
Article:
Crowther, P.A., Rate, G. and Bestenlehner, J.M. orcid.org/0000-0002-0859-5139 (2023) Line luminosities of Galactic and Magellanic Cloud Wolf–Rayet stars. Monthly Notices of the Royal Astronomical Society, 521 (1). pp. 585-612. ISSN 0035-8711

https://doi.org/10.1093/mnras/stad418

Monthly Notices of the ROYAL ASTRONOMICAL SOCIETY

MNRAS **521,** 585–612 (2023) https://doi.org/10.1093/mnras/stad418
Advance Access publication 2023 February 7

Line luminosities of Galactic and Magellanic Cloud Wolf–Rayet stars

Paul A. Crowther,* G. Rate and Joachim M. Bestenlehner
Department of Physics and Astronomy, University of Sheffield, Hounsfield Road, Sheffield S3 7RH, UK

Accepted 2023 February 3. Received 2023 February 2; in original form 2023 January 11

ABSTRACT

We provide line luminosities and spectroscopic templates of prominent optical emission lines of 133 Galactic Wolf–Rayet (WR) stars by exploiting *Gaia* DR3 parallaxes and optical spectrophotometry, and provide comparisons with 112 counterparts in the Magellanic Clouds. Average line luminosities of the broad blue (He II λ4686, C III λλ4647,51, N III λλ4634,41, and N V λλ4603,20) and yellow (C IV λλ5801,12) emission features for WN, WN/C, WC, and WO stars have application in characterizing the WR populations of star-forming regions of distant, unresolved galaxies. Early-type WN stars reveal lower line luminosities in more metal-poor environments, but the situation is less clear for late-type WN stars. LMC WC4–5 line luminosities are higher than their Milky Way counterparts, with line luminosities of Magellanic Cloud WO stars higher than Galactic stars. We highlight other prominent optical emission lines, N IV λλ3478,85 for WN and WN/C stars, O IV λλ3403,13 for WC and WO stars, and O VI λλ3811,34 for WO stars. We apply our calibrations to representative metal-poor and metal-rich WR galaxies, IC 4870 and NGC 3049, respectively, with spectral templates also applied based on a realistic mix of subtypes. Finally, the global blue and C IV λλ5801,12 line luminosities of the Large Magellanic Clouds or LMCs (Small Magellanic Clouds) are 2.6×10^{38} erg s^{-1} (9×10^{36} erg s^{-1}) and 8.8×10^{37} erg s^{-1} (4×10^{36} erg s^{-1}), respectively, with the cumulative WR line luminosity of the Milky Way estimated to be an order of magnitude higher than the LMC.

Key words: galaxies: Magellanic Clouds – galaxies: stellar content – stars: massive – stars: Wolf–Rayet.

1. INTRODUCTION

Wolf–Rayet (WR) stars, the evolved descendants of (very) high-mass stars, exhibit broad optical emission lines owing to their dense stellar winds (Crowther 2007). There are three flavours of WR stars known, nitrogen-sequence (WN) stars dominated by helium and nitrogen features, carbon-sequence (WC) stars with prominent carbon and helium lines, and rare oxygen-sequence (WO) stars with dominant oxygen and carbon features.[1] Their unusual spectroscopic signatures permit their use as tracers of star-formation in galaxies (Allen, Wright & Goss 1976; Kunth & Sargent 1981). Indeed, a subset of starburst galaxies have been coined WR galaxies owing to the presence of broad He II λ4686 emission from WN stars, and occasionally C IV λ5808 emission from WC stars (Vacca & Conti 1992). The advent of highly multiplexed instrumentation (e.g. SDSS) and large-field integral field spectroscopic capabilities (e.g. MUSE) has identified large numbers of WR stars in external galaxies (Brinchmann, Kunth & Durret 2008; Miralles-Caballero et al. 2016; Monreal-Ibero et al. 2017; Gómez-González et al. 2021; Senchyna et al. 2021).

Population synthesis models have incorporated WR stars via either empirical calibrations (Schaerer & Vacca 1998) or synthetic spectra (Smith, Norris & Crowther 2002; Eldridge et al. 2017). The former approach has relied heavily on calibrations of WR stars in the metal-poor Magellanic Clouds (Smith, Shara & Moffat 1990a; Crowther & Hadfield 2006) while the latter depend on predictions from single or binary evolutionary models and suitable prescriptions for theoretical wind densities at a range of metallicities. Various mass-loss prescriptions are available, and differ between very massive stars exhibiting WR spectral morphologies (Bestenlehner 2020) and classical WR stars (Nugis & Lamers 2000; Sander, Vink & Hamann 2020) although these are generally untested for a broad range of metallicities. By way of example, Eldridge et al. (2017) utilize the grid of PoWR (Gräfener, Koesterke & Hamann 2002) model atmospheres[2] for spectral synthesis, yet predictions are highly dependent on the choice of WR models.

Empirical calibrations have been produced for WR stars in the Magellanic Clouds, but uncertain distances to Milky Way WR stars have severely hindered calibrations at high metallicity to date. The advent of reliable Galactic WR distances from *Gaia* (Rate & Crowther 2020) has opened up the possibility of solar metallicity calibrations and spectral templates. In this study, we exploit *Gaia* DR3 parallaxes and archival spectrophotometry of large numbers of Galactic WR stars to provide calibrations at (near) solar composition, with which to complement synthetic spectroscopy, and revisit Magellanic Cloud calibrations in view of new discoveries and higher quality observations since Crowther & Hadfield (2006).

This paper is structured as follows. Section 2 discusses the observational data sets employed to construct WR line luminosities, Section 3 compares Milky Way WR line luminosities with Magellanic Cloud counterparts and includes templates for each environment, and

* E-mail: Paul.crowther@sheffield.ac.uk

[1]The WR phenomenon is common to evolved massive stars (classical WN, WC, and WO), very massive main-sequence stars (H-rich WN and Of/WN), and a subset of central stars of Planetary Nebulae ([WC] and [WN]).

[2]https://www.astro.physik.uni-potsdam.de/PoWR/

Table 1. Source of optical spectrophotometry of Galactic and Magellanic Cloud WR stars for this study, including representative spectral resolutions at $\lambda = 5000$ Å.

ID	Telescope	Instrument	Epoch	Sp. Res (Å)	Wavelength Coverage (Å)	Flux Calib. (per cent)	Ref	Notes
AD	ANU 2.3m	DBS	Dec 1997	5	3200–11 000	10	2	Southern WR stars; 6070–6400 Å detector gap
AR	AAT	RGO	Mar 1992–Dec 1994	2	3680–6000	10	1	LMC/SMC WN and WN/C stars
CS	CTIO 1.5m	SIT	Nov 1981–Feb 1985	10	3400–7270	10	16	Southern Milky Way WR stars; variable λ_{max}
HF	*HST*	FOS	Jan 1996–Jan 1997	3	3230–6820	10	4–6	LMC WN stars; G400 only ($\lambda_{max} = 4780$ Å) except for R136
HS	*HST*	STIS	Mar 2014–Sep 2016	10	2900–10 250	10	17	AB5 (HD 5980)
II91	INT	IDS	Sep 1991	2	3320–7300	20	7	Northern Milky Way WN and WN/C stars; variable $\lambda_{min/max}$
II96	INT	IDS	Jul 1996	3	3620–6810	10	8	Northern Milky Way WN stars
II13	INT	IDS	Sep 2013	5	3800–9350	20	9	Northern Milky Way WR stars
KI	KPNO 0.91m	IRS	Oct 1980–Feb 1983	9	3450–6900	10	10	Northern Milky Way WR stars
MM	Magellan	MagE	Sep 2014-Dec 2020	1.2	3170–9440	10	13, 14	LMC WR stars
SC	Mt Stromlo 1.9m	Coudé	Dec 1995	1	4700–6700	20	1	LMC late-type WN stars
WI94	WHT	ISIS	Jun 1994	3	4450–6030	10	11	Northern Milky Way WN and WN/C stars
WI02	WHT	ISIS	Aug 2002	3.5	3400–9500	10	12	Northern Milky Way WC stars
VM	VLT	MUSE	Aug 2014	3	4600–9350	10	15	LMC WN stars; calibration via BAT99–100 (*HST*/FOS)
VU	VLT	UVES	Jan 2002–Jan 2003	0.1	3200–10 240	10	18, 19	Southern Milky Way WR stars
VX	VLT	Xshooter	Nov 2011–Aug 2013	0.8	3100–24 700	10	20, 21	Southern Milky Way and LMC WR stars

Notes. 1: Crowther & Smith (1997); 2: Crowther et al. (2002), 3: Crowther & Hadfield (2006); 4: de Koter, Heap & Hubeny (1997); 5: Massey & Hunter (1998); 6: Walborn et al. (1999); 7: Crowther et al. (1995a); 8: Crowther (1997); 9: This study; 10: Massey (1984); 11: Crowther, Smith & Willis (1995c); 12: Crowther, Morris & Smith (2006b); 13: Neugent et al. (2017); 14: Aadland et al. (2022b); 15: Castro et al. (2018); 16: Torres-Dodgen & Massey (1988); 17: Hillier et al. (2019); 18: Bagnulo et al. (2003); 19: Borisov et al. (2022); 20: Tramper et al. (2015); 21: M. Rubin-Diez et al. (in preparation).

Section 4 applies calibrations and templates to representative WR galaxies at low and high metallicity, with conclusions drawn in Section 5.

2. OBSERVATIONS

Our primary objective is to provide line luminosities of prominent optical emission lines in Milky Way WR stars, requiring (i) spectrophotometric data sets; (ii) interstellar extinctions drawn from spectroscopic studies; and (iii) distances from *Gaia* DR3 parallaxes.

2.1 Milky Way WR stars

A subset of flux calibrated spectroscopic data sets involved observations through large apertures, while others involved relatively flux calibrated data sets adjusted to literature photometry, primarily narrow-band *ubvr* photometry of Massey (1984) or Torres-Dodgen & Massey (1988). In instances of discrepant photometric measurements, inspection of large aperture low resolution (LORES) LWR or LWP (1850–3350 Å) spectrophotometry from *International Ultraviolet Explorer (IUE)*[3] provided the primary reference. We also utilize *IUE* SWP (1150–1980 Å) spectrophotometry, where available.

Our primary optical spectroscopic data sets are summarized in Table 1, with typical spectral resolutions of 1–5 Å, although some historical data sets were obtained at low spectral resolution. In view of the (typically) broad WR emission lines, this does not adversely impact on line flux measurements, but full width at half-maximum (FWHM) of narrow-lined stars (typically WN8–11) are impacted, so all quoted FWHM are corrected for instrumental broadening (typical uncertainties are ± 100 km s^{-1}). All data sets have been previously discussed with the exception of Isaac Newton Telescope (INT) IDS spectroscopy from 2013 September 16–17 (PI Rosslowe), involving observations of WR138–1,[4] WR140, and WR149 with the 235-mm camera, R300V grating, and EEV10 detector. Relative flux calibration was achieved using standard star BD + 25° 4655. Flux calibrated UVES Paranal Observatory Project (POP) data sets (Bagnulo et al. 2003; Borisov et al. 2022) are included if the key C IV λλ5801,12 line, missing due to the UVES detector gap, is available from other sources. In some instances spectroscopy extends to or beyond 1 μm (e.g. Australian National University (ANU) 2.3m/DBS and Very Large Telescope (VLT)/Xshooter) which are supplemented by additional near-infrared (near-IR) spectrophotometry (e.g. Infrared Telescope Facility (IRTF)/SpeX, Crowther et al. 2006a). For inclusion in the present sample, we require He II λ4686 for WN and Of/WN stars, C IV λλ5801,12 for WC stars, and O IV λλ3811,34 for WO stars, thereby excluding heavily reddened stars, such as the rich WR population in Westerlund 1 (Crowther et al. 2006a). We also omit WR + WR binaries involving differing subtypes (e.g. WR70–16; Callingham et al. 2020).

Line fluxes were measured using the multiple Gaussian Emission Line Fitting (ELF) routines within the Starlink DIPSO spectroscopic package (Howarth et al. 2004). Spectral coverage varies by instrument/telescope, but usually includes λ4000–λ7000, so may exclude some violet (e.g. O IV λλ3403,13 and N IV λλ3478,85) or red (e.g. N IV λλ7103,29 and C III λλ9701,19 diagnostics). We adopt uncertainties of 10 per cent for the majority of line flux

[3]INES data sets obtained from http://sdc.cab.inta-csic.es/ines/.

[4]Gvaramadze et al. (2009) discovered WR138a, which was subsequently reclassified as WN9 by Flagey et al. (2014) and its WR catalogue number was revised to WR138-1 following Rosslowe & Crowther (2015).

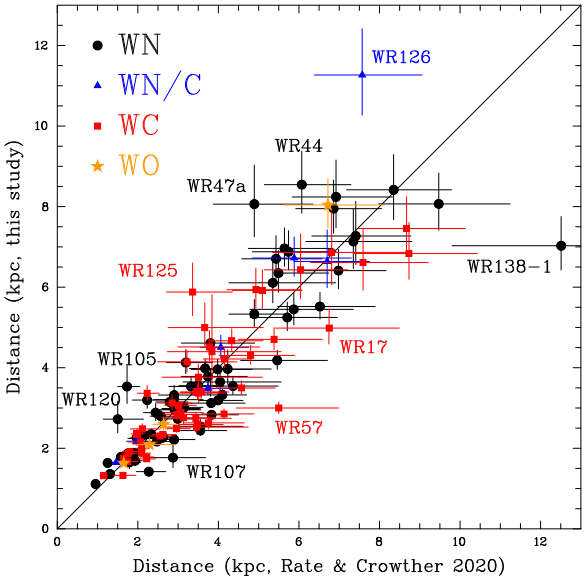

Figure 1. Comparison between Galactic WR distances (in kpc) following a common Bayesian methodology of Rate & Crowther (2020) using either *Gaia* DR2 parallaxes incorporating global zero-point corrections of Lindegren et al. (2018), versus DR3 parallaxes incorporating local zero-point corrections of Lindegren et al. (2021) and Maíz Apellániz (2022). The key distinguishes between WN (black circles), WN/C (blue triangles), WC (red squares), and WO (orange stars) subtypes. In general, DR3 and revised zero-points provides improved uncertainties on distances, with some outliers labelled.

measurements, 20 per cent for Mt Stromlo 1.9m/Coudé and INT/IDS spectroscopy from 1991 and 2013. Comparisons between He II λ4686 line fluxes and literature results for WN stars from Leitherer, Lee & Faisst (2019) reveal $\log F_{\rm HeII4686} - F^{\rm L19}_{\rm HeII4686} = 0.00 \pm 0.10$ for 35 stars in common, while comparisons between C IV λλ5801,12 line fluxes and literature results for WC stars from Smith, Shara & Moffat (1990b) reveal $\log F_{\rm CIV5801,12} - F^{\rm S90b}_{\rm CIV5801,12} = 0.00 \pm 0.11$ for 48 stars in common.

In the era of reliable Galactic distances courtesy of *Gaia*, interstellar extinctions are of critical importance for line luminosity determinations. Here, we adopt E_{B-V} and R_V values from contemporary spectroscopic studies (Hamann, Gräfener & Liermann 2006; Sander, Hamann & Todt 2012). For stars (usually WR + O binaries) lacking modern extinction determinations, we follow the approach adopted by Crowther & Hadfield (2006) involving the relationship between the He II λ4686 equivalent width ($W_{\rm HeII\,4686}$) and intrinsic colour of WN stars, or adopt $(b-v)_0 = -0.30$ mag, and $E_{B-V} = 1.21 \times E_{b-v}$ and $R_V = 3.1$. In order to determine intrinsic fluxes, we adopt the Milky Way extinction law of Seaton (1979), parametrized by Howarth (1983), which provided the default law for the majority of Galactic WN and WC stars studied by Hamann et al. (2006) and Sander et al. (2012), respectively.[5] For error calculations, we assume A_V magnitudes are reliable to 10 per cent throughout. By way of example, we measure $W_{\rm HeII\,4686} = 19$ Å for WR138–1, which implies $(b-v)_0 \sim -0.31$ mag (Crowther & Hadfield 2006, their fig. 1), so $E_{b-v} = 1.87$ mag, based on $b - v = 1.56$ mag from our INT/IDS spectroscopy, resulting in $A_V = 7.0 \pm 0.7$ mag (versus $A_V = 7.4$ mag from Gvaramadze et al. 2009).

Distances to Galactic WR stars follow from *Gaia* DR3 parallaxes (Gaia Collaboration 2021), using star-specific zero-point corrections from Lindegren et al. (2021) updated by Maíz Apellániz (2022), and the Bayesian methods set out in Rate & Crowther (2020). Inferred distances are generally in good agreement with Bailer-Jones et al. (2021). A comparison between distances obtained from Rate & Crowther (2020) based on DR2 parallaxes and the global zero-point correction of Lindegren et al. (2018) versus DR3 parallaxes and updated zero-point corrections is presented in Fig. 1. In general, DR3 and star-specific zero-point corrections provide significantly improved uncertainties on WR distances. Sources with DR3 warning flags (e.g. WR2, WR31, WR66, WR104, and WR115) are excluded, while we include H-rich WN stars within NGC 3603 (WR43) for which we adopt the distance of $7.27^{+0.38}_{-0.35}$ kpc determined by Drew, Monguió & Wright (2021). Average distances to Galactic WN and WN/C stars in our sample are 4.0 ± 2.2 kpc while average distances to WC and WO stars are 3.5 ± 1.7 kpc. For Galactic stars, *Gaia* DR3 distance uncertainties are typically ≤10 per cent, so extinctions usually dominate uncertainties in line luminosities.

We group WN stars into five categories, namely strong-lined ('WN3–7s'), weak-lined, early-type ('WN2–5w'), weak-lined late-type ('WN6–8'), very late-type ('WN9–11'), and (main sequence) very massive H-rich stars ('WN5–7h'), and additionally include transition Of/WN stars ('O2–3.5If/WN'). The division between strong- and weak-lined stars was set at $W_{\rm HeII\,5412} = 40$ Å (Koesterke et al. 1991). We follow this approach with the exception of BAT99-5 which is assigned as a weak-lined star despite $W_{\rm HeII\,5412} = 41 \pm 1$ Å. Weak-/strong-lined categories are preferred to narrow-/broad-lined (Smith, Shara & Moffat 1996) whose threshold is FWHM(He II λ4686) = 30 Å (corresponding to ∼1900 km s^{-1}), since a subset of broad-lined stars possesses a very weak emission line spectrum (e.g. WR46; Crowther, Smith & Hillier 1995b), although the majority of strong-lined stars also possess broad lines, and Smith et al. (1996) included W_λ(He II λ5412) = 40 Å as one of their criteria for broad-lined WN stars. The majority of strong-lined stars have WN3–4 subtypes, although examples in the Milky Way extend as late as WN6 (WR134 and WR136) or WN7 (WR91). Large Magellanic Cloud (LMC) 170–2 (WN3/O3; Neugent et al. 2017) is included as a WN2–5w star, although H β absorption would usually favour an O-type classification in preference to either WN or Of/WN (Crowther & Walborn 2011). In order to discriminate between classical WN and main-sequence WN5–7h stars, we consider spectral morphologies as well as association with young star-forming regions (e.g. Carina Nebula, NGC 3603). WC stars are categorized as early-type ('WC4–5'), mid-type ('WC6–7'), or late-type ('WC8–9').

Line luminosities of individual Galactic WN, WN/C, WC, and WO stars are presented in Tables A1–A4 in the Appendix. For WN and WN/C stars, aside from the blends at λ4100 and λ4630, we have endeavoured to exclude the contribution of He I λ7065 and He II λ7177 from the N IV λλ7103,29 multiplet. For early-type WC and WO stars, C IV λ4658 (6-5), λ4686 (8-6), and λ4689 (11-7) will also contribute to the C,III λλ4647,51 + He II λ4686 blend. Uncertainties in absolute luminosities involve a combination of absolute flux calibration, distance and extinction, with the latter dominating uncertainties for the majority of Galactic WR stars. Uncertainties on stellar luminosities from literature results account for distance and extinction, but exclude systematic uncertainties resulting from individual studies which vary between studies (typically 0.1–0.2 dex).

In general, WR stars within unresolved star-forming regions are detected via blue (λ4686) or yellow (λ5808) bumps. Binaries comprise a significant subset of our sample, but WR fluxes/luminosities are not generally impacted with a few exceptions. Strong absorption lines of OB companions impact measurements of features in the proximity of (usually) upper Balmer lines, while a few systems

[5]Contemporary extinction laws are available (e.g. Fitzpatrick et al. 2019).

are host to multiple WR stars in which case calibrations adopt equal contribution from each component, which is a reasonable approximation for systems with mass ratios of order unity (e.g. WR43A; Schnurr et al. 2008). Excess line emission is also observed in colliding wind systems, usually witnessed in C III λ5696 in WC + O binaries (Luehrs 1997).

2.2 Magellanic Cloud WR stars

We supplement Galactic WR data sets with Magellanic Cloud counterparts, updated from Crowther & Hadfield (2006) to include additional data sets (e.g. Tramper et al. 2015; Neugent et al. 2017; Aadland et al. 2022b). Observations of Small Magellanic Cloud (SMC) WN2–5w stars suffer from poor sound-to-noise ratio (S/N), so we also calibrate higher quality data sets from Foellmi et al. (2003). We also make use of archival ultraviolet (UV) *IUE* or *Hubble Space Telescope (HST)* spectrophotometry, the latter involving FOS (Crowther et al. 2002), STIS (Crowther et al. 2016; Aadland et al. 2022b), and COS (Aadland et al. 2022b) instruments. VLT/Xshooter and ANU/2.3m/DBS spectrophotometry extend to the near-IR, with Magellan/FIRE data sets also utilized for LMC WC and WO stars (Aadland et al. 2022b). Again, we assume typical uncertainties of 10 per cent for line flux measurements obtained from spectrophotometric data sets (e.g. Crowther & Hadfield 2006).

Comparisons between He II λ4686 line fluxes and literature results for LMC WN stars from Leitherer et al. (2019) reveal $\log F_{\rm HeII4686} - F^{\rm L19}_{\rm HeII4686} = +0.02 \pm 0.05$ for 30 stars in common, while comparisons between C IV λ5808 line fluxes and literature results for LMC WC stars from Smith et al. (1990a) reveal $\log F_{\rm CIV5801,12} - F^{\rm S90a}_{\rm CIV5801,12} = -0.07 \pm 0.09$ for 10 stars in common. Several Magellanic Cloud systems are host to multiple WN + WN stars, including BAT99-116 (Mk 34; Tehrani et al. 2019), and BAT99-118 (R144; Shenar et al. 2021), so we adopt equal line contributions from each component since mass ratios are close to unity, which should be a reasonable assumption with the potential exception of AB5 (HD 5980; Koenigsberger et al. 2014). Since AB5 is known to be spectroscopically variable (Koenigsberger et al. 2022), we have selected the *HST*/STIS data set from 2016 (phase 0.36) instead of 2014 (phase 0.0) (Hillier et al. 2019). R140a is omitted since it involves a mix of WN and WC populations which are difficult to deblend (Castro et al. 2018).

Revised interstellar extinctions are again drawn from spectroscopic studies where available (e.g. Hainich et al. 2014), or $(b-v)_0 = -0.30$ mag otherwise, and $E_{B-V} = 1.21\,E_{b-v}$ and $R_V = 3.1$. Again, we assume that literature A_V values are reliable to 10 per cent. For reference, the average difference between values of E_{B-V} adopted here for LMC WC + O binaries is -0.03 ± 0.13 mag with respect to Bartzakos et al. (2001). The LMC distance of 49.6 kpc adopted from Pietrzyński et al. (2019) and a SMC distance of 61.2 kpc obtained from the 0.458 mag difference in distance moduli between the Magellanic Clouds (Graczyk et al. 2014). We assume an uncertainty of 2 per cent for individual distances within the Magellanic Clouds. We adopt the LMC extinction law of Howarth (1983) for both Clouds, in common with the studies of Magellanic Cloud WR stars by Hainich et al. (2014, 2015), noting that alternative prescriptions are available (Gordon et al. 2003; Maíz Apellániz et al. 2014).

Line luminosities of individual Magellanic Cloud WN, Of/WN, WN/WC, WC, and WO stars are included in Tables A1–A4 in the Appendix. The largest source of uncertainty in line luminosities of Magellanic Cloud stars is usually flux calibration since distances are well established and extinctions are generally low, with a few exceptions (e.g. VFTS 682; Rubin-Diez et al., in preparation). Since Rubin-Diez et al. adopt the 30 Dor extinction law of Maíz Apellániz et al. (2014) for the heavily reddened star VFTS 682 (WN5–7h) we are able to quantify differences in line intensities following Howarth (1983). We typically obtain line intensities within 10–20 per cent, higher intensities for violet lines following Howarth (1983), and higher intensities for red lines following Maíz Apellániz et al. (2014). Uncertainties on stellar luminosities from literature results account for distance and extinction, but exclude systematic uncertainties resulting from individual studies (variable, albeit typically 0.1–0.2 dex).

3. RESULTS

3.1 WN, Of/WN, and WN/C stars

In Fig. 2, we compare He II λ4686 FWHM and line luminosities for Milky Way and Magellanic Cloud WN and OIf/WN stars. Galactic strong-lined WN stars exhibit the highest line luminosities and largest FWHM λ4686. LMC strong-lined WN stars overlap with Galactic counterparts, but typically have lower luminosities and FWHM. Weak-lined WN2–5 stars in the Milky Way span a broad range of line luminosities, ranging from $\log(L_{4686}/{\rm erg\,s^{-1}}) = 36.1 \pm 0.2$ (WR141) to 34.6 ± 0.1 (WR3), with similar results obtained for LMC stars, except that LMC 170–2 (Neugent et al. 2017) has a very low luminosity of $\log(L_{4686}/{\rm erg\,s^{-1}}) = 34.2$, and is morphologically similar to WR3 and WR46 in the Milky Way (Crowther et al. 1995b). SMC WN2–5w stars possess uniformly low λ4686 line luminosities, spanning $\log(L_{4686}/{\rm erg\,s^{-1}}) = 35.6$ (AB3) to 34.7 (AB11), which has previously been highlighted by Crowther & Hadfield (2006). Sander et al. (2020) have investigated wind driving of WR stars, and establish a dependence on metallicity (Fe-group elements) and Eddington parameter Γ_e ($\propto L/M$) so strong-lined WN stars likely differ in

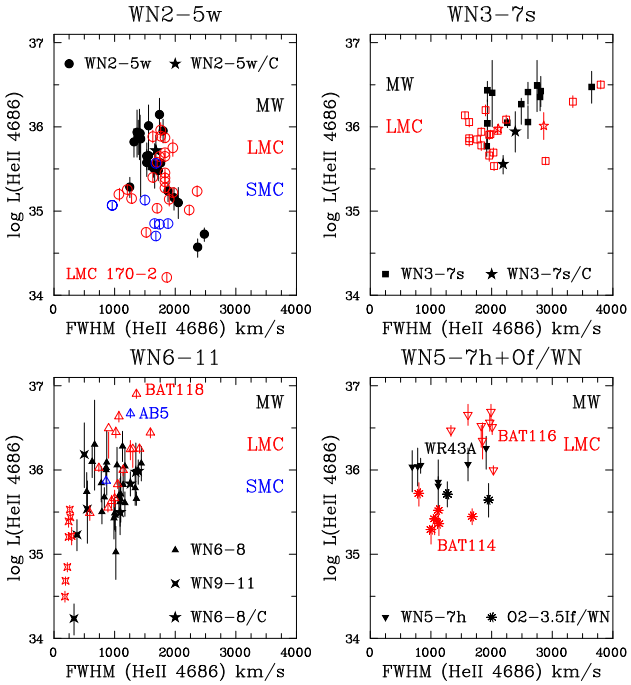

Figure 2. He II λ4686 line luminosities of WN2–5w (top-left panel), WN3–7s (top-right panel), WN6–8 (bottom-left panel), and WN5–7h + Of/WN (bottom-right panel) stars in the Milky Way (black, filled), LMC (red, open), and SMC (blue, open) versus FWHM (km s^{-1}). Weak- and strong-lined early-type WN stars are indicated as circles and squares, respectively, WN/C stars as stars, WN6–8 as triangles, WN9–11 as crosses, H-rich main sequence WN5–7h stars as inverted triangles, and Of/WN stars as asterisks.

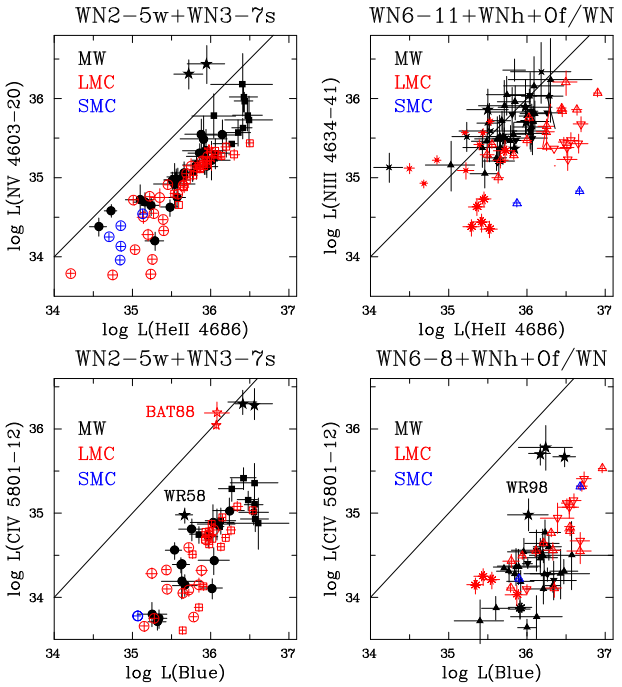

Figure 3. (Upper panels): He II λ4686 versus N V λλ4603,20 + N III λλ4634,41 line luminosities of WN, Of/WN, and WN/C stars in the Milky Way (black), LMC (red), and SMC (blue). C III λ4647,51 also contributes for WN/C subtypes, N III λλ4634,41 for WN6–7s subtypes, and N II λλ460,43 for WN10–11 subtypes. (Lower panels): Blue (He II λ4686, N V λλ4603,20, N III λλ4634,41, and C III λ4647,51) versus C IV λλ5801,12 line luminosities. C IV λλ5801,12 is an order of magnitude stronger in WN/C stars than WN stars. The solid line indicates equal line luminosities. Symbols as in Fig. 2 (WN9–11 are omitted from lower panels since C IV λλ5801,12 is weak/absent).

their wind properties from weak-lined WN stars owing to higher luminosity-to-mass ratios. He II λ4686 properties of Galactic and LMC WN/C stars are similar to normal WN stars in these galaxies.

Galactic weak-lined WN6–8 stars possess relatively low FWHM λ4686, albeit a wide range of line luminosities, spanning $\log(L_{4686}/\mathrm{erg\,s^{-1}}) = 36.3 \pm 0.5$ (WR147) to 35.0 ± 0.3 (WR107). LMC weak-lined WN6–8 stars extend the Galactic sequence to higher luminosities, including R144 (BAT99–118), which is host to a multiple WN + WN system (Shenar et al. 2021) and R145 (BAT99–119) which is also a binary system (Shenar et al. 2019). There are too few SMC late-type WN stars to draw robust conclusions, although the high-luminosity SMC system AB 5 (HD 5980) is also multiple (Koenigsberger et al. 2014, 2022). Milky Way and LMC WN9–11 stars possess very low FWHM and line luminosities, with the notable exception of WR105 (WN9) whose λ4686 line luminosity is comparable with WN6–8 stars. H-rich main sequence WN6–7h stars in the Milky Way form a relatively homogenous group, overlapping with weak-lined classical WN stars in He II λ4686 properties, and includes the WN + WN binary system WR43A. LMC counterparts extend to higher luminosity, broader lines (WN5h) stars, including the WN5h + WN5h binary Mk 34 (BAT99-116; Tehrani et al. 2019) with Of/WN stars, such as Mk 35 (BAT99-114; Crowther & Walborn 2011), possessing lower line luminosities.

Fig. 3 (upper panels) compares He II λ4686 and N V λλ4603,20 + N III λ4634,41 line luminosities of WN, Of/WN, and WN/C stars. For early subtypes N V λλ4603,20/He II λ4686 ∼ 0.2–0.3 in all environments, with the exception of Galactic WN/C stars which also exhibit a contribution from C III λλ4647,51. In contrast, for late subtypes N III λλ4634,41/He II λ4686 ∼ 0.8 in the Milky Way, ∼0.2 in the LMC, and ≤0.1 in the SMC, with the exception of WN9–11 stars for which N II λλ4601,43 + N III λλ4634,41/He II λ4686 ≥ 1. Fig. 3 (lower panels) compares the blue (He II λ4686, N V λλ4603,20, N III λ4634,41, and C III λλ4647,51) and C IV λλ5801,12 line luminosities of WN, Of/WN, and WN/C stars. For Galactic early-type WN stars the line luminosity of C IV λλ5801,12 is an order of magnitude weaker than the blue feature, with late-type WN stars somewhat weaker still (and usually resolved into individual components). A broadly similar dependence is obtained for Magellanic Cloud counterparts, with C IV λλ5801,12 undetected in a subset of WN stars from all environments. In contrast, C IV λλ5801,12 luminosities of WN/C stars exceed normal WN stars by an order of magnitude, and are more typical of WC stars. The least extreme examples of WN/C stars in our sample are WR58 and WR98 (Conti & Massey 1989).

Tables 2–3 provide calibrations of He II λ4686 line luminosities for WN2–8 (N = 140), WN9–11 (N = 12), Of/WN (N = 8), and WN/C (N = 9) stars, respectively, together with other prominent optical emission lines. This highlights features that may be detectable in high-S/N observations of WR galaxies, notably the λ4100 complex in WN stars which is largely unaffected by nebular emission, in contrast with Hα, Hβ, and He I λ5876. Although Hβ is omitted here, $L_{\mathrm{H}\alpha}/L_{\mathrm{H}\beta} = 1.9 \pm 0.8$ for 141 Milky Way and Magellanic Cloud WN and WN/C stars.

3.2 WC and WO stars

In Fig. 4 (left-hand and centre panels), we compare the FWHM and line luminosities of C IV λλ5801,12 for Milky Way and Magellanic Cloud WO and WC stars. WO stars possess exceptionally high FWHM though span a wide range of C IV λλ5801,12 line luminosities, ranging from $\log(L_{\mathrm{CIV\,5801,\,12}}/\mathrm{erg\,s^{-1}}) = 36.52 \pm 0.05$ (AB8, SMC) to 34.25 ± 0.15 (WR102, Milky Way). In contrast, LMC WC4–5 stars possess uniformly high luminosities, with the WC4 + O binary BAT99-70 possessing the highest luminosity C IV λλ5801,12. Galactic counterparts overlap with LMC stars, though extend to lower luminosities. Galactic WC6–7 stars overlap with WC4–5 subtypes, although these extend to lower luminosities, unusually so for WR39. Galactic WC8–9 stars exhibit a narrow range of FWHM but a broad range of line luminosities, ranging from $\log(L_{\mathrm{CIV\,5801,\,12}}/\mathrm{erg\,s^{-1}}) = 36.1 \pm 0.2$ (WR60) to 34.85 ± 0.15 (WR77). Smith et al. (1990b) have previously studied Galactic WC stars in clusters and associations to suggest uniform C IV λ5801–12 fluxes for Galactic WC5–7 stars, with lower line fluxes for WC8–9 stars. Fig. 4 (right-hand panel) compares O VI λλ3811,34 FWHM and line luminosities of Milky Way and Magellanic Cloud WO stars, revealing uniformly high FWHM, though an order of magnitude spread in line luminosity from $\log(L_{\mathrm{OVI\,3811,\,34}}/\mathrm{erg\,s^{-1}}) = 36.35 \pm 0.05$ (AB8) to 35.4 ± 0.3 (WR93b).

Fig. 5 compares blue (C III λλ4647,51, C IV λ4658, and He II λ4686) to yellow (C IV λλ5801,12) line luminosities of WC and WO stars. For Galactic WC4–5 stars the blue and yellow features are well correlated, with the former exceeding C IV λλ5801,12 by a factor of 2–3, while these features are more comparable in strength in LMC WC4–5 and WO stars. Blue and yellow features are also tightly correlated for WC6–9 stars, with the former exceeding C IV λλ5801,12 by a factor of 3 (WC6–7) to 5 (WC8–9).

Tables 4–5 provide calibrations of C IV λλ5801,12 line luminosities for WC (N = 68) and WO (N = 8) stars, respectively. Other strong WC features include C III λλ4647,51, λ5696, the latter having

Table 2. WN and Of/WN line luminosity calibrations for Milky Way, LMC, and SMC stars, including He II λ4686 FWHM in km s^{-1}. The complex at λ4100 involves N III λλ4097,4103, Si IV λλ4088,4116, and He II λ4100 + H δ, while the feature at λ4630 involves N V λλ4603,20 and N III λλ4634,41 (or N II λλ4601,43 for very late WN subtypes). Line luminosities have been adjusted for systems host to WN + WN binaries (marked with ⋄), namely WR43A, BAT99-116, BAT99-118, and AB5.

Category	N	HeII 4686 FWHM	$L_{\rm HeII\ 4686}$ 10^{35} erg s^{-1}	$L_{\rm HeII\ 4686}$ 10^{-3} $L_{\rm Bol}$	$\frac{L_{\rm NIV\ 3478,85}}{L_{\rm HeII\ 4686}}$	$\frac{L_{\rm NIV\ 4058}}{L_{\rm HeII\ 4686}}$	$\frac{L_{4100}}{L_{\rm HeII\ 4686}}$	$\frac{L_{4630}}{L_{\rm HeII\ 4686}}$	$\frac{L_{\rm HeII\ 5412}}{L_{\rm HeII\ 4686}}$	$\frac{L_{\rm CIV\ 5801,12}}{L_{\rm HeII\ 4686}}$	$\frac{L_{\rm HeI\ 5876}}{L_{\rm HeII\ 4686}}$	$\frac{L_{\rm H\alpha}}{L_{\rm HeII\ 4686}}$	$\frac{L_{\rm NIV\ 7103,29}}{L_{\rm HeII\ 4686}}$
						Milky Way ($Z_\odot$)							
WN2–5w	22	1680 ± 310	4.9±3.7	0.37 ± 0.23	0.68 ± 0.21	0.26 ± 0.14	0.27 ± 0.14	0.29 ± 0.15	0.12 ± 0.03	0.06 ± 0.05	0.03 ± 0.02	0.20 ± 0.08	0.21 ± 0.15
WN3–7s	12	2480 ± 510	20.3±8.9	1.25 ± 0.40	0.49 ± 0.14	— 0.40 ± 0.25 —		0.27 ± 0.16	0.13 ± 0.02	0.07 ± 0.03	0.05 ± 0.03	0.15 ± 0.04	0.16 ± 0.04
WN6–8	25	990 ± 240	7.4±5.0	0.44 ± 0.20	0.30 ± 0.16	0.18 ± 0.09	0.65 ± 0.28	0.86 ± 0.44	0.11 ± 0.04	0.03 ± 0.02	0.32 ± 0.31	0.51 ± 0.43	0.12 ± 0.10
WN9–11	4	440 ± 100	5.1±6.9	0.13 ± 0.11	···	0.00 ± 0.00	6.2 ± 10.2	3.1 ± 3.2	0.03 ± 0.03	0.01 ± 0.01	9.7 ± 18.0	45 ± 87	0.01 ± 0.0
WN5–7h	7⋄	1260 ± 510	11.0±3.8	0.15 ± 0.04	0.37 ± 0.39	0.18 ± 0.07	0.54 ± 0.23	0.58 ± 0.32	0.06 ± 0.01	0.03 ± 0.02	0.05 ± 0.02	0.64 ± 0.13	0.09 ± 0.01
Of/WN	2	1610 ± 470	4.8 ± 0.5	0.05 ± 0.01	0.16 ± 0.08	0.25 ± 0.09	0.26 ± 0.24	0.48 ± 0.16	0.06	0.01	0.00	0.58	···
						LMC (0.4 $Z_\odot$)							
WN2–5w	24	1750 ± 280	3.3±2.6	0.21 ± 0.14	0.79 ± 0.19	0.10 ± 0.11	0.13 ± 0.12	0.19 ± 0.12	0.11 ± 0.03	0.04 ± 0.03	0.00 ± 0.01	0.22 ± 0.06	0.08 ± 0.04
WN3–7s	18	2170 ± 600	10.1±6.9	0.70 ± 0.24	0.50 ± 0.23	— 0.12 ± 0.04 —		0.16 ± 0.03	0.13 ± 0.01	0.05 ± 0.03	0.01 ± 0.02	0.16 ± 0.03	0.07 ± 0.03
WN6–8	13⋄	1080 ± 270	17.8 ± 14.0	0.39 ± 0.16	0.20 ± 0.08	0.17 ± 0.03	0.33 ± 0.14	0.34 ± 0.19	0.09 ± 0.03	0.03 ± 0.02	0.09 ± 0.06	0.41 ± 0.24	0.06 ± 0.01
WN9–11	8	240±40	1.6 ± 1.1	0.09 ± 0.07	···	0.01 ± 0.02	1.50 ± 0.93	1.9 ± 1.1	0.05 ± 0.09	0.00 ± 0.00	1.8 ± 1.5	6.5 ± 5.1	···
WN5–7h	8⋄	1830 ± 250	30.2 ± 13.6	0.24 ± 0.12	0.44 ± 0.14	0.18 ± 0.05	0.18 ± 0.09	0.07 ± 0.03	0.09 ± 0.02	0.03 ± 0.01	0.01 ± 0.01	0.34 ± 0.08	0.11 ± 0.04
Of/WN	6	1130 ± 300	3.7 ± 1.9	0.05 ± 0.02	0.30	0.22	0.00	0.18 ± 0.12	0.02 ± 0.02	0.04 ± 0.04	0.00 ± 0.00	0.59 ± 0.13	0.11 ± 0.05
						SMC (0.2 $Z_\odot$)							
WN2–5w	9	1630 ± 280	1.7±1.3	0.05 ± 0.03	0.58	0.04 ± 0.08	0.00 ± 0.01	0.19 ± 0.13	0.06 ± 0.02	0.01 ± 0.02	0.00 ± 0.00	0.25 ± 0.14	0.22
WN6–8	2⋄	1060 ± 280	15.5 ± 11.4	0.35 ± 0.06	0.23 ± 0.07	0.09 ± 0.07	0.10 ± 0.03	0.04 ± 0.03	0.10 ± 0.00	0.03 ± 0.02	0.03 ± 0.02	0.23 ± 0.02	0.06 ± 0.01
All WN2–8	140⋄	1570 ± 610	9.7 ± 10.1	0.42 ± 0.37	0.48 ± 0.27	0.14 ± 0.11	0.26 ± 0.25	0.34 ± 0.33	0.10 ± 0.04	0.04 ± 0.03	0.08 ± 0.17	0.30 ± 0.23	0.12 ± 0.14
All WN9–11	12	300 ± 120	2.8 ± 4.1	0.10 ± 0.07	···	0.01 ± 0.01	3.1±5.9	2.3 ± 1.9	0.02 ± 0.02	0.00 ± 0.01	4.4 ± 10.3	20 ± 52	0.01 ± 0.00
All Of/WN	8	1250 ± 380	3.5 ± 1.3	0.05 ± 0.02	0.21 ± 0.10	0.24 ± 0.07	0.18 ± 0.23	0.26 ± 0.19	0.03 ± 0.02	0.03 ± 0.03	0.00 ± 0.00	0.59 ± 0.12	0.11 ± 0.05

Table 3. WN/C line luminosity calibrations for Milky Way and LMC stars, including He II λ4686 FWHM in km s^{-1}. The complex at λ4100 involves N III λλ4097,4103, Si IV λλ4088,4116, and He II λ4100 + H δ, while the feature at λ4603–51 involves N V λλ4603,20, N III λλ4634,41, and C III λλ4647,51.

Category	N	HeII 4686 FWHM	$L_{\rm HeII\,4686}$ 10^{35} erg s^{-1}	10^{-3} $L_{\rm Bol}$	$\frac{L_{\rm NIV\,3478-85}}{L_{\rm HeII\,4686}}$	$\frac{L_{\rm NIV\,4058}}{L_{\rm HeII\,4686}}$	$\frac{L_{4100}}{L_{\rm HeII\,4686}}$	$\frac{L_{4603,51}}{L_{\rm HeII\,4686}}$	$\frac{L_{\rm HeII\,5412}}{L_{\rm HeII\,4686}}$	$\frac{L_{\rm CIII\,5696}}{L_{\rm HeII\,4686}}$	$\frac{L_{\rm CIV\,5801,12}}{L_{\rm HeII\,4686}}$	$\frac{L_{\rm H\alpha}}{L_{\rm HeII\,4686}}$	$\frac{L_{\rm NIV\,7103,29}}{L_{\rm HeII\,4686}}$
Three Milky Way ($Z_\odot$) and two LMC (0.4 $Z_\odot$)													
WNE/C	5	2240 ± 430	7.5 ± 2.9	0.47 ± 0.30	0.64 ± 0.04	0.14 ± 0.12	0.26 ± 0.19	1.54 ± 1.82	0.18 ± 0.08	0.01 ± 0.02	1.38 ± 1.39	0.21 ± 0.08	0.19 ± 0.20
Milky Way ($Z_\odot$)													
WNL/C	4	1270 ± 130	7.3 ± 3.1	0.36 ± 0.17	0.82	0.91	0.87	1.75 ± 1.32	0.15 ± 0.05	0.06 ± 0.08	0.53 ± 0.17	0.18 ± 0.09	0.20
All WN/C	9	1810 ± 600	7.4 ± 2.8	0.43 ± 0.25	0.68 ± 0.10	0.27 ± 0.33	0.36 ± 0.30	1.63 ± 1.53	0.17 ± 0.06	0.03 ± 0.06	1.26 ± 1.21	0.20 ± 0.08	0.19 ± 0.14

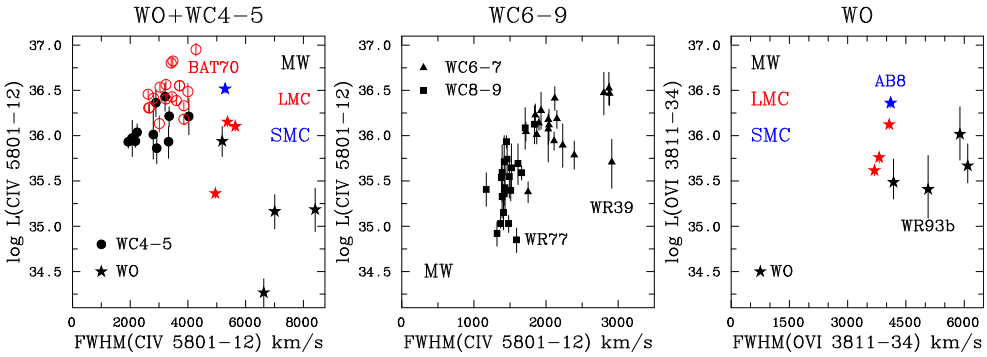

Figure 4. Left-hand panel: C IV λ5808 line luminosities of WO (stars) and WC4–5 (circles) stars in the Milky Way, LMC, and SMC versus FWHM (km s^{-1}). Central panel: C IV λλ5801,12 line luminosities of Milky Way WC6–7 (black triangles) and WC8–9 (black squares) versus FWHM (km s^{-1}). Right-hand panel: O VI λλ3811,34 line luminosities of WO stars in the Milky Way, LMC, and SMC versus FWHM (km s^{-1}).

occasionally been reported in WR galaxies (e.g. Schaerer et al. 1999), with O IV λλ3403,13 also prominent in WC and WO stars.

3.3 Calibrations

In order to analyse distant, unresolved star-forming regions host to WR stars we shall primarily focus on the broad blue bump, involving a blend of N V λλ4603,20, N III λλ4634,41, and C III λλ4647,51. He II λ4686, and the yellow C IV λλ5801,12 bump. Although C IV λλ5801,12 is present in the majority of WN stars, it is typically much weaker than the blue bump (Fig. 3), with upper limits measured for many weak-lined WN stars. WN/C stars possess high C IV λλ5801,12 line luminosities, with an average value of log ($L_{\rm CIV\,5801,\,12}$/erg s^{-1}) = 36.0, although one would not expect prominent C IV emission from such stars in an unresolved stellar population since they only comprise a small fraction of the overall WR population. The strength of the bumps are tightly correlated for WC stars, confirming results from Smith et al. (1990b), with $L_{\rm Blue}/L_{\rm CIV\,5801,\,12}$ = 1.9 ± 0.6 for WC4–5 stars, 3.0 ± 0.4 for WC6–7 stars, and 4.8 ± 1.2 for WC8–9 stars. In contrast, these features are poorly correlated in WO stars.

Previous optical calibrations have been obtained by Smith et al. (1990a) for LMC WC stars, Schaerer & Vacca (1998) for Milky Way and LMC WR stars, and Crowther & Hadfield (2006) for Magellanic Cloud WN stars, which have also been adapted for other metallicities (López-Sánchez & Esteban 2010). In Table 6, we compare our current results with previous calibrations. Overall we reinforce the decrease in line luminosity of early-type WN stars with metallicity established by Crowther & Hadfield (2006) by the addition of Milky Way stars, and higher line luminosities of WC4–5 stars in the LMC with respect to the Milky Way. However, we find no clear metallicity dependence for late-type WN or WO stars (hindered by low number of SMC stars), with significantly improved statistics for Galactic WC6–7 and WC8–9 stars with respect to Smith et al. (1990b) and Schaerer & Vacca (1998). The lack of strong metallicity dependence

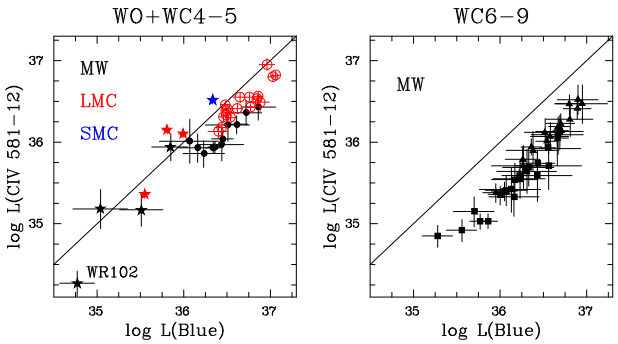

Figure 5. Blue (C III λλ4647,51, C IV λ4658, and He II λ4686) versus yellow (C IV λλ5801,12) line luminosities of WC and WO stars in the Milky Way (black), LMC (red), and SMC (blue). Symbols as in Fig. 4. The solid line indicates equal blue and yellow luminosities.

for some subtypes is somewhat surprising, recalling Sander et al. (2020). However, the lower (luminosity) threshold to the formation of WR stars increases at lower metallicity (Shenar et al. 2020, their figure 3) so reduced wind strengths at low metallicity are countered by a shift to higher stellar luminosities on average.

Schaerer & Vacca (1998) have previously adopted $L_{\rm HeII\,4686}$ = 6.5 × 10^{35} erg s^{-1} and 2.5 × 10^{35} erg s^{-1} for (LMC) Of/WN and Of stars, respectively. We obtain $L_{\rm HeII\,4686}$ = (3.5 ± 1.3) × 10^{35} erg s^{-1} for Of/WN stars (Table 2), whereas $L_{\rm HeII\,4686} \leq 10^{35}$ erg s^{-1} is more typical of Magellanic Cloud Of supergiants. For example, $L_{\rm HeII\,4686}$ = 8 × 10^{34} erg s^{-1} for the O2 supergiant Mk 42 (BAT99-105) based on our MUSE data set and the interstellar extinction from Hainich et al. (2014). Definitive results await analysis of VLT/Xshooter flux calibrated spectroscopy of Magellanic Cloud OB stars obtained via the X-Shooting ULLYSES initiative (Vink et al., in preparation).

Beyond the usual blue and yellow WR bumps, we include line luminosities for prominent violet features, O IV λλ3403,13, N IV

Table 4. WC line luminosity calibrations for Milky Way and LMC stars, including C IV λλ5801,12 FWHM in km s^{-1}. The blue feature involves C III λλ4647,51, C IV λ4658, and He II λ4686, while the feature at λ6559,81 involves He II λ6560 and C II λλ6559,81.

Category	N	CIV 5801,12 FWHM	$L_{\rm CIV5801.12}$ 10^{35} erg s^{-1}	10^{-3} $L_{\rm Bol}$	$\frac{L_{\rm OIV\ 3403,13}}{L_{\rm CIV\ 5801,\ 12}}$	$\frac{L_{\rm Blue}}{L_{\rm CIV\ 5801,\ 12}}$	$\frac{L_{\rm CIII\ 5696}}{L_{\rm CIV\ 5801,\ 12}}$	$\frac{L_{\rm HeI\ 5876}}{L_{\rm CIV\ 5801,\ 12}}$	$\frac{L_{6559,81}}{L_{\rm CIV\ 5801,\ 12}}$	$\frac{L_{\rm CIII\ 6727,73}}{L_{\rm CIV\ 5801,\ 12}}$	$\frac{L_{\rm CIV\ 7725}}{L_{\rm CIV\ 5801,\ 12}}$	$\frac{L_{\rm CIII\ 9701,19}}{L_{\rm CIV\ 5801,\ 12}}$
Milky Way ($Z_\odot$)												
WC4–5	11	2790 ± 630	13.3±6.6	1.43 ± 0.44	0.55 ± 0.25	2.30 ± 0.51	0.02 ± 0.03	0.08 ± 0.01	0.07 ± 0.03	0.11 ± 0.03	0.09 ± 0.02	0.13 ± 0.07
WC6–7	18	2180 ± 400	15.3±9.0	0.89 ± 0.43	0.77 ± 0.24	3.11 ± 0.50	0.35 ± 0.24	0.16 ± 0.11	0.16 ± 0.06	0.17 ± 0.03	0.11 ± 0.01	0.28 ± 0.06
WC8–9	21	1480 ± 140	4.1±3.5	0.41 ± 0.20	1.32 ± 0.92	4.82 ± 1.19	3.21 ± 1.01	0.56 ± 0.26	1.12 ± 0.48	0.60 ± 0.27	0.11 ± 0.04	0.99 ± 0.28
LMC (0.4 $Z_\odot$)												
WC4–5	18	3370 ± 490	34.1 ± 19.8	2.19 ± 0.27	0.55 ± 0.26	1.63 ± 0.40	0.02 ± 0.03	0.02 ± 0.03	0.05 ± 0.01	0.06 ± 0.02	0.06 ± 0.01	0.06 ± 0.03
All WC	68	2380 ± 850	16.4 ± 16.2	0.98 ± 0.68	0.79 ± 0.53	3.12 ± 1.48	1.09 ± 1.54	0.26 ± 0.28	0.45 ± 0.56	0.26 ± 0.27	0.08 ± 0.03	0.34 ± 0.38

Table 5. WO line luminosity calibrations for Milky Way, LMC, and SMC stars, including C IV λλ5808 FWHM in km s^{-1}. The blue feature involves C IV λ4658 and He II λ4686.

Subtype	N	CIV 5801,12 FWHM	$L_{\rm CIV\ 5801,\ 12}$ 10^{35} erg s^{-1}	10^{-3} $L_{\rm Bol}$	$\frac{L_{\rm OIV\ 3403,13}}{L_{\rm CIV\ 5801,\ 12}}$	$\frac{L_{\rm OVI\ 3811,34}}{L_{\rm CIV\ 5801,\ 12}}$	$\frac{L_{\rm Blue}}{L_{\rm CIV\ 5801,\ 12}}$	$\frac{L_{\rm OV\ 5572,607}}{L_{\rm CIV\ 5801,\ 12}}$	$\frac{L_{\rm HeII\ 6560}}{L_{\rm CIV\ 5801,\ 12}}$	$\frac{L_{\rm CIV\ 7725}}{L_{\rm CIV\ 5801,\ 12}}$
Milky Way ($Z_\odot$)										
WO2–4	4	6800 ± 1300	3.0 ± 3.9	0.25 ± 0.20	1.8 ± 0.8	8.6 ± 12.2	1.7 ± 1.2	0.5 ± 0.6	0.22 ± 0.16	0.45 ± 0.47
LMC (0.4 $Z_\odot$)										
WO3–4	3	5300 ± 300	9.7 ± 6.5	1.18 ± 0.84	1.9 ± 2.0	2.2 ± 3.1	0.9 ± 0.6	0.16 ± 0.14	0.08 ± 0.08	0.14 ± 0.13
SMC (0.2 $Z_\odot$)										
WO4	1	5300	32.9	0.59	1.0	0.7	0.65	0.16	0.04	0.19
All WO	8	6100 ± 1200	9 ± 11	0.70 ± 0.69	1.7 ± 1.3	5.2 ± 8.5	1.3 ± 1.0	0.3 ± 0.4	0.13 ± 0.13	0.30 ± 0.36

λλ3478,85, and O IV λλ3811,34, noting that the latter is challenging to measure in WC stars due to line blends with other features, primarily the λ3700 complex of O III–IV and C IV on its blue wing. Although these are weaker than the standard WR diagnostics, they may be detectable in suitable host galaxies, especially those below the Balmer jump. The absence of O VI λλ3811,34 from WO stars in integrated populations is not wholly unexpected in view of the low line luminosity with respect to C IV λλ5801,12 in WC4–5 stars (Table 6) and location adjacent to stellar absorption lines (e.g. H9 at λ3835; Sidoli, Smith & Crowther 2006). Longward of the visible range, N IV λλ7103,29 and He II λ10124 are the strongest emission lines in WNE and WNE/C stars, with $L_{\rm HeII\ 10124}/L_{\rm HeII\ 4686} = 0.13 \pm 0.02$ while He I λ10830 is the strongest feature in WN6–8 (WN9–11) stars with $L_{\rm HeI\ 10830}/L_{\rm HeII\ 4686} = 0.7 \pm 0.6$ (0.9 ± 0.8). C IV λ7725 and C III λλ9701,19 are the strongest red features in WC4–5 stars, albeit an order of magnitude weaker than C IV λλ5801,12, the former also prominent in WO stars. C III λλ9701,19 is prominent in late WC subtypes, with $L_{\rm CIII\ 9701\text{-}19}/L_{\rm CIV\ 5801\text{-}12} = 0.3 \pm 0.1$ and 1.0 ± 0.3 for WC6–7 and WC8–9 stars, respectively. C II λλ7231,37 is prominent in WC8–9 subtypes, with He I λ10830 also very strong with $L_{\rm HeI\ 10830}/L_{\rm CIV\ 5801\text{-}12} = 0.5 \pm 0.4$.

In the vacuum UV, attention has usually been focused on He II λ1640 (n = 3–2) since it is prominent in most WR subtypes, and its line luminosity exceeds He II λ4686 (n = 4-3) by an order of magnitude (Crowther & Hadfield 2006, their fig. 3). Schaerer & Vacca (1998) obtained $L_{1640}/L_{4686} = 7.8$ for Milky Way and LMC WN stars, supported by the comprehensive study of Leitherer et al. (2019), while Crowther & Hadfield (2006) obtained $L_{4686}/L_{1640} = 10$ from LMC WN stars and theoretical models. Based on our adopted extinctions and λ1640 line fluxes measured from LORES *IUE*/SWP spectroscopy we obtain $L_{4686}/L_{1640} = 12 \pm 4$ for Galactic, and Magellanic Cloud WN and WN/C stars. N IV λλ1238,42 is also strong in early WN stars, although this line and C IV λλ1548,51 are present in early O stars (Crowther et al. 2016). N IV] λ1486 and N IV λ1718 are also prominent in early WN stars, with emission line luminosities 20–30 per cent of He II λ1640. In late WN stars, He II λ1640 is less dominant, in part due to the forest of iron lines in its vicinity (Crowther et al. 1995a, their fig. 2), especially Fe IV λ1633, with C IV λλ1548,51, Si IV λλ1393,1402, and N IV λ1718 P Cygni profiles also prominent. In the near-UV, the strongest WN emission line is He II λ3203 (n = 5–3) with $L_{3203}/L_{4686} = 0.7 \pm 0.2$ for Milky Way and Magellanic Cloud WN stars.

The strongest far-UV feature in WC4–7 stars is C IV λλ1548,51 (Crowther & Hadfield 2006, their fig. 5), with He II λ1640, C III] λ1909, O IV λλ1338,43, O IV] λλ1397,1407, and C III λ1247 also prominent. For LMC and Milky Way WC4–5 stars, $L_{\rm CIV\ 1548,\ 51}/L_{\rm CIV\ 5801,\ 12} = 8 \pm 2$ and $L_{\rm HeII\ 1640}/L_{\rm CIV\ 5801,\ 12} = 5 \pm 2$, somewhat higher than the ratios of 6.0 and 2.6 obtained by Crowther & Hadfield (2006) for single LMC WC4–5 stars indicating the sensitivity to extinction determinations and sample size. C IV λλ1548,51 remains the strongest far-UV line in WC6–7 stars, with C III] λ1909 the strongest far-UV emission line in WC8–9 stars. We obtain $L_{\rm CIII]\ 1909}/L_{\rm CIV\ 5801,\ 12} = 4 \pm 2$, 7 ± 4, and 23 ± 8 for Galactic WC4–5, WC6–7, and WC8–9 stars, respectively. In the near-UV, the strongest WC emission line is C III λ2297, followed by C IV λ2530 in early WC stars. $L_{\rm CIII\ 2297}/L_{\rm CIV\ 5801,\ 12} = 5 \pm 2$, 6 ± 4, and 23 ± 10 for Galactic WC4–5, WC6–7, and WC8–9 stars, respectively.

3.4 Line-to-bolometric luminosity ratio

In view of the range of properties of WR stars within different environments, one can compare the ratios of line to bolometric luminosities for WR stars whose physical properties have been determined from spectroscopic analysis. Results are primarily drawn from Hamann et al. (2019) and Sander et al. (2019) for Galactic WR stars, Hainich et al. (2014), Shenar et al. (2019), Aadland et al. (2022a), and Aadland et al. (2022b) for LMC WR stars, and Hainich et al. (2015) and Shenar et al. (2016) for SMC WR stars. These are supplemented by studies of WO stars (Tramper et al. 2015) and very massive WNh and Of/WN stars in dense clusters (Crowther et al. 2010; Brands et al. 2022).

In Fig. 6, we compare bolometric luminosities with the ratio of He II λ4686 line to bolometric luminosity for Milky Way, LMC, and

Table 6. Comparison to literature calibrations of violet (O IV λλ3403,11, N IV λλ3478,85, and O VI λλ3811,34), blue (He II λ4686, C III λλ4647,51, and N III–V λλ4603,41), yellow (C III λ5696 and C IV λλ5801,12), and red (N IV λλ7103,29 and C III λλ9701,19) WR line luminosities. Wind features associated with strong nebular emission (H α, β) are excluded.

$L_{\rm OIV\ 3403,\ 13}$ 10^{35} erg s^{-1}	N	$L_{\rm NIV\ 3478,\ 85}$ 10^{35} erg s^{-1}	N	$L_{\rm OVI\ 3811,\ 34}$ 10^{35} erg s^{-1}	N	$L_{\rm Blue}$ 10^{35} erg s^{-1}	N	$L_{\rm CIII\ 5696}$ 10^{35} erg s^{-1}	N	$L_{\rm CIV\ 5801,\ 12}$ 10^{35} erg s^{-1}	N	$L_{\rm NIV\ 7103,\ 29}$ 10^{35} erg s^{-1}	N	$L_{\rm CIII\ 9701,\ 19}$ 10^{35} erg s^{-1}	N	Sample	Ref
								WN3–7s									
···		9.5 ± 5.7	10	···		26 ± 12	12	···		1.3 ± 0.7	11	3.3 ± 1.7	8	···		MW	3
···		5.4 ± 3.7	15	···		12±7	18	···		0.5 ± 0.4	18	0.7 ± 0.5	16	···		LMC	3
								WN2–5w									
···		···		···		5 ± 3	26	···		0.4 ± 0.1	5	···		···		MW + LMC[b]	1
···		3.8 ± 2.7	13	0.1[a]	1	6 ± 5	23	···		0.3 ± 0.3	19	1.0 ± 0.7	11	···		MW	3
···		3.0 ± 1.8	12	···		4 ± 3	24	···		0.2 ± 0.2	23	0.3 ± 0.3	20	···		LMC	3
···		2.1	1	···		2 ± 1	9	···		0.01 ± 0.02	7	0.3	1	···		SMC	3
								WN6–8									
···		···		···		21 ± 18	19	···		1.0 ± 0.6	10	···		···		MW + LMC[c]	1
···		2.2 ± 1.4	12	···		13±8	25	···		0.2 ± 0.1	24	0.9 ± 1.0	6	···		MW	3
···		2.8 ± 2.6	8	···		26 ± 25	15	···		0.6 ± 0.6	13	1.3 ± 0.1	4	···		LMC	3
···		3.2 ± 1.6	2	···		10±3	2	···		0.6 ± 0.6	2	0.9 ± 0.6	2	···		SMC	3
								WN9–11									
···		···		···		7 ± 10	12	···		0.01 ± 0.01	4	0.03 ± 0.02	2	···		MW + LMC	3
								WN5–7h + Of/WN									
···		3.1 ± 3.8	8	···		14±7	9	···		0.2 ± 0.1	6	···		···		MW	3
···		11.8 ± 7.1	8	···		20 ± 18	14	···		0.7 ± 0.7	13	1.9 ± 1.6	8	···		LMC	3
								WN/C									
···		4.9 ± 1.6	4	···		18 ± 10	9	0.1 ± 0.2	3	9.5 ± 7.8	9	1.4 ± 0.8	3	···		MW + LMC	3
								WC4–5									
···		···		···		50	5	···		32	5	···		···		LMC	2
···		···		···		49 ± 17	32	0.7 ± 0.4	20	28 ± 12	20	···		···		MW + LMC	1
6±4	8	···		0.9 ± 0.5	9	31 ± 18	11	0.2 ± 0.3	11	13±7	11	···		1.5 ± 1.1	4	MW	3
16±7	7	···		2.0 ± 1.6	15	53 ± 29	17	0.5 ± 0.8	17	34 ± 20	17	···		2.1 ± 1.2	7	LMC	3
								WC6–7									
···		···		···		37 ± 11	25	5.5 ± 4.1	25	12 ± 5	7	···		···		MW	1
9±5	12	···		1.1 ± 0.7	15	45 ± 23	18	5.6 ± 6.9	18	15 ± 9	18	···		4.7 ± 2.1	7	MW	3
								WC8–9									
···		···		···		10±2	24	7.3 ± 1.4	25	2.9 ± 2.5	5	···		···		MW	1
9±7	7	···		···		19 ± 14	21	11 ± 8	21	4.1 ± 3.5	21	···		2.7 ± 1.6	5	MW	3
								WO									
19 ± 14	3	···		15 ± 9	3	8 ± 3	3	···		11±2	3	···		···		MC + IC1613	1
9 ± 10	8	···		8 ± 7	8	7 ± 7	8	···		9 ± 11	8	···		···		MW + MC	3

Notes. 1: Schaerer & Vacca (1998); 2: Smith et al. (1990a); 3: This work.
[a]O VI is observed in WR46 (Crowther et al. 1995b) with $L_{\rm OVI\ 3811,\ 34}/L_{\rm HeII\ 4686} = 0.17$.
[b]WN2–4 weak and strong lined.
[c]WN6–9 weak and strong lined.

SMC WN, WN/C, and Of/WN stars, with average values provided in Table 2. This reinforces the difference in line strength of He II λ4686 between strong- and weak-lined WN stars in view of their comparable bolometric luminosities, since $\log L_{\rm HeII\ 4686}/L_{\rm Bol} = -3.0^{+0.1}_{-0.3}$ for strong-lined WN stars, whereas $\log L_{\rm HeII\ 4686}/L_{\rm Bol} = -3.6^{+0.2}_{-0.9}$ for weak-lined WN2–5 stars, with the lowest ratio for LMC 170–2 (Neugent et al. 2017). The metallicity dependence for weak-lined early-type WN stars is also apparent (compare Milky Way and SMC stars). The situation is less clear for weak-lined WN6–8 stars, since Milky Way and Magellanic Cloud stars are broadly similar in their ratios of line to bolometric luminosities, $\log L_{\rm HeII\ 4686}/L_{\rm Bol} = -3.4^{+0.2}_{-0.2}$. WN9–11 stars universally exhibit very low ratios (e.g. WR31a; Smith et al. 1994) with $\log L_{\rm HeII\ 4686}/L_{\rm Bol} = -4.0^{+0.3}_{-0.5}$. Fig. 6 also reveals a low line-to-bolometric luminosity ratio for BAT99-111 (R136b) which has previously been classified O4 If/WN8 (Crowther et al. 2016) although WN8 is preferred on the basis of its H β morphology from MUSE/NFM observations (Crowther & Walborn 2011; Castro et al. 2021). Bolometric luminosities of WN5–7h stars are high in both galaxies, with $\log L/L_{\rm Bol} = 6.3 \pm 0.2$ and 6.5 ± 0.2 for the Milky Way and LMC respectively, with typical ratios of $\log L_{\rm HeII\ 4686}/L_{\rm Bol} = -3.7^{+0.2}_{-0.3}$, and ratios of line to bolometric luminosities for Of/WN stars somewhat lower still, $\log L_{\rm HeII\ 4686}/L_{\rm Bol} = -4.3^{+0.2}_{-0.2}$.

Fig. 7 compares bolometric luminosities with the ratio of C IV λλ5801,12 line to bolometric luminosity for Milky Way and Magellanic Cloud WC and WO stars, and bolometric luminosities with the ratio of O VI λ3811,34 line to bolometric luminosity for WO stars. Galactic WC4–5 stars reveal significantly higher ratios than WC8–9 stars, with intermediate ratios for most WC6–7 stars (WR39 is an notable outlier), and very high ratios for LMC WC4–5 stars. WO stars show a broad range of C IV λλ5801,12 line ratios, some in common with WC4–5 stars (BAT99-123 and LH 41-1042) with others revealing far lower ratios (e.g. WR102 in Milky Way, LMC195–1 in LMC). Line ratios of O VI λλ3811,34 to bolometric luminosity for WO stars suggest a weak metallicity dependence, with higher ratios for Milky Way stars than those in Magellanic Clouds.

3.5 Templates

In addition to calibrations, we have produced WR emission line templates for each environment, although this is hindered by the variation in spectral coverage of individual data sets (Table 1), so stars with limited spectral coverage are generally excluded. We have degraded composite spectra to a resolution of 10 Å, and produced

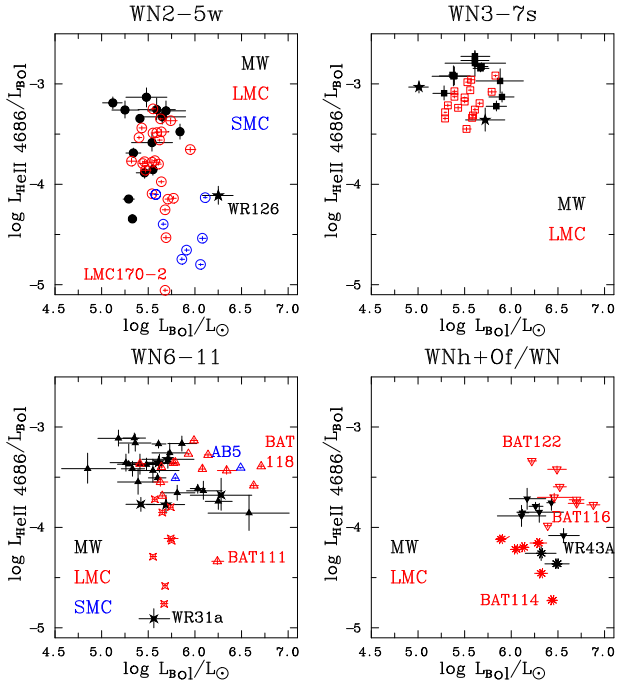

Figure 6. Bolometric luminosity versus ratio of He II λ4686 line to bolometric luminosity for weak-lined WN2–5 (top-left panel), strong lined WN3–7 (top-right panel), weak lined WN6–11 (bottom-left panel), and WNh + Of/WN (bottom-right panel) stars in the Milky Way (black), LMC (red), and SMC (blue). Symbols as in Fig. 2.

continuum-subtracted templates based on single WR stars and all (single and binary) WR stars, since the latter are often contaminated by (Balmer) absorption lines from companion OB stars. Templates incorporate velocity corrections of 284 and 162 km s^{-1} for the LMC and SMC, respectively (Tully, Courtois & Sorce 2016). Templates generally correct for atmospheric telluric effects, but no adjustment for interstellar atomic features (Ca II H&K and Na I D) lines or diffuse interstellar bands (e.g. λ4430) is made.

Fig. B1 presents templates for Galactic, LMC, and SMC early-type WN stars from single and combined (single and binary) samples, separated into weak and strong lined subsets. Aside from He II λ4686, the strongest feature in metal-rich early-type WN stars is N IV λλ3478,85 followed by He II λ5412, λ6560 and the complex involving N IV λ4058, He II λ4100, Si IV λλ4088,4116, and N III λλ4097,4103. C IV λλ5801,12 is present, though relatively weak, in Galactic and LMC early-type WN stars.

Fig. B2 presents templates for Galactic, LMC, and SMC late-type WN stars, separated into classical (WN6–8) and main-sequence H-rich (WN5–7h) subsets. The scarcity of LMC main-sequence WN stars required the use of 30 Doradus MUSE data sets (Castro et al. 2018) which exclude the spectral region shortward of λ4600. He II λ4686 aside, the strongest stellar features in WN6–8 stars include N IV λλ3478,85, the λ4100 complex, N III λλ4634,41, and H α, H β, and He I λ5876 in the Milky Way. The change in N III λλ4634,41/He II λ4686 ratio from high to low metallicity is apparent. H-rich main sequence WN5–7h stars resemble WN6–8 stars aside from the relative strength of N IV λ4058, weakness of N III λ4634,41, and He I lines and higher λ4686 FWHM (Fig. 2).

Fig. B3 presents templates for Of/WN and WN9–11 stars in the Milky Way and LMC. Of/WN stars reveal weak, narrow He II λ4686 emission, and N IV λ4058 and H α, with the upper Balmer series in absorption. WN9–11 stars also exhibit weak, narrow weak He II λ4686 emission, with either the N III λλ4634,41 triplet or N II λλ4601,43 multiplet prominent and strong Balmer and He I emission lines. Guseva, Izotov & Thuan (2000) have highlighted N III λλ4512,48 and Si III λλ4554,76 from late WN stars in WR galaxies. Such features are present in late WN stars, albeit with the λ4100 complex and N III λλ4634,41/N II λλ4601,43 more prominent.

Fig. B4 presents templates for Galactic and LMC WN/C stars, separated into early- and late-type categories. Early subtypes are dominated by C IV λλ5801,12 and the blend of C III λλ4647,51 and He II λ4686, while the latter dominates late WN/C subtypes. C III λ5696 is present, albeit weakly in late WN/C templates. We combine Galactic and LMC WN/C stars to construct templates, noting that some exhibit strong C III λλ4647,51 (e.g. WR26 and WR126), while this feature is absent in others (e.g. WR58, BAT99-36, and BAT99-88) such that spectroscopy of C IV λλ5801,12 is essential in discriminating between WN and WN/C stars.

Fig. B5 presents templates for Galactic WC4–5, WC6–7, and WC8–9 stars from single and combined (single and binary) samples. C III λλ4647,51 (and He II λ4686) dominates the blue WR bump for all subtypes, while the transition from C IV λλ5801,12 to C III λ5696 in the yellow from early to late subtypes is apparent, with O IV λλ3403,13 prominent in WC4–7 stars. At late subtypes, C II λλ6559,81, λλ7231,7 are particularly strong in the red. The forest of blue features in WC8–9 stars primarily involves C II–III (Crowther et al. 2006b).

The upper panel of Fig. B6 presents templates of LMC WC4–5 emission lines. Aside from C III λ4647–51 + He II λ4686 and C IV λλ5801,12, O IV λλ3403,13 is also prominent, in common with Milky Way counterparts. The lower panel presents templates of our combined WO sample, incorporating Milky Way, LMC, and SMC stars, highlighting the defining O VI λλ3811,34 feature, together with prominent O IV λλ3403,13, C IV λ4658 + He II λ4686, and C IV λλ5801,12. Comparing WO and LMC WC4–5 stars, the average O VI λλ3811,34 line luminosity is factor of ∼4 stronger in the former group, while C III λλ4647,51 + C IV λ4658 + He II λ4686 and C IV λ5801,12 are 4–8 times weaker (Table 6).

3.6 Cumulative WR line luminosities

Armed with line luminosities for a large subset of (optically detected) WR stars in the Milky Way and Magellanic Clouds, we can also consider their cumulative blue and yellow line luminosities, and contributions from different WR populations. Our sample includes all known WR stars in the SMC, 66 per cent of the WR population in the LMC (Neugent et al. 2018),[6] though only ∼7 per cent of the estimated Milky Way population (N = 1900 ± 250; Rosslowe & Crowther 2015). 18 per cent of the LMC population are carbon or oxygen sequence WR stars, whereas these comprise 21 per cent of our sample. In the Milky Way carbon and oxygen sequence stars represent 42 per cent of the known population, in close agreement with our data set.[7]

Table 7 summarizes cumulative blue and yellow WR line luminosities from our current data set in the Milky Way, LMC, and SMC. As expected, WC and WO stars dominate the integrated C IV λλ5801,12

[6]The global WR population of the LMC is 153, following Neugent et al. (2018) after including the WN8 star BAT99-111 (R136b), excluding two Of stars (Mk 42 and LH 99-3), and noting that their catalogue entry 125 is Mk 37 rather than Mk 30 (also listed as entry 129).

[7]275 WC or WO stars from a total of 667 stars according to v1.25 of the Galactic WR catalogue https://pacrowther.staff.shef.ac.uk/WRcat.

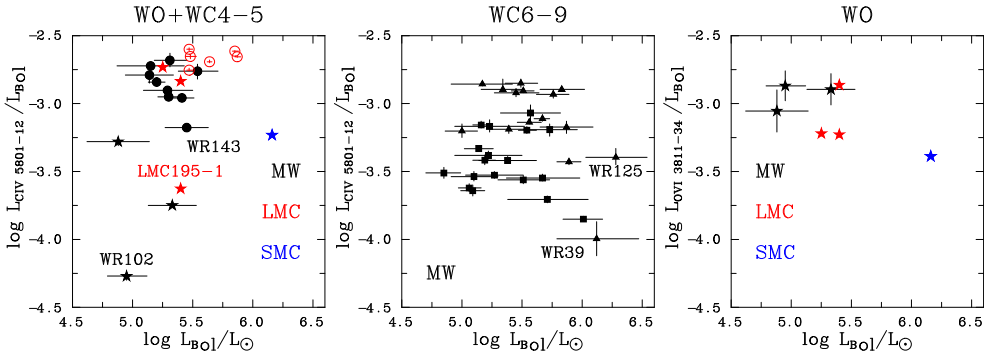

Figure 7. Left-hand panel: Bolometric luminosity versus ratio of C IV λλ5801,12 line to bolometric luminosity for WO and WC4–5 stars. Central panel: Bolometric luminosity versus ratio of C IV λλ5801,12 line to bolometric luminosity for WC6–7 (triangles) and WC8–9 (squares) stars. Right-hand panel: Bolometric luminosity versus ratio of O VI λλ3811,34 line to bolometric luminosity for WO stars. Symbols as in Fig. 4.

line luminosity in all environments, but also contribute significantly to the blue feature: 58 per cent in the Galaxy, 49 per cent in the LMC, and 23 per cent in the SMC, for the samples included. AB5 (HD 5980) alone contributes half of the integrated blue WR bump of the SMC. If we utilize our LMC calibrations for the remainder of the known WR population, we estimate total blue and yellow line luminosities of 2.6×10^{38} erg s^{-1} (51 per cent from WN, Of/WN, and WN/C stars, 49 per cent from WC and WO stars) and 8.8×10^{37} erg s^{-1} (8 per cent from WN, Of/WN, and WN/C stars, 92 per cent from WC and WO stars), respectively. The fractional contributions from WN and WC stars are not affected because the overwhelming majority of omitted nitrogen-sequence stars possess weak lines (weak-lined WNE, WN10–11, and Of/WN and LMC 170–2 type).

Accounting for line luminosities of all known WR stars in the Milky Way, we obtain cumulative blue and C IV λλ5801,12 line luminosities of 1.2×10^{39} and 2.7×10^{38} erg s^{-1}, respectively. If these are representative of the total (∼1900) the blue (3.6×10^{39} erg s^{-1}) and yellow (7.7×10^{38} erg s^{-1}) sum is an order of magnitude higher than the LMC. This is reasonable, given their relative star-formation rates of 1.9 $M_\odot$ yr^{-1} (Chomiuk & Povich 2011) and 0.25 $M_\odot$ yr^{-1} (Kennicutt et al. 2008), respectively, and environmental differences in WR line luminosities.

The fractional contributions to the cumulative WR bumps are further highlighted in Fig. 8, which provides the integrated line spectrum of 102 Galactic stars (upper panel), 80 LMC stars (middle panel), and 10 SMC stars (lower panel). The integrated Milky Way template highlights that strong-lined and late-type WN stars are the primary contributors to He II λ4686, WC4–7, and WC8–9 and late-type WN subtypes dominating the λ4650 feature, and WC4–7 and WC8–9 subtypes dominating C IV λλ5801,12 and C III λ5696, respectively. Similar results are obtained for the LMC, aside from the lack of WC6–9 stars, while the cumulative SMC bumps are dominated by late-type WN stars (primarily AB5) and the WO star AB8. Fig. 8 is reminiscent of WR bumps observed in star-forming galaxies (Vacca & Conti 1992; Schaerer et al. 1999; Brinchmann et al. 2008; Senchyna et al. 2021), but serves as a caution to approximating WR populations by restricted WC and WN flavours, which additional (violet or red) WR diagnostics would help discriminate.

4. APPLICATIONS

We now undertake analysis of two WR galaxies with our revised line luminosity calibration, selected at low and high metallicities. Historically, two methods have been employed to quantify the number of WR stars from optical emission line bumps, Gaussian fits to emission lines calibrated with reference line luminosities or template fitting. The former approach is more straightforward, but discards line profile information and may result in unphysical solutions through independent solutions to blue and red bumps. The latter approach incorporates line profile information but may involve templates ill-suited to the host galaxy metallicity. Here, we apply both approaches to our selected WR galaxies.

4.1 NGC 3049 (Mrk 710)

Our high metallicity target, NGC 3049 is a barred spiral at a distance of 19.3 Mpc (Tully et al. 2013) which was identified as a WR galaxy by Kunth & Schild (1986). WR populations of NGC 3049 have been studied using ESO 2.2m/EFOSC2 (Schaerer et al. 1999) and *HST*/STIS (González Delgado et al. 2002), and exhibits broad emission at N III λλ4634,41/C III λλ4647,51, He II λ4686, C III λ5696, and C IV λλ5801,12. NGC 3049 is unusual in the λ4634,41 feature being comparable in strength with He II λ4686 (see Schmutz & Vacca 1999). Fig. 9 (left-hand panel) presents de-reddened, velocity-corrected WR bumps including Gaussian fits to stellar and nebular emission lines. Table 8 provides a summary of nebular and stellar line luminosities in NGC 3049, remeasured from EFOSC observations, which provides a spectral coverage of 4370–6550 Å at a resolving power of R ∼750 (Schaerer et al. 1999). The spectroscopic L(H β) corresponds to an ionizing output of $Q_H = 1.6 \times 10^{52}$ photon s^{-1}, comparable with 30 Doradus in the LMC, although the integrated output is likely to be considerably higher.

Strong-line calibrations indicate NGC 3049 is supersolar ($\log$ O/H + 12 ≥ 8.9; Guseva et al. 2000) so we apply Galactic calibrations to estimate its WR populations. The C IV λλ5801,12 to C III λ5696 ratio suggests a dominant WC6–7 subclass, requiring 380 WC stars. The contribution from WC6–7 stars to the He II λ4686 is considered to be negligible, so we adopt a WN6–8 population of ∼1300.

Fig. 9 (right-hand panel) presents continuum-subtracted line luminosities of blue and yellow WR bumps in NGC 3049, together with emission line templates for Milky Way WN (red) and WC (blue) stars, and their sum (pink). For the yellow bump we prefer a reduced WC4–7 content of 260 stars in order to reproduce the C IV λλ5801,12 and C III λ5696 emission line, whose FWHM is well reproduced (we adopt a similar mix of WC4–5 and WC6–7 stars to the Milky Way sample, i.e. 1:3). For the blue bump, N V λ4603–20 is not apparent, but we adhere to a mix of WNEw:WN3–7s:WN6–8 stars corresponding to the Milky Way (1:1:3), requiring ∼750 stars to reproduce the He II λ4686 line, accounting for the contribution of

Table 7. Cumulative blue and yellow line luminosities for our sample of WR systems in the Milky Way, LMC and SMC, with completeness fractions of ∼7 per cent, 66 per cent, and 100 per cent (Rosslowe & Crowther 2015; Neugent, Massey & Morrell 2018). Systems involved WN + WN binaries (WR43A, BAT99-116, BAT199-118, and AB5) are reflected in + statistics. WC and WO stars dominate the C IV λλ5801,12 feature, and also contribute the majority of the integrated blue feature in Milky Way and LMC. AB5 (HD 5980) alone contributes half of the integrated blue WR bump of the SMC. We estimate total LMC (Milky Way) blue and yellow line luminosities of 2.6×10^{38} erg s^{-1} (3.6×10^{39} erg s^{-1}) and 8.8×10^{37} erg s^{-1} (7.7×10^{38} erg s^{-1}), respectively.

Galaxy	Milky Way			LMC			SMC			Milky Way			LMC			SMC		
	N	ΣL erg s^{-1}	per cent	N	ΣL erg s^{-1}	per cent	N	ΣL erg s^{-1}	per cent	N	ΣL erg s^{-1}	per cent	N	ΣL erg s^{-1}	per cent	N	ΣL erg s^{-1}	per cent
Subtype	—— Blue bump (N III-V λλ4603,41, C III λλ4647,51, and He II λ4686) ——									—— Yellow bump (C IV λλ5801,12) ——								
WN3–7*s*	12	3.1×10^{37}	12	18	2.1×10^{37}	10	.	...	...	12	1.4×10^{36}	2	18	0.9×10^{36}	1	.	...	...
WN2–5w	22	1.4×10^{37}	5	24	0.9×10^{37}	5	9	1.7×10^{36}	18	19	0.6×10^{36}	1	22	0.3×10^{36}	0	7	0.1×10^{35}	0
WN6–11	29	3.9×10^{37}	15	21+1	4.2×10^{37}	21	2+1	5.6×10^{36}	59	25	0.5×10^{36}	1	15+1	1.0×10^{36}	1	2+1	2.2×10^{35}	6
WN5-7h[a]	9+1	1.3×10^{37}	5	14+1	3.0×10^{37}	15	.	...	...	6+1	0.1×10^{36}	0	13+1	1.0×10^{36}	1	.	...	...
WN/C	7	1.4×10^{37}	5	2	0.2×10^{37}	1	.	...	...	7	5.9×10^{36}	10	2	2.7×10^{36}	4	.	...	...
WC4–5	11	3.4×10^{37}	13	18	9.7×10^{37}	48	.	...	...	11	14.7×10^{36}	24	17	61.5×10^{36}	88	.	...	...
WC6–9	39	12.0×10^{37}	45	.	...	...	.	...	...	39	36.1×10^{36}	59	.	...	...	.	...	...
WO	4	0.1×10^{37}	0	3	0.2×10^{37}	1	1	2.2×10^{36}	23	4	1.2×10^{36}	2	3	2.9×10^{36}	4	1	32.9×10^{35}	93
Total	133+1	26.7×10^{37}	100	100+2	20.4×10^{37}	100	12+1	9.5×10^{36}	100	123+1	60.4×10^{36}	100	91+2	70.2×10^{36}	100	10+1	35.2×10^{35}	100

Note.
[a]Includes Of/WN stars.

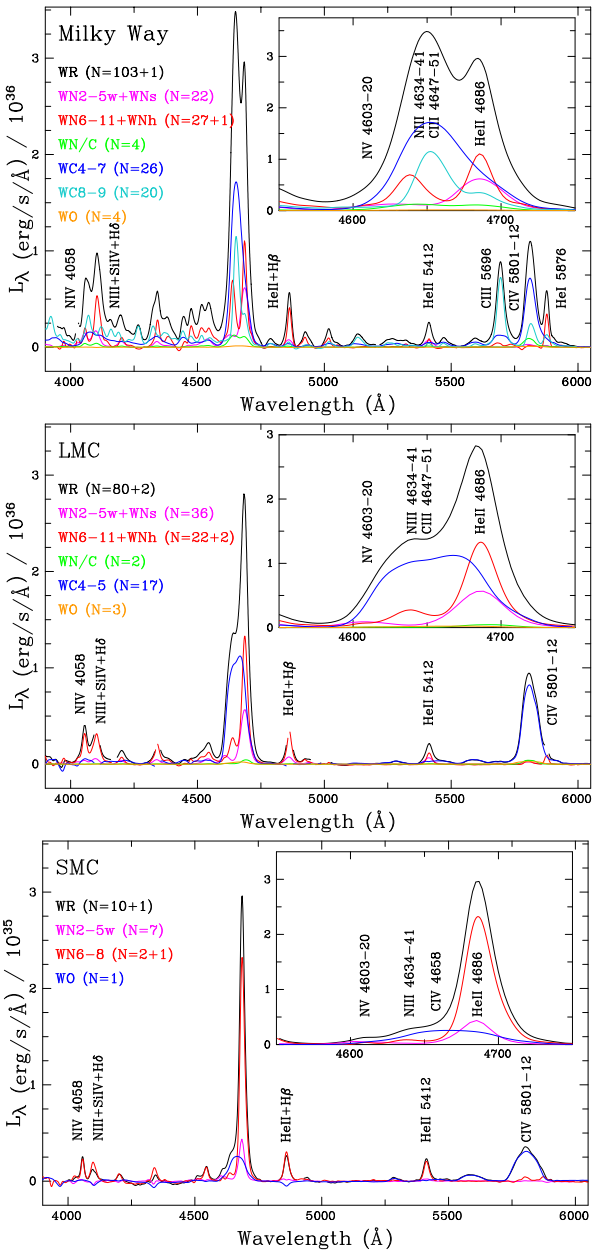

Figure 8. Top panel: Cumulative λλ3950–6050 emission line spectrum of 103+1 Milky Way WR stars (black) together, and inset for the blue WR bump, including contributions from WN2–5w + WN3–7s (N = 22), WN6–11 + WNh (N = 27+1), WN/C (N = 4), WC4–7 (N = 26), WC8–9 (N = 20), and WO (N = 4) stars, indicating the primary contributors to the blue and yellow WR bumps. The global Milky Way WR line luminosity is estimated to be a factor of ∼13 times higher than presented here based on the known WR subtype distribution. Middle panel: As above, for 80+2 LMC WR stars (black), highlighting contributions from WN2–5w + WN3–7s (N = 36), WNL + WNh (N = 22+2), WN/C (N = 2), WC4–5 (N = 17), and WO (N = 3) stars. The global LMC WR line luminosity is estimated to be ∼25 per cent higher than presented here, accounting for incompleteness. Bottom panel: As above for 10+1 SMC WR stars (black), highlighting contributions from WNE (N = 7), WNL (N = 2 + 1), and WO (N = 1) stars. The global SMC WR line luminosity is estimated to be a few per cent higher than presented here, owing to the omission of two WN2–5w stars.

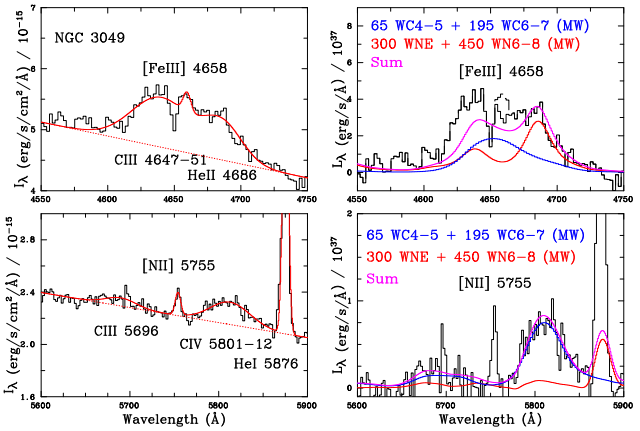

Figure 9. Left-hand panels: De-reddened, velocity corrected, blue and yellow WR bumps in NGC 3049 from Schaerer et al. (1999), including Gaussian fits (red) to broad (C III λλ4647,51, He II λ4686, C III λ5696, and C IV λλ5801,12) and nebular ([Fe III] λ4658, [N II] λ5755, and He I λ5876) lines, with the continuum indicated as dotted lines. Also, ∼1300 WN6-8 and ∼380 WC6–7 stars are estimated from Galactic calibrations, adopting a distance of 19.3 Mpc. Right-hand panels: Continuum subtracted luminosities of blue and yellow WR bumps in NGC 3049 (black, nebular [Fe III] component indicated in dashed lines) and composite template fits adopting 750 Milky Way WN stars (red, distributed 1:1:3 between WN2–5w:WN3-7s:WN6–8 stars as observed in the Milky Way), 260 Milky Way WC4–7 stars (blue, distributed between WC4–5 and WC6–7 stars as observed in the Milky Way), and their sum (pink). Nebular [N II] λ5755 and He I λ5876 are not reproduced by the stellar WR templates. The poor match to the λ4640–4650 blend may arise from the use of solar metallicity WN6—8 stars (NGC 3049 is considered to be supersolar).

Table 8. Line luminosities of selected nebular and stellar emission lines in NGC 3049 (Schaerer, Contini & Kunth 1999) based on $c(\mathrm{H}\,\beta) = 0.22$, a distance of 19.3 Mpc and Milky Way calibrations from this study. Results in parenthesis are from Galactic template fits.

Line	FWHM	F_λ	I_λ	L_λ	N (WR)
				10^{37}	
	km s^{-1}	10^{-15} erg s^{-1} cm^{-2}		erg s^{-1}	
C III λλ4647,51	3300 ± 800	26.2 ± 5.8	45.2 ± 9.9	202 ± 44	
[Fe III] λ4658	···	1.3 ± 1.1	2.3 ± 2.1	10 ± 9	
He II λ4686	2200 ± 600	13.0 ± 4.9	21.9 ± 8.2	98 ± 37	1300 WN6–8
H β	···	98.9 ± 1.2	169±2	755 ± 9	(750 WN2–8)
[O III] λ4959	···	11.8 ± 0.5	19.8 ± 0.9	88 ± 4	
[O III] λ5007	···	36.2 ± 0.7	60.6 ± 1.1	271 ± 5	
C III λ5696	2100 ± 500	1.9 ± 0.5	2.7 ± 0.7	12 ± 3	
[N II] λ5755	···	0.9 ± 0.2	1.3 ± 0.3	6 ± 1	
C IV λλ5801,12	2700 ± 300	6.5 ± 0.7	9.6 ± 1.0	43 ± 5	380 WC6–7
He I λ5876	···	11.9 ± 0.2	18.1 ± 0.3	81 ± 1	(260 WC4–7)

WC stars to this region. The combination of N III λλ4634,41 (from WN6–8 stars) and C III λλ4647,51 (from WC4–7 stars) reproduces the majority of the blue bump reasonably well. The residual mismatch likely arises from stronger N III λλ4634,41 emission than our Galactic templates since N III/He II is observed to scale with metallicity (recall Fig. 3) and NGC 3049 is likely supersolar. C III λ5696 is reasonably well matched, and includes modest contributions from WN6–8 stars via N IV λ5737/Si III λ5740 and the N II λ5680 multiplet (note also nebular [N II] λ5755). The use of empirical templates requires fewer WR stars, owing to the contribution of WN stars to the yellow bump, and WC stars to the blue bump, which are usually not accounted for, and suggests a WN to WC ratio of ∼3.

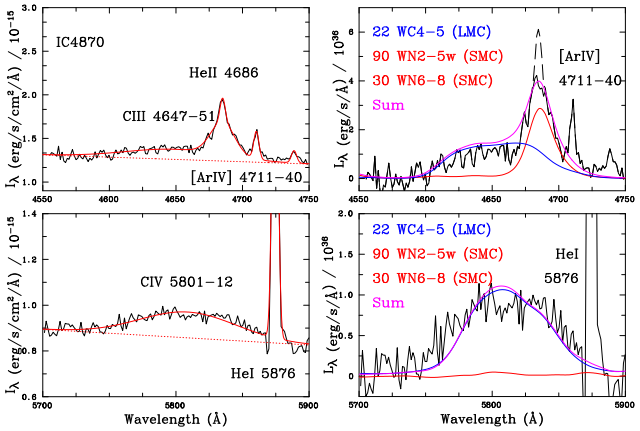

Figure 10. Left-hand panels: De-reddened, velocity corrected, blue and yellow WR bumps in IC 4870 (black), including Gaussian fits (red) to broad (C III λλ4647,51, He II λ4686, and C IV λλ5801,12) and nebular ([Ar IV] λλ4711,40 and He I λ5876) lines, with the continuum indicated as dotted lines. Also, ∼47 SMC WN6–8 and 26 LMC WC4–5 stars are estimated from calibrations, adopting a distance of 8.5 Mpc. Right-hand panels: Continuum subtracted luminosities of blue and yellow WR bumps in IC 4870 (black, nebular He II λ4686 component indicated in dashed lines) and template fits adopting 120 SMC WN stars (red), 22 LMC WC4–5 stars (blue), and their sum (pink).

4.2 IC 4870 (ESO 105–IG 011)

Our low metallicity target IC 4870 is a nearby barred irregular galaxy at a distance of 8.5 Mpc (Tully et al. 2013) which was identified as a WR galaxy by Joguet et al. (2001). Spectroscopy reported by Joguet et al. (2001) focuses on the blue WR bump, so we have utilized archival New Technology Telescope (NTT)/EMMI spectroscopy from 1999 May (PA = 0 and $T_{\rm exp}$ = 600 s). Grism #5 and a 1-arcsec slit provided a spectral coverage of 3975–6685 Å at a resolving power of R = 1000–1300. The brightest knot reveals a strong emission line spectrum, including broad C III λ4647–51/C IV λ4658, He II λ4686, and C IV λλ5801,12, and extended nebular emission. After standard reduction techniques, including flux calibration, we obtained $c(\mathrm{H}\,\beta) = 0.19$ from the observed flux ratio $F(\mathrm{H}\,\alpha)/F(\mathrm{H}\,\beta) = 3.37$. Since the spectral coverage does not extend to [O II] λ3727, we are unable to determine a direct oxygen abundance, but strong line calibrations (N2 and O3N2; Pettini & Pagel 2004) indicate IC 4870 is metal-poor (log O/H + 12 ∼7.9, or 1/6 $Z_\odot$), which is supported by the high electron temperature of $T_{\rm e}$ = 13.7 kK obtained from [O III] λ4363/5007.

Fig. 10 (left-hand panel) presents de-reddened, velocity corrected WR bumps including Gaussian fits to stellar and nebular emission lines. Fluxes of selected nebular and stellar emission lines in IC 4870 measured from fits are presented in Table 9. He II λ4686 comprises both stellar (86 per cent) and nebular (14 per cent) components, with a nebular He II λ4686)/H β intensity ratio of 2 per cent. Indeed, Joguet et al. (2001) attribute 16 per cent of the He II λ4686 to nebular origin in their higher resolution 1.5m ESO Boller & Chivens spectroscopy of IC 4870 (R = 2100 at λ4686). The spectroscopic H α luminosity corresponds to an ionizing output of $Q_{\rm H} = 1.5 \times 10^{51}$ photon s^{-1}, typical of nearby giant H II regions (e.g. NGC 595 in M33), although the integrated ionizing output is likely to be significantly larger. The yellow C IV λλ5801,12 feature is very broad, exceeding the average value of LMC WC4–5 stars (Table 4).

Ideally one would apply SMC-metallicity calibrations to IC 4870, but since WC stars are not observed in the SMC we revert to LMC

Table 9. Line luminosities of selected emission lines in IC 4870 from Gaussian fits, based on $c(\mathrm{H}\,\beta) = 0.18$, a distance of 8.5 Mpc and calibrations from this study. Separate nebular (n) and broad (b) entries are provided for He II λ4686. Calibrations are from SMC (WN6–8) and LMC (WC4–5) samples, while results shown in parenthesis arise from LMC (WC) and SMC (WN) template fits.

Line	FWHM	F_λ	I_λ	L_λ	N (WR)
				10^{37}	
	km s^{-1}	10^{-15} erg s^{-1} cm^{-2}		erg s^{-1}	
H δ	···	13.5 ± 0.2	22.5 ± 0.4	19.5 ± 0.3	
H γ	···	23.2 ± 0.2	37.8 ± 0.4	32.8 ± 0.3	
[O III] λ4363	···	4.5 ± 0.2	7.2 ± 0.3	6.3 ± 0.3	
He I λ4471	···	2.1 ± 0.2	3.4 ± 0.3	2.9 ± 0.3	
C III λλ4647,51	5700 ± 2200	7.0 ± 3.2	10.8 ± 4.8	9.0 ± 4.0	
He II λ4686 (b)	1300 ± 300	5.4 ± 0.9	8.5 ± 1.4	7.3 ± 1.2	47 WN6–8
He II λ4686 (n)	···	0.8 ± 0.4	1.3 ± 0.6	1.1 ± 0.5	(120 WN2–8)
[Ar IV] λ4711	···	1.0 ± 0.3	1.5 ± 0.5	1.4 ± 0.3	
H β	···	51.0 ± 0.3	78.6 ± 0.5	68.1 ± 0.4	
[O III] λ4959	···	114±2	174±4	151±3	
[O III] λ5007	···	339±3	515±4	446±3	
C IV λλ5801,12	4300 ± 200	7.3 ± 0.5	10.3 ± 0.7	8.9 ± 0.6	26 WC4–5
He I λ5876	···	6.6 ± 0.1	9.3 ± 0.1	8.1 ± 0.1	(22 WC4–5)
H α	···	172±1	231±2	200±2	
[N II] λ6584	···	2.7 ± 1.1	3.6 ± 1.5	3.1 ± 1.3	

calibrations, allowing us to estimate a population of ∼26 WC4–5 stars in IC 4870 from the yellow bump. FWHM(He II λ4686) is intermediate between early and late WN subtypes (Table 2), so we apply a SMC WN6–8 (WN2–5w) calibration to estimate a population of 47 (440) stars, excluding the nebular component. At SMC metallicity, N III λλ4634,41/He II λ4686 ∼ 0.04, so accounting for this modest contribution to the broad C III λλ4647,51 feature, we can estimate the number of WC4–5 stars from this diagnostic, again based on LMC calibrations. We estimate a slightly lower population of 19 WC4–5 stars from the blue bump.

Fig. 10 (right-hand panel) presents continuum-subtracted line luminosities of blue and yellow WR bumps in IC 4870, together with emission line templates for WN and WC stars, and their sums (pink). For the yellow WR bump, 22 (LMC) WC4–5 stars provide a satisfactory match to the broad C IV λλ5801,12 emission line, with negligible contribution from WN stars. For the blue bump, a mix of early and late WN stars is more plausible than a purely early or late WN population, recalling the WNE:WNL ratio is 2 (LMC) to 3 (SMC) in local metal-poor galaxies. Consequently we adopt a ratio of 3:1 for the WN2–5w:WN6–8 population in IC 4870, with both comprising SMC templates. We require a total of 120 WN stars to reproduce the non-nebular He II λ4686 feature, accounting for the contribution of 22 WC4–5 stars, which also provide a satisfactory fit to C III λλ4647,51 + C IV λ4658.

Although there is a no direct evidence supporting the presence of WN2–5w stars in IC 4870, they are capable of producing the observed nebular He II λ4686 emission, in contrast to WN6–8 or WC4–5 stars (Crowther & Hadfield 2006). The measured nebular He II λ4686 luminosity (Table 9) corresponds to an ionizing budget of $\mathrm{Q(He^+)} = 1.3 \times 10^{49}$ photon s^{-1}, an order of magnitude higher than individual nebular He III λ4686 producing H II regions in Local Group galaxies (Garnett et al. 1991). Adopting $\mathrm{Q(He^+)}$ ionizing photons of SMC WN2–5w stars from Hainich et al. (2015), only ∼10 stars are required to produce sufficient ionizing photons in order to reproduce the observed nebular emission. Consequently only ∼10 per cent of the inferred population would need to be located within H II regions to match observations. This more realistic WN population inferred for this metal-poor galaxy produces a WN:WC ratio of ∼5.5:1, which is more plausible than 2:1 if solely WN6–8 and WC4–5 calibrations are adopted (Table 9). The modest He II λ4686 line luminosity of metal-poor WN2–5w stars would severely hinder their direct detection, so the spectroscopic absence of WR bumps in nebular λ4686 emitting galaxies does not necessarily exclude them from being responsible for the observed nebular emission (Schaerer 1996; Shirazi & Brinchmann 2012), although several alternative candidates exist (Götberg et al. 2019; Schaerer, Fragos & Izotov 2019; Oskinova & Schaerer 2022).

5. OUTLOOK AND CONCLUSIONS

We report calibrations of line luminosities of optical emission lines of Galactic WR stars, greatly expanding on previous studies owing to the availability of *Gaia* DR3 parallaxes, and provide revised line luminosities for Magellanic Cloud counterparts, updated from previous calibrations (Smith et al. 1990a; Schaerer & Vacca 1998; Crowther & Hadfield 2006).

Overall we confirm previous results for a reduction in He II λ4686 line luminosity for early-type WN stars at low metallicity, providing separate calibrations for strong- and weak-lined stars. Sander et al. (2020) have investigated wind driving of WR stars, and establish a dependence on metallicity (Fe-group elements) and Eddington parameter Γ_e ($\propto L/M$) so strong-lined stars likely differ from weak-lined stars in their wind properties owing to their higher luminosity-to-mass ratios.

The situation is less clear for late-type WN stars since average line luminosities of LMC stars are higher than Galactic counterparts and one of the two late WN stars in the SMC is the complex multiple system HD 5980, whose primary potentially dominates the line emission (Hillier et al. 2019). This does not necessarily argue against a metallicity dependence of wind strengths since the lower (luminosity) threshold to the formation of WR stars increases at lower metallicity (Shenar et al. 2020), so reduced wind strengths at low metallicity are countered by a shift to higher stellar luminosities on average. We find very massive main-sequence stars in the Milky Way and LMC possess similar He II λ4686 line luminosities to classical late WN stars, albeit with broader lines and weaker N III λλ4634,41 and He I λ5876 lines. C IV λλ5801,12 is an order of magnitude weaker than the blue bump in early WN stars, and is weaker still in late subtypes, though has comparable strength in WN/C subtypes.

LMC WC4–5 stars possess higher C IV λλ5801,12 line luminosities than Galactic counterparts, while we provide the first calibration of line luminosities for WC6–7 and WC8–9 stars based on large samples. C III λλ4647,51 + He II λ4686 is strong for all WC subtypes, with C III λ5696 is the dominant emission line in the yellow region for WC9 stars. The blue WC bump is well correlated with C IVλλ5801,12 in all subtypes. We also provide line luminosities of O VI λλ3811,34 in WO stars, and other prominent lines (O IV λλ3403,13, C IV λ4658 + He II λ4686, and C IV λλ5801,12). We also utilize spectroscopic studies to quantify the line-to-bolometric luminosity ratios for each spectral type, which ranges from $L_{\mathrm{HeII\,4686}}/L_{\mathrm{Bol}} = 3 \times 10^{-5}$ for SMC WNEw stars, to $L_{\mathrm{CIV\,5801,\,12}}/L_{\mathrm{Bol}} = 2 \times 10^{-3}$ for LMC WC4–5 stars.

Figs 2 and 4 emphasize the diversity in line luminosities within our various WR categories, so average properties should be used with caution. For example, Littlefield et al. (2012) have presented optical line fluxes of WR142–1 (WN6w) from Hobby Eberly Telescope observations. Applying their derived extinction ($A_V = 8.1^{+0.6}_{-0.7}$ mag) and the average He II λ4686 line luminosity of Galactic WN6–8 stars (Table 2) implies a distance of $2.1^{+0.6}_{-0.9}$ kpc, whereas the *Gaia* DR3 distance to WR142-1 is 1.58 ± 0.05 kpc.

Flux-calibrated spectroscopy also permits us to produce templates for single and composite (single and binary) subtypes at each metallicity. We construct cumulative emission line luminosities for the Milky Way (∼7 per cent completeness), LMC (66 per cent complete), and SMC (100 per cent complete), with global blue WR line luminosities of $\approx 3.7 \times 10^{39}$, 2.6×10^{38}, and 9.5×10^{37} erg s^{-1}, respectively. We also apply our templates to representative metal-poor (IC 4870) and metal-rich (NGC 3049) galaxies that exhibit strong WR bumps at optical wavelengths. Reasonable consistency is achieved, although templates are preferred since they exploit line profile information and incorporate contributions from WN stars to the yellow WR bump, and contributions from WC stars to the blue WR bump.

The prospect for additional empirical WR line luminosities is promising at high metallicity, thanks to large numbers of detections in M31 (Neugent & Massey 2019), while the situation is less satisfactory at low metallicity. IC10 has a relatively high star-formation rate, although it suffers from high foreground extinction and its metallicity is close to that of the LMC (Tehrani, Crowther & Archer 2017). Other nearby dwarf galaxies suffer from very low star-formation rates (Crowther 2019, their fig.11), so only a handful of WR stars are known in NGC 6822 and IC 1613 (Armandroff & Massey 1991). Consequently there is little alternative to the use of theoretical spectra below SMC metallicity, providing these are carefully calibrated against empirical results.

ACKNOWLEDGEMENTS

PAC and JMB are supported by the Science and Technology Facilities Council research grant ST/V000853/1 (PI V. Dhillon). Thanks to Bill Vacca for sharing his IRTF/SpeX data set, Frank Tramper for providing his VLT/Xshooter spectra of WO stars, Nidia Morrell for sharing her Magellan/MagE spectrum of LMC 170–2, Paco Najarro for providing his VLT/Xshooter spectrum of VFTS 682, Gloria Koenigsberger for providing her *HST*/STIS spectra of HD 5980, and Daniel Schaerer for providing his flux calibrated ESO 2.2m EFOSC2 spectrum of NGC 3049.

This research has made extensive use of NASA's Astrophysics Data System Bibliographic Services, and the SIMBAD data base, operated at CDS, Strasbourg, France, and the European Space Agency (ESA) *Gaia* archive whose website is https://archives.esac.esa.int/gaia and the ESO Science Archive Facility (IC 4870 was observed under programme 59.A-9004). The INES System has been developed by the ESA *IUE* Project at VILSPA. Data and access software are distributed and maintained by INTA through the INES Principal Centre at LAEFF. The Starlink software (Currie et al. 2014) is currently supported by the East Asian Observatory.

For the purpose of open access, the author has applied a Creative Commons Attribution (CC BY) license to any Author Accepted Manuscript version arising.

DATA AVAILABILITY

Template continuum subtracted emission line spectra of Milky Way and Magellanic Cloud WR stars will be publicly available in a Zenodo collection upon publication (ascii format, wavelength units of Å, monochromatic luminosity units of erg s^{-1} Å^{-1}) at 10.5281/zenodo.7573775, separately for single and single + binary WN2–5w, WN3–7s, WN6–8, WN9–11, WN5–7h + Of/WN (main sequence), WN/C, WC4–5, WC6–7, WC8–9, and WO stars.

REFERENCES

Aadland E., Massey P., Hillier D. J., Morrell N. I., Neugent K. F., Eldridge J. J., 2022b, ApJ, 931, 157
Aadland E., Massey P., Hillier D. J., Morrell N., 2022a, ApJ, 924, 44
Allen D. A., Wright A. E., Goss W. M., 1976, MNRAS, 177, 91
Armandroff T. E., Massey P., 1991, AJ, 102, 927
Bagnulo S., Jehin E., Ledoux C., Cabanac R., Melo C., Gilmozzi R., ESO Paranal Science Operations Team, 2003, The Messenger, 114, 10
Bailer-Jones C. A. L., Rybizki J., Fouesneau M., Demleitner M., Andrae R., 2021, AJ, 161, 147
Bartzakos P., Moffat A. F. J., Niemela V. S., 2001, MNRAS, 324, 18
Bestenlehner J. M., 2020, MNRAS, 493, 3938
Bohannan B., Crowther P. A., 1999, ApJ, 511, 374
Borisov S. et al., 2022, preprint (arXiv:2211.09130)
Brands S. A. et al., 2022, A&A, 663, A36
Brinchmann J., Kunth D., Durret F., 2008, A&A, 485, 657
Callingham J. R., Crowther P. A., Williams P. M., Tuthill P. G., Han Y., Pope B. J. S., Marcote B., 2020, MNRAS, 495, 3323
Castro N., Crowther P. A., Evans C. J., Mackey J., Castro-Rodriguez N., Vink J. S., Melnick J., Selman F., 2018, A&A, 614, A147
Castro N. et al., 2021, The Messenger, 182, 50
Chomiuk L., Povich M. S., 2011, AJ, 142, 197
Conti P. S., Massey P., 1989, ApJ, 337, 251
Crowther P. A., 1997, MNRAS, 290, L59
Crowther P. A., 2007, ARA&A, 45, 177
Crowther P. A., 2019, Galaxies, 7, 88
Crowther P. A., Hadfield L. J., 2006, A&A, 449, 711
Crowther P. A., Smith L. J., 1997, A&A, 320, 500
Crowther P. A., Walborn N. R., 2011, MNRAS, 416, 1311
Crowther P. A., Smith L. J., Hillier D. J., Schmutz W., 1995a, A&A, 293, 427
Crowther P. A., Smith L. J., Hillier D. J., 1995b, A&A, 302, 457
Crowther P. A., Smith L. J., Willis A. J., 1995c, A&A, 304, 269
Crowther P. A., Dessart L., Hillier D. J., Abbott J. B., Fullerton A. W., 2002, A&A, 392, 653
Crowther P. A., Hadfield L. J., Clark J. S., Negueruela I., Vacca W. D., 2006a, MNRAS, 372, 1407
Crowther P. A., Morris P. W., Smith J. D., 2006b, ApJ, 636, 1033
Crowther P. A., Schnurr O., Hirschi R., Yusof N., Parker R. J., Goodwin S. P., Kassim H. A., 2010, MNRAS, 408, 731
Crowther P. A. et al., 2016, MNRAS, 458, 624
Currie M. J., Berry D. S., Jenness T., Gibb A. G., Bell G. S., Draper P. W., 2014, in Manset N., Forshay P., eds, ASP Conf. Ser. Vol. 485, Astronomical Data Analysis Software and Systems XXIII. Astron. Soc. Pac., San Francisco. p. 391
de Koter A., Heap S. R., Hubeny I., 1997, ApJ, 477, 792
Drew J. E., Monguió M., Wright N. J., 2021, MNRAS, 508, 4952
Eldridge J. J., Stanway E. R., Xiao L., McClelland L. A. S., Taylor G., Ng M., Greis S. M. L., Bray J. C., 2017, Publ. Astron. Soc. Aust., 34, e058
Fitzpatrick E. L., Massa D., Gordon K. D., Bohlin R., Clayton G. C., 2019, ApJ, 886, 108
Flagey N., Noriega-Crespo A., Petric A., Geballe T. R., 2014, AJ, 148, 34
Foellmi C., Moffat A. F. J., Guerrero M. A., 2003, MNRAS, 338, 360
Gaia Collaboration, 2021, A&A, 649, A1
Garnett D. R., Kennicutt R. C. J., Chu Y.-H., Skillman E. D., 1991, ApJ, 373, 458
Gómez-González V. M. A., Mayya Y. D., Toalá J. A., Arthur S. J., Zaragoza-Cardiel J., Guerrero M. A., 2021, MNRAS, 500, 2076
González Delgado R. M., Leitherer C., Stasińska G., Heckman T. M., 2002, ApJ, 580, 824
Gordon K. D., Clayton G. C., Misselt K. A., Landolt A. U., Wolff M. J., 2003, ApJ, 594, 279
Götberg Y., de Mink S. E., Groh J. H., Leitherer C., Norman C., 2019, A&A, 629, A134
Graczyk D. et al., 2014, ApJ, 780, 59
Gräfener G., Koesterke L., Hamann W. R., 2002, A&A, 387, 244
Guseva N. G., Izotov Y. I., Thuan T. X., 2000, ApJ, 531, 776

Gvaramadze V. V. et al., 2009, MNRAS, 400, 524
Hainich R. et al., 2014, A&A, 565, A27
Hainich R., Pasemann D., Todt H., Shenar T., Sander A., Hamann W. R., 2015, A&A, 581, A21
Hamann W. R., Gräfener G., Liermann A., 2006, A&A, 457, 1015
Hamann W. R. et al., 2019, A&A, 625, A57
Hillier D. J., Koenigsberger G., Nazé Y., Morrell N., Barbá R. H., Gamen R., 2019, MNRAS, 486, 725
Howarth I. D., 1983, MNRAS, 203, 301
Howarth I. D., Murray J., Mills D., Berry D. S., 2004, Starlink User Note, 50
Joguet B., Kunth D., Melnick J., Terlevich R., Terlevich E., 2001, A&A, 380, 19
Kennicutt R. C. J., Lee J. C., Funes J. G. J. S., Sakai S., Akiyama S., 2008, ApJS, 178, 247
Koenigsberger G., Morrell N., Hillier D. J., Gamen R., Schneider F. R. N., González-Jiménez N., Langer N., Barbá R., 2014, AJ, 148, 62
Koenigsberger G., Morrell N., Hillier D. J., Schmutz W., Gamen R., Arias J. I., Barbá R., Ferrero G., 2022, Rev. Mex. Astron. Astrofis., 58, 403
Koesterke L., Hamann W. R., Schmutz W., Wessolowski U., 1991, A&A, 248, 166
Kunth D., Sargent W. L. W., 1981, A&A, 101, L5
Kunth D., Schild H., 1986, A&A, 169, 71
Leitherer C., Lee J. C., Faisst A., 2019, AJ, 158, 192
Lindegren L. et al., 2018, A&A, 616, A2
Lindegren L. et al., 2021, A&A, 649, A4
Littlefield C., Garnavich P., Marion G. H. H., Vinkó J., McClelland C., Rettig T., Wheeler J. C., 2012, AJ, 143, 136
López-Sánchez Á. R., Esteban C., 2010, A&A, 516, A104
Luehrs S., 1997, PASP, 109, 504
Maíz Apellániz J., 2022, A&A, 657, A130
Maíz Apellániz J. et al., 2014, A&A, 564, A63
Massey P., 1984, ApJ, 281, 789
Massey P., Hunter D. A., 1998, ApJ, 493, 180
Miralles-Caballero D. et al., 2016, A&A, 592, A105
Monreal-Ibero A., Walsh J. R., Iglesias-Páramo J., Sandin C., Relaño M., Pérez-Montero E., Vílchez J., 2017, A&A, 603, A130
Neugent K., Massey P., 2019, Galaxies, 7, 74
Neugent K. F., Massey P., Hillier D. J., Morrell N., 2017, ApJ, 841, 20
Neugent K. F., Massey P., Morrell N., 2018, ApJ, 863, 181
Nugis T., Lamers H. J. G. L. M., 2000, A&A, 360, 227
Oskinova L. M., Schaerer D., 2022, A&A, 661, A67
Pettini M., Pagel B. E. J., 2004, MNRAS, 348, L59
Pietrzyński G. et al., 2019, Nature, 567, 200
Rate G., Crowther P. A., 2020, MNRAS, 493, 1512
Rosslowe C. K., Crowther P. A., 2015, MNRAS, 447, 2322
Sander A., Hamann W. R., Todt H., 2012, A&A, 540, A144
Sander A. A. C., Hamann W. R., Todt H., Hainich R., Shenar T., Ramachandran V., Oskinova L. M., 2019, A&A, 621, A92
Sander A. A. C., Vink J. S., Hamann W. R., 2020, MNRAS, 491, 4406
Schaerer D., 1996, ApJ, 467, L17
Schaerer D., Vacca W. D., 1998, ApJ, 497, 618
Schaerer D., Contini T., Kunth D., 1999, A&A, 341, 399
Schaerer D., Fragos T., Izotov Y. I., 2019, A&A, 622, L10
Schmutz W., 1997, A&A, 321, 268
Schmutz W., Vacca W. D., 1999, New Astron., 4, 197
Schnurr O., Casoli J., Chené A. N., Moffat A. F. J., St-Louis N., 2008, MNRAS, 389, L38
Seaton M. J., 1979, MNRAS, 187, 73
Senchyna P., Stark D. P., Charlot S., Chevallard J., Bruzual G., Vidal-García A., 2021, MNRAS, 503, 6112
Shenar T. et al., 2016, A&A, 591, A22
Shenar T. et al., 2019, A&A, 627, A151
Shenar T., Gilkis A., Vink J. S., Sana H., Sander A. A. C., 2020, A&A, 634, A79
Shenar T. et al., 2021, A&A, 650, A147
Shirazi M., Brinchmann J., 2012, MNRAS, 421, 1043
Sidoli F., Smith L. J., Crowther P. A., 2006, MNRAS, 370, 799
Smith L. F., Shara M. M., Moffat A. F. J., 1990a, ApJ, 348, 471
Smith L. F., Shara M. M., Moffat A. F. J., 1990b, ApJ, 358, 229
Smith L. J., Crowther P. A., Prinja R. K., 1994, A&A, 281, 833
Smith L. F., Shara M. M., Moffat A. F. J., 1996, MNRAS, 281, 163
Smith L. J., Norris R. P. F., Crowther P. A., 2002, MNRAS, 337, 1309
Tehrani K., Crowther P. A., Archer I., 2017, MNRAS, 472, 4618
Tehrani K. A., Crowther P. A., Bestenlehner J. M., Littlefair S. P., Pollock A. M. T., Parker R. J., Schnurr O., 2019, MNRAS, 484, 2692
Torres-Dodgen A. V., Massey P., 1988, AJ, 96, 1076
Tramper F. et al., 2015, A&A, 581, A110
Tully R. B. et al., 2013, AJ, 146, 86
Tully R. B., Courtois H. M., Sorce J. G., 2016, AJ, 152, 50
Vacca W. D., Conti P. S., 1992, ApJ, 401, 543
Walborn N. R., Drissen L., Parker J. W., Saha A., MacKenty J. W., White R. L., 1999, AJ, 118, 1684

APPENDIX A: LINE LUMINOSITIES OF GALACTIC AND MAGELLANIC CLOUD WR STARS

Line luminosities of individual Galactic and Magellanic Cloud WN + Of/WN, WN/WC, WC, and WO stars are provided in Tables A1–A4, sorted by catalogue number (WR for Milky Way, BAT for LMC, and AB for SMC). Optical data sets refer to Table 1, Galactic distances are from *Gaia* DR3 parallaxes (Gaia Collaboration 2021), using zero-point corrections from Lindegren et al. (2021) updated by Maíz Apellániz (2022), and the Bayesian methods set out in Rate & Crowther (2020), while Magellanic Cloud distances are from Pietrzyński et al. (2019) and Graczyk et al. (2014). References are provided for A_V (mag) and stellar luminosities ($L_\odot$), with the latter adjusted to our adopted distances. Observed line fluxes, line luminosities, and FWHM of He II λ4686 (for WN, WN/C, and Of/WN stars) or C IV λλ5801,12 are provided in erg s^{-1} cm^{-2}, erg s^{-1}, and km s^{-1}, the latter corrected for instrumental broadening. The He II λ4686 or C IV λλ5801,12 line luminosity (in 10^{-3} $L_{\rm Bol}$) is restricted to stars with a measured stellar luminosity, with other optical line luminosities provided with respect to He II λ4686 or C IV λλ5801,12 (··· refers to a lack of data). For WN and WN/C stars, aside from the blends at λ4100 and λ4630, we have endeavoured to exclude the contribution of He I λ7065 and He II λ7177 to the N IV λλ7103,29 multiplet. For early-type WC and WO stars, C IV λ4658 (6-5), λ4686 (8-6), and λ4689 (11-7) will also contribute to the C,III λλ4647,51 + He II λ4686 blend.

Table A1. Luminosities of prominent optical emission lines of Galactic (WR), LMC (BAT99), and SMC (AB) WN stars, categorized as weak-lined early-type (WN2–5w), strong-lined (WN3–7s), late-type (WN6–8), very late-type (WN9–11), or (main sequence) very massive H-rich (WN5–7h) stars. He II λ4686 FWHM are also provided in km s^{-1} (±100 km s^{-1}). The feature at λ4100 involves N III λλ4097,4103, Si IV λλ4088,4116, and He II λ4100 + H δ, while the feature at λ4630 involves N V λλ4603,20 and N III λλ4634,41. Stars included in spectral templates are indicated in bold (the remainder are excluded owing to limited spectral coverage).

Star	Category	Data ID	d kpc	A_V mag	log $L_{Bol}/L_\odot$	Ref	log $F_{HeII\ 4686}$ erg s^{-1} cm^{-2}	HeII 4686 FWHM	$L_{HeII\ 4686}$ 10^{35} erg s^{-1}	$L_{HeII\ 4686}$ 10^{-3} L_{Bol}	$\frac{L_{NIV\ 3478,85}}{L_{HeII\ 4686}}$	$\frac{L_{NIV\ 4058}}{L_{HeII\ 4686}}$	$\frac{L_{4100}}{L_{HeII\ 4686}}$	$\frac{L_{4630}}{L_{HeII\ 4686}}$	$\frac{L_{HeII\ 5412}}{L_{HeII\ 4686}}$	$\frac{L_{CIV\ 5801,12}}{L_{HeII\ 4686}}$	$\frac{L_{HeI\ 5876}}{L_{HeII\ 4686}}$	$\frac{L_{H\alpha}}{L_{HeII\ 4686}}$	$\frac{L_{NIV\ 7103.29}}{L_{HeII\ 4686}}$
WR1	WN3–7s	II91	3.0 ± 0.1	2.5 ± 0.3	$5.84^{+0.11}_{-0.11}$	1	$-10.06^{+0.08}_{-0.10}$	2500	$15.9^{+6.1}_{-5.1}$	0.60 ± 0.07	$0.28^{+0.03}_{-0.02}$	— 0.21$^{+0.01}_{-0.00}$ —		0.17	$0.16^{+0.01}_{-0.01}$	$0.12^{+0.01}_{-0.01}$	0.04	$0.21^{+0.02}_{-0.02}$	$0.21^{+0.02}_{-0.03}$
WR3	WN2–5w	II91	2.2 ± 0.1	$1.4^{+0.2}_{-0.1}$	$5.33^{+0.07}_{-0.07}$	1	$-10.89^{+0.08}_{-0.10}$	2400	$0.4^{+0.1}_{-0.1}$	$0.05^{+0.00}_{-0.01}$	···	···	···	0.65	$0.16^{+0.01}_{-0.00}$	0.02	0.00	$0.24^{+0.01}_{-0.01}$	···
WR6	WN3–7s	VU	1.4 ± 0.1	$0.4^{+0.1}_{-0.0}$	$5.37^{+0.05}_{-0.04}$	1	$-8.55^{+0.04}_{-0.05}$	2300	$11.2^{+1.4}_{-1.4}$	$1.23^{+0.26}_{-0.05}$	$0.60^{+0.01}_{-0.01}$	— 0.28 —		0.16	0.13	[a]0.06	0.03	0.14	$0.15^{+0.00}_{-0.01}$
WR7	WN3–7s	AR	4.0 ± 0.4	2.0 ± 0.2	$5.28^{+0.12}_{-0.12}$	1	$-10.48^{+0.04}_{-0.04}$	1900	$5.9^{+1.7}_{-1.4}$	$0.81^{+0.14}_{-0.12}$	$0.50^{+0.03}_{-0.03}$	0.02	$0.07^{+0.01}_{-0.00}$	0.20	$0.15^{+0.01}_{-0.00}$	$0.09^{+0.01}_{-0.00}$	0.02	$0.18^{+0.01}_{-0.02}$	[b]$0.07^{+0.01}_{-0.00}$
WR10	WN2–5w	CS	4.2 ± 0.2	2.2 ± 0.2	$5.55^{+0.10}_{-0.10}$	1	$-11.10^{+0.04}_{-0.04}$	1300	$1.9^{+0.6}_{-0.5}$	$0.14^{+0.02}_{-0.02}$	$0.63^{+0.05}_{-0.03}$	$0.62^{+0.03}_{-0.02}$	$0.38^{+0.01}_{-0.01}$	0.08	$0.08^{+0.01}_{-0.00}$	0.03	0.00	$0.27^{+0.02}_{-0.02}$	···
WR12	WN6–8	CS	$5.2^{+0.4}_{-0.3}$	$3.6^{+0.3}_{-0.4}$	$5.86^{+0.16}_{-0.15}$	1	$-10.94^{+0.05}_{-0.04}$	1100	$19.1^{+9.4}_{-6.6}$	$0.68^{+0.13}_{-0.10}$	$0.18^{+0.02}_{-0.01}$	$0.22^{+0.01}_{-0.01}$	$0.58^{+0.03}_{-0.03}$	$0.56^{+0.01}_{-0.00}$	$0.09^{+0.01}_{-0.00}$	0.01	$0.18^{+0.02}_{-0.01}$	$0.50^{+0.06}_{-0.05}$	···
WR16	WN6–8	CS	2.3 ± 0.1	$2.3^{+0.2}_{-0.3}$	$5.60^{+0.09}_{-0.10}$	1	$-10.21^{+0.05}_{-0.04}$	600	$4.7^{+1.4}_{-1.2}$	$0.31^{+0.04}_{-0.03}$	···	0.10	$0.83^{+0.03}_{-0.02}$	$1.11^{+0.01}_{-0.00}$	$0.08^{+0.00}_{-0.01}$	0.01	$0.33^{+0.02}_{-0.02}$	$0.65^{+0.05}_{-0.05}$	···
WR18	WN3–7s	AR	3.1 ± 0.1	$3.3^{+0.3}_{-0.4}$	$5.90^{+0.13}_{-0.14}$	1	$-10.27^{+0.04}_{-0.04}$	2800	$22.6^{+10.0}_{-7.2}$	$0.74^{+0.09}_{-0.08}$	···	— 0.28$^{+0.01}_{-0.01}$ —		$0.16^{+0.01}_{-0.00}$	$0.12^{+0.01}_{-0.00}$	$0.12^{+0.00}_{-0.01}$	0.02	$0.15^{+0.02}_{-0.01}$	$0.17^{+0.03}_{-0.02}$
WR20	WN2–5w	CS	$6.4^{+0.5}_{-0.4}$	4.8 ± 0.5	$5.69^{+0.21}_{-0.20}$	1	$-12.03^{+0.04}_{-0.04}$	1600	$10.3^{+7.5}_{-4.5}$	$0.54^{+0.14}_{-0.11}$	$0.64^{+0.10}_{-0.08}$	$0.24^{+0.02}_{-0.02}$	$0.29^{+0.02}_{-0.02}$	0.16	$0.12^{+0.01}_{-0.01}$	$0.07^{+0.01}_{-0.01}$	0.02	$0.10^{+0.02}_{-0.02}$	$0.15^{+0.04}_{-0.03}$
WR21	WN2–5w + O	CS	3.2 ± 0.1	2.1 ± 0.2	···	2	$-10.56^{+0.05}_{-0.04}$	1800	$3.7^{+1.1}_{-0.9}$	···	$0.61^{+0.03}_{-0.04}$	$0.09^{+0.01}_{-0.00}$	$0.12^{+0.01}_{-0.00}$	0.15	$0.08^{+0.00}_{-0.01}$	$0.07^{+0.00}_{-0.01}$	0.00	$0.15^{+0.02}_{-0.01}$	$0.28^{+0.03}_{-0.03}$
WR22	WN5–7h + O	VU	$2.4^{+0.1}_{-0.2}$	1.6 ± 0.2	$6.26^{+0.08}_{-0.07}$	1	$-9.52^{+0.04}_{-0.05}$	800	$11.4^{+2.5}_{-2.2}$	$0.16^{+0.02}_{-0.01}$	$0.03^{+0.01}_{-0.00}$	0.13	$0.55^{+0.01}_{-0.01}$	0.61	$0.05^{+0.01}_{-0.00}$	[a]0.02	0.05	$0.59^{+0.03}_{-0.03}$	$0.09^{+0.00}_{-0.01}$
WR24	WN5–7h	VU	$2.4^{+0.2}_{-0.1}$	0.9 ± 0.1	$6.12^{+0.07}_{-0.05}$	1	$-9.44^{+0.05}_{-0.04}$	1100	$7.2^{+1.1}_{-1.1}$	$0.14^{+0.01}_{-0.01}$	0.09	0.20	0.34	0.41	$0.06^{+0.01}_{-0.00}$	[a]$0.04^{+0.00}_{-0.01}$	0.00	$0.49^{+0.02}_{-0.01}$	0.10
WR25	Of/WN + O	**CS**	2.3 ± 0.1	3.0 ± 0.3	$6.49^{+0.13}_{-0.13}$	1,3	$-10.47^{+0.04}_{-0.05}$	1300	$5.1^{+2.0}_{-1.5}$	$0.04^{+0.01}_{-0.00}$	$0.10^{+0.01}_{-0.01}$	$0.31^{+0.01}_{-0.01}$	$0.43^{+0.01}_{-0.01}$	0.60	$0.06^{+0.01}_{-0.00}$	0.01	0.00	$0.58^{+0.05}_{-0.04}$	···
WR28	WN6–8 + O	CS	6.9 ± 0.5	$4.5^{+0.5}_{-0.4}$	$6.09^{+0.20}_{-0.18}$	1	$-11.91^{+0.04}_{-0.04}$	1200	$11.1^{+7.4}_{-4.6}$	$0.23^{+0.06}_{-0.04}$	$0.29^{+0.04}_{-0.04}$	$0.21^{+0.02}_{-0.01}$	$0.39^{+0.03}_{-0.02}$	0.33	$0.09^{+0.01}_{-0.01}$	$0.03^{+0.00}_{-0.01}$	0.02	$0.26^{+0.05}_{-0.05}$	···
WR29	WN6–8 + O	CS	7.0 ± 0.5	3.6 ± 0.4	···	2	$-12.06^{+0.04}_{-0.04}$	1000	$2.9^{+1.4}_{-1.0}$	···	$0.15^{+0.01}_{-0.02}$	$0.19^{+0.01}_{-0.01}$	$0.37^{+0.02}_{-0.02}$	0.39	$0.08^{+0.00}_{-0.01}$	$0.03^{+0.00}_{-0.01}$	0.04	$0.27^{+0.04}_{-0.04}$	···
WR31a	WN9–11	AR	$7.1^{+0.8}_{-0.6}$	$3.5^{+0.4}_{-0.3}$	$5.56^{+0.17}_{-0.16}$	4	$-13.28^{+0.05}_{-0.04}$	300	$0.2^{+0.1}_{-0.1}$	$0.01^{+0.01}_{-0.00}$	···	0.00	21^{+2}_{-1}	7.8	0.00	0.00	37^{+4}_{-4}	175^{+26}_{-23}	···
WR34	WN2–5w	CS	$7.3^{+0.8}_{-0.7}$	$4.4^{+0.5}_{-0.4}$	$5.59^{+0.20}_{-0.20}$	1	$-12.04^{+0.04}_{-0.05}$	1400	$8.4^{+5.6}_{-3.5}$	$0.55^{+0.17}_{-0.12}$	$0.64^{+0.09}_{-0.08}$	$0.24^{+0.02}_{-0.01}$	$0.26^{+0.02}_{-0.02}$	$0.22^{+0.01}_{-0.00}$	···	···	···	···	···
WR35	WN6–8	CS	$7.9^{+0.8}_{-0.6}$	4.3 ± 0.4	$5.73^{+0.19}_{-0.19}$	1	$-11.93^{+0.04}_{-0.04}$	1000	$11.4^{+7.3}_{-4.6}$	$0.55^{+0.14}_{-0.11}$	$0.40^{+0.05}_{-0.05}$	$0.30^{+0.02}_{-0.02}$	$0.46^{+0.03}_{-0.03}$	$0.38^{+0.01}_{-0.00}$	$0.07^{+0.01}_{-0.00}$	$0.04^{+0.00}_{-0.01}$	$0.02^{+0.01}_{-0.00}$	$0.20^{+0.04}_{-0.03}$	···
WR36	WN3–7s	CS	$6.7^{+0.6}_{-0.5}$	$3.8^{+0.3}_{-0.4}$	$5.39^{+0.17}_{-0.16}$	1	$-11.51^{+0.05}_{-0.04}$	2600	$11.4^{+6.2}_{-4.2}$	$1.20^{+0.27}_{-0.21}$	$0.58^{+0.07}_{-0.06}$	$0.10^{+0.01}_{-0.01}$	$0.19^{+0.01}_{-0.01}$	0.18	$0.11^{+0.01}_{-0.01}$	$0.07^{+0.01}_{-0.01}$	$0.07^{+0.00}_{-0.01}$	$0.12^{+0.01}_{-0.02}$	$0.18^{+0.03}_{-0.03}$
WR37	WN3–7s	CS	$6.8^{+0.7}_{-0.6}$	6.1 ± 0.6	$5.88^{+0.25}_{-0.26}$	1	$-12.24^{+0.05}_{-0.04}$	2800	$31.0^{+31.0}_{-16.0}$	$1.07^{+0.37}_{-0.26}$	$0.36^{+0.07}_{-0.06}$	0.03	$0.15^{+0.01}_{-0.02}$	0.17	$0.09^{+0.01}_{-0.01}$	$0.07^{+0.02}_{-0.01}$	0.02	$0.11^{+0.03}_{-0.03}$	···
WR40	WN6–8	CS	$2.8^{+0.2}_{-0.1}$	$1.6^{+0.2}_{-0.1}$	$5.61^{+0.08}_{-0.07}$	1	$-9.74^{+0.04}_{-0.05}$	900	$10.7^{+2.5}_{-2.1}$	$0.68^{+0.07}_{-0.06}$	$0.33^{+0.01}_{-0.02}$	$0.11^{+0.00}_{-0.01}$	$0.76^{+0.02}_{-0.02}$	$0.99^{+0.01}_{-0.00}$	$0.08^{+0.01}_{-0.00}$	0.01	$0.48^{+0.02}_{-0.02}$	$0.71^{+0.05}_{-0.04}$	$0.28^{+0.02}_{-0.02}$
WR43A	2×WN5–7h	HF	7.3 ± 0.4	3.9 ± 0.4	$6.56^{+0.17}_{-0.16}$	5	$-11.64^{+0.04}_{-0.04}$	1600	$11.7^{+6.6}_{-4.3}$	$0.08^{+0.02}_{-0.01}$	$0.19^{+0.03}_{-0.02}$	$0.31^{+0.02}_{-0.02}$	$0.47^{+0.03}_{-0.02}$	0.27	···	···	···	···	···
WR43B	WN5–7h	HF	7.3 ± 0.4	3.9 ± 0.4	$6.43^{+0.16}_{-0.16}$	5	$-11.44^{+0.05}_{-0.04}$	1900	$18.1^{+10.0}_{-6.7}$	$0.18^{+0.03}_{-0.03}$	$0.26^{+0.03}_{-0.03}$	$0.25^{+0.01}_{-0.02}$	$0.46^{+0.03}_{-0.02}$	$0.37^{+0.00}_{-0.01}$	···	···	···	···	···
WR43C	Of/WN	HF	7.3 ± 0.4	3.9 ± 0.4	$6.32^{+0.16}_{-0.17}$	5	$-12.07^{+0.04}_{-0.05}$	1900	$4.4^{+2.5}_{-1.6}$	$0.06^{+0.01}_{-0.01}$	$0.21^{+0.03}_{-0.02}$	$0.18^{+0.01}_{-0.01}$	$0.10^{+0.00}_{-0.01}$	$0.37^{+0.00}_{-0.01}$	···	···	···	···	···
WR44	WN2–5w + O	CS	$8.5^{+0.9}_{-0.7}$	2.7 ± 0.3	$5.84^{+0.14}_{-0.13}$	1	$-11.27^{+0.04}_{-0.05}$	1800	$9.0^{+3.3}_{-2.6}$	$0.33^{+0.07}_{-0.05}$	$0.83^{+0.06}_{-0.06}$	$0.11^{+0.00}_{-0.01}$	$0.15^{+0.01}_{-0.00}$	$0.16^{+0.00}_{-0.01}$	···	···	···	···	···
WR46	WN2–5w	CS	$2.3^{+0.0}_{-0.1}$	1.3 ± 0.1	$5.29^{+0.04}_{-0.06}$	1	$-10.68^{+0.04}_{-0.05}$	2500	$0.5^{+0.1}_{-0.1}$	$0.07^{+0.01}_{-0.00}$	···	···	···	$0.72^{+0.01}_{-0.01}$	0.11	0.01	0.00	$0.16^{+0.01}_{-0.00}$	···
WR47	WN6–8 + O	CS	3.6 ± 0.2	$4.0^{+0.3}_{-0.4}$	···	2	$-11.03^{+0.04}_{-0.05}$	1400	$12.0^{+6.9}_{-4.5}$	···	···	$0.24^{+0.02}_{-0.01}$	$0.41^{+0.03}_{-0.02}$	$0.43^{+0.00}_{-0.01}$	$0.12^{+0.00}_{-0.01}$	$0.05^{+0.00}_{-0.01}$	$0.06^{+0.01}_{-0.00}$	$0.13^{+0.02}_{-0.02}$	···
WR47a	WN6–8	AD	$8.1^{+1.0}_{-0.8}$	$7.6^{+0.8}_{-0.7}$	···	2	$-13.53^{+0.04}_{-0.04}$	900	$12.3^{+16.9}_{-7.3}$	···	···	$0.10^{+0.01}_{-0.01}$	$0.72^{+0.09}_{-0.08}$	$1.17^{+0.02}_{-0.02}$	$0.07^{+0.01}_{-0.01}$	$0.02^{+0.00}_{-0.01}$	$0.61^{+0.14}_{-0.12}$	$1.00^{+0.35}_{-0.26}$	$0.03^{+0.02}_{-0.01}$
WR49	WN2–5w	CS	$8.4^{+0.9}_{-0.7}$	3.0 ± 0.3	$5.25^{+0.15}_{-0.14}$	1	$-11.82^{+0.04}_{-0.04}$	1500	$3.8^{+1.6}_{-1.2}$	$0.55^{+0.12}_{-0.10}$	$0.66^{+0.07}_{-0.05}$	$0.29^{+0.01}_{-0.02}$	$0.27^{+0.01}_{-0.01}$	0.25	$0.11^{+0.01}_{-0.01}$	$0.04^{+0.00}_{-0.01}$	0.01	$0.22^{+0.03}_{-0.02}$	···
WR51	WN2–5w	CS	4.0 ± 0.2	$5.3^{+0.5}_{-0.6}$	$5.54^{+0.22}_{-0.22}$	1	$-12.30^{+0.04}_{-0.05}$	1700	$3.5^{+2.8}_{-1.6}$	$0.26^{+0.06}_{-0.05}$	$0.71^{+0.11}_{-0.11}$	$0.20^{+0.02}_{-0.02}$	$0.27^{+0.02}_{-0.02}$	0.24	$0.11^{+0.01}_{-0.01}$	$0.04^{+0.01}_{-0.00}$	0.01	$0.20^{+0.04}_{-0.04}$	···
WR54	WN2–5w	CS	$5.5^{+0.4}_{-0.3}$	3.1 ± 0.3	$5.41^{+0.14}_{-0.13}$	1	$-11.41^{+0.04}_{-0.05}$	1500	$4.5^{+1.9}_{-1.4}$	$0.45^{+0.08}_{-0.06}$	$1.01^{+0.10}_{-0.08}$	$0.28^{+0.02}_{-0.01}$	$0.32^{+0.01}_{-0.02}$	0.23	···	···	···	···	···
WR55	WN6–8	CS	3.0 ± 0.3	2.8 ± 0.1	$5.35^{+0.12}_{-0.12}$	1	$-10.55^{+0.04}_{-0.05}$	1100	$6.7^{+2.5}_{-1.9}$	$0.78^{+0.10}_{-0.10}$	$0.12^{+0.01}_{-0.01}$	$0.24^{+0.01}_{-0.01}$	$0.49^{+0.01}_{-0.02}$	0.53	···	···	···	···	···
WR61	WN2–5w	CS	6.4 ± 0.5	1.9 ± 0.2	$5.12^{+0.10}_{-0.11}$	1	$-11.13^{+0.05}_{-0.04}$	1600	$3.2^{+0.9}_{-0.8}$	$0.65^{+0.10}_{-0.09}$	$0.53^{+0.03}_{-0.03}$	$0.25^{+0.01}_{-0.01}$	$0.32^{+0.01}_{-0.01}$	$0.28^{+0.01}_{-0.00}$	$0.12^{+0.01}_{-0.00}$	$0.07^{+0.01}_{-0.00}$	$0.02^{+0.01}_{-0.00}$	$0.13^{+0.01}_{-0.01}$	···
WR67	WN6–8	CS	3.2 ± 0.2	3.9 ± 0.4	$5.36^{+0.17}_{-0.17}$	1	$-11.23^{+0.05}_{-0.04}$	1300	$6.1^{+3.5}_{-2.3}$	$0.69^{+0.15}_{-0.12}$	$0.40^{+0.05}_{-0.05}$	$0.30^{+0.02}_{-0.02}$	$0.46^{+0.03}_{-0.02}$	0.48	$0.11^{+0.01}_{-0.00}$	$0.06^{+0.00}_{-0.01}$	0.04	$0.14^{+0.02}_{-0.02}$	···
WR71	WN6–8	CS	4.1 ± 0.3	$1.1^{+0.2}_{-0.1}$	$5.29^{+0.08}_{-0.07}$	1	$-10.23^{+0.04}_{-0.05}$	1400	$4.6^{+0.9}_{-0.8}$	$0.61^{+0.06}_{-0.05}$	$0.62^{+0.03}_{-0.02}$	$0.32^{+0.01}_{-0.01}$	$0.55^{+0.01}_{-0.01}$	0.52	$0.12^{+0.01}_{-0.00}$	0.04	0.04	$0.13^{+0.00}_{-0.01}$	···

Table A1 – *continued*

Star	Category	Data ID	d kpc	A_V mag	log $L_{Bol}/L_\odot$	Ref	log $F_{HeII\ 4686}$ erg s^{-1} cm^{-2}	HeII 4686 FWHM	$L_{HeII\ 4686}$ 10^{35} erg s^{-1}	$L_{HeII\ 4686}$ 10^{-3} L_{Bol}	$\frac{L_{NIV\ 3478.85}}{L_{HeII\ 4686}}$	$\frac{L_{NIV\ 4058}}{L_{HeII\ 4686}}$	$\frac{L_{4100}}{L_{HeII\ 4686}}$	$\frac{L_{4630}}{L_{HeII\ 4686}}$	$\frac{L_{HeII\ 5412}}{L_{HeII\ 4686}}$	$\frac{L_{CIV\ 5801,12}}{L_{HeII\ 4686}}$	$\frac{L_{HeI\ 5876}}{L_{HeII\ 4686}}$	$\frac{L_{H\alpha}}{L_{HeII\ 4686}}$	$\frac{L_{NIV\ 7103.29}}{L_{HeII\ 4686}}$
WR74	WN6–8	CS	$4.0^{+0.2}_{-0.3}$	$5.6^{+0.6}_{-0.5}$	$5.41^{+0.23}_{-0.24}$	1	$-12.40^{+0.04}_{-0.05}$	1100	$4.2^{+3.7}_{-2.0}$	$0.43^{+0.10}_{-0.09}$	…	$0.16^{+0.01}_{-0.02}$	$0.29^{+0.02}_{-0.03}$	$0.74^{+0.01}_{-0.01}$	$0.16^{+0.01}_{-0.02}$	$0.06^{+0.00}_{-0.01}$	$0.16^{+0.03}_{-0.02}$	$0.15^{+0.04}_{-0.03}$	$0.20^{+0.07}_{-0.04}$
WR75	WN3–7s	CS	$3.5^{+0.3}_{-0.2}$	$3.5^{+0.3}_{-0.4}$	$5.61^{+0.15}_{-0.15}$	1	$-10.45^{+0.04}_{-0.05}$	2800	$26.6^{+13.2}_{-9.2}$	$1.71^{+0.32}_{-0.27}$	$0.72^{+0.08}_{-0.07}$	—	$0.77^{+0.03}_{-0.04}$	—	0.39	$0.12^{+0.01}_{-0.01}$	$0.03^{+0.01}_{-0.00}$	$0.08^{+0.01}_{-0.00}$	$0.11^{+0.02}_{-0.01}$	…
WR78	WN6–8	VU	1.6 ± 0.1	1.8 ± 0.2	$6.03^{+0.08}_{-0.08}$	1	$-9.37^{+0.04}_{-0.04}$	900	$10.0^{+2.5}_{-2.1}$	$0.24^{+0.03}_{-0.02}$	$0.05^{+0.01}_{-0.00}$	0.10	$0.47^{+0.01}_{-0.02}$	$0.61^{+0.00}_{-0.01}$	$0.11^{+0.00}_{-0.01}$	[a]0.03	$0.12^{+0.01}_{-0.00}$	$0.37^{+0.03}_{-0.02}$	$0.09^{+0.01}_{-0.01}$
WR82	WN6–8	CS	3.8 ± 0.3	$3.8^{+0.3}_{-0.4}$	$5.26^{+0.16}_{-0.17}$	1	$-11.58^{+0.04}_{-0.05}$	1000	$3.1^{+1.7}_{-1.1}$	$0.44^{+0.10}_{-0.08}$	$0.31^{+0.03}_{-0.04}$	$0.23^{+0.02}_{-0.01}$	$0.73^{+0.05}_{-0.04}$	$0.94^{+0.01}_{-0.00}$	$0.11^{+0.01}_{-0.00}$	0.01	$0.17^{+0.02}_{-0.02}$	$0.40^{+0.07}_{-0.05}$	…
WR83	WN2–5w	CS	$4.6^{+0.4}_{-0.3}$	4.0 ± 0.4	…	2	$-11.46^{+0.04}_{-0.05}$	1400	$7.6^{+4.4}_{-2.9}$	…	$0.75^{+0.09}_{-0.08}$	$0.37^{+0.03}_{-0.02}$	$0.50^{+0.03}_{-0.03}$	$0.47^{+0.00}_{-0.01}$	$0.10^{+0.00}_{-0.01}$	$0.04^{+0.00}_{-0.01}$	0.01	$0.19^{+0.03}_{-0.03}$	…
WR84	WN6–8	CS	2.7 ± 0.1	$5.4^{+0.6}_{-0.5}$	$5.18^{+0.22}_{-0.22}$	1	$-11.94^{+0.04}_{-0.05}$	1100	$4.5^{+3.8}_{-2.1}$	$0.77^{+0.16}_{-0.11}$	$0.31^{+0.06}_{-0.04}$	$0.27^{+0.02}_{-0.03}$	$0.65^{+0.05}_{-0.05}$	$0.74^{+0.01}_{-0.00}$	$0.14^{+0.01}_{-0.01}$	$0.05^{+0.01}_{-0.01}$	$0.09^{+0.02}_{-0.01}$	$0.12^{+0.03}_{-0.02}$	…
WR85	WN6–8	CS	$2.2^{+0.1}_{-0.0}$	$3.5^{+0.3}_{-0.4}$	$5.48^{+0.15}_{-0.14}$	1	$-10.75^{+0.04}_{-0.04}$	1100	$4.9^{+2.4}_{-1.7}$	$0.42^{+0.07}_{-0.05}$	$0.45^{+0.05}_{-0.04}$	$0.34^{+0.02}_{-0.02}$	$0.62^{+0.03}_{-0.03}$	$0.67^{+0.01}_{-0.00}$	$0.11^{+0.01}_{-0.00}$	0.03	$0.04^{+0.00}_{-0.01}$	$0.32^{+0.04}_{-0.04}$	…
WR87	WN5–7h	CS	$3.0^{+0.1}_{-0.2}$	$6.4^{+0.6}_{-0.7}$	$6.11^{+0.26}_{-0.26}$	1	$-12.32^{+0.04}_{-0.05}$	1100	$6.5^{+6.8}_{-3.4}$	$0.13^{+0.03}_{-0.03}$	$0.57^{+0.12}_{-0.10}$	$0.14^{+0.01}_{-0.01}$	$0.70^{+0.07}_{-0.06}$	$1.04^{+0.01}_{-0.01}$	$0.06^{+0.01}_{-0.01}$	$0.06^{+0.01}_{-0.01}$	$0.06^{+0.02}_{-0.01}$	$0.77^{+0.22}_{-0.17}$	…
WR89	WN5–7h	CS	3.2 ± 0.2	5.9 ± 0.6	$6.30^{+0.26}_{-0.24}$	1	$-11.95^{+0.04}_{-0.04}$	700	$10.9^{+10.4}_{-5.5}$	$0.14^{+0.03}_{-0.03}$	$1.07^{+0.21}_{-0.17}$	$0.16^{+0.01}_{-0.02}$	$0.95^{+0.09}_{-0.08}$	$1.01^{+0.01}_{-0.01}$	$0.03^{+0.01}_{-0.00}$	$0.01^{+0.01}_{-0.00}$	$0.07^{+0.01}_{-0.01}$	$0.73^{+0.19}_{-0.15}$	…
WR91	WN3–7s	CS	$3.6^{+0.3}_{-0.2}$	$8.0^{+0.7}_{-0.8}$	$5.61^{+0.33}_{-0.32}$	1	$-12.68^{+0.04}_{-0.05}$	2000	$25.4^{+36.9}_{-15.3}$	$1.61^{+0.54}_{-0.40}$	…	…	…	$0.60^{+0.00}_{-0.01}$	$0.12^{+0.02}_{-0.02}$	$0.03^{+0.01}_{-0.01}$	$0.11^{+0.03}_{-0.02}$	$0.14^{+0.05}_{-0.04}$	…
WR94	WN2–5w	CS	1.1 ± 0.0	6.1 ± 0.6	$5.65^{+0.25}_{-0.24}$	1	$-11.21^{+0.04}_{-0.04}$	1400	$8.1^{+7.9}_{-4.1}$	$0.47^{+0.08}_{-0.07}$	$1.04^{+0.19}_{-0.16}$	$0.41^{+0.04}_{-0.04}$	$0.54^{+0.05}_{-0.04}$	$0.38^{+0.00}_{-0.01}$	…	…	…	…	…
WR97	WN3–7s + O	CS	$2.3^{+0.1}_{-0.0}$	3.7 ± 0.4	…	2	$-11.53^{+0.05}_{-0.04}$	2000	$1.3^{+0.7}_{-0.5}$	…	$0.54^{+0.06}_{-0.06}$	$0.12^{+0.01}_{-0.01}$	0.07	0.42	$0.09^{+0.01}_{-0.01}$	$0.05^{+0.01}_{-0.00}$	0.00	$0.26^{+0.04}_{-0.04}$	…
WR100	WN3–7s	CS	$2.5^{+0.2}_{-0.1}$	$5.6^{+0.6}_{-0.5}$	$5.38^{+0.23}_{-0.23}$	1	$-11.60^{+0.05}_{-0.04}$	1900	$11.0^{+9.8}_{-5.3}$	$1.19^{+0.31}_{-0.24}$	$0.37^{+0.07}_{-0.06}$	$0.26^{+0.02}_{-0.02}$	$0.59^{+0.05}_{-0.05}$	$0.55^{+0.01}_{-0.00}$	…	…	…	…	…
WR105	WN9–11	II96	$3.5^{+0.6}_{-0.4}$	$7.7^{+0.7}_{-0.8}$	$6.28^{+0.33}_{-0.33}$	6	$-12.72^{+0.04}_{-0.05}$	500	$15.3^{+21.0}_{-9.1}$	$0.21^{+0.10}_{-0.06}$	…	0.00	$0.72^{0.08}_{-0.08}$	$1.42^{+0.02}_{-0.02}$	0.02:	0.00	$0.82^{+0.19}_{-0.15}$	$1.6^{+0.5}_{-0.4}$	…
WR107	WN6–8	II96	1.8 ± 0.3	6.3 ± 0.6	$4.85^{+0.30}_{-0.28}$	1	$-12.54^{+0.04}_{-0.05}$	1000	$1.1^{+1.0}_{-0.6}$	$0.38^{+0.17}_{-0.10}$	…	$0.22^{+0.02}_{-0.02}$	$0.87^{+0.07}_{-0.07}$	$1.36^{+0.01}_{-0.01}$	$0.17^{+0.02}_{-0.01}$	$0.05^{+0.01}_{-0.01}$	$0.49^{+0.07}_{-0.07}$	$0.17^{+0.04}_{-0.03}$	…
WR108	WN9–11	II91	$3.1^{+0.2}_{-0.1}$	$3.7^{+0.3}_{-0.4}$	$5.42^{+0.15}_{-0.16}$	6	$-11.63^{+0.04}_{-0.05}$	400	$1.7^{+0.9}_{-0.6}$	$0.17^{+0.03}_{-0.02}$	…	0.00	$1.20^{+0.07}_{-0.06}$	$1.93^{+0.01}_{-0.01}$	0.02	0.02	$0.25^{+0.03}_{-0.02}$	$1.13^{+0.17}_{-0.14}$	0.01
WR110	WN3–7s	AR	1.8 ± 0.1	3.8 ± 0.4	$5.61^{+0.16}_{-0.15}$	1	$-9.93^{+0.04}_{-0.05}$	3600	$29.8^{+15.8}_{-10.7}$	$1.88^{+0.27}_{-0.23}$	$0.57^{+0.07}_{-0.05}$	—	$0.47^{+0.02}_{-0.03}$	—	$0.20^{+0.01}_{-0.00}$	$0.11^{+0.01}_{-0.01}$	$0.03^{+0.01}_{-0.00}$	$0.07^{+0.01}_{-0.00}$	$0.13^{+0.02}_{-0.01}$	$0.17^{+0.02}_{-0.03}$
WR116	WN6–8	II96	2.9 ± 0.2	$6.6^{+0.6}_{-0.7}$	$5.56^{+0.27}_{-0.27}$	1	$-12.49^{+0.04}_{-0.05}$	1100	$5.2^{+5.7}_{-2.8}$	$0.37^{+0.11}_{-0.09}$	…	$0.11^{+0.01}_{-0.01}$	$1.25^{+0.12}_{-0.12}$	$1.58^{+0.02}_{-0.02}$	$0.07^{+0.01}_{-0.00}$	0.01	$0.69^{+0.14}_{-0.11}$	$1.04^{+0.30}_{-0.24}$	…
WR120	WN6–8	WI94	$2.7^{+0.5}_{-0.4}$	4.7 ± 0.5	$5.39^{+0.23}_{-0.22}$	1	$-11.81^{+0.04}_{-0.05}$	1000	$2.7^{+1.9}_{-1.2}$	$0.28^{+0.10}_{-0.07}$	…	…	…	$0.89^{+0.01}_{-0.01}$	$0.24^{+0.02}_{-0.02}$	$0.08^{+0.01}_{-0.01}$	$0.41^{+0.06}_{-0.05}$	…	…
WR123	WN6–8	AR + II91	$6.1^{+0.6}_{-0.5}$	$2.5^{+0.3}_{-0.2}$	$5.33^{+0.13}_{-0.12}$	1	$-11.41^{+0.04}_{-0.05}$	800	$3.2^{+1.2}_{-0.9}$	$0.38^{+0.08}_{-0.06}$	…	$0.12^{+0.00}_{-0.01}$	$1.15^{+0.05}_{-0.05}$	$1.54^{+0.00}_{-0.01}$	$0.17^{+0.01}_{-0.01}$	0.02	$0.68^{+0.06}_{-0.05}$	$0.15^{+0.02}_{-0.01}$	[b]$0.08^{+0.01}_{-0.01}$
WR124	WN6–8	II91	$5.4^{+0.5}_{-0.3}$	3.8 ± 0.4	$5.62^{+0.17}_{-0.16}$	1	$-11.58^{+0.08}_{-0.10}$	800	$7.0^{+4.1}_{-2.9}$	$0.43^{+0.10}_{-0.07}$	…	…	…	$1.31^{+0.01}_{-0.01}$	$0.08^{+0.00}_{-0.01}$	0.02	$0.92^{+0.11}_{-0.09}$	$1.29^{+0.23}_{-0.19}$	…
WR128	WN2–5w	II91	$3.3^{+0.3}_{-0.2}$	1.4 ± 0.1	$5.34^{+0.08}_{-0.08}$	1	$-10.55^{+0.08}_{-0.09}$	1900	$1.7^{+0.5}_{-0.4}$	$0.20^{+0.02}_{-0.02}$	…	…	…	0.26	$0.11^{+0.00}_{-0.01}$	0.03	0.00	$0.23^{+0.02}_{-0.01}$	$0.13^{+0.01}_{-0.01}$
WR131	WN5–7h	II96 + WI94	$8.2^{+1.0}_{-0.7}$	4.3 ± 0.4	$6.17^{+0.20}_{-0.19}$	1	$-11.97^{+0.04}_{-0.05}$	800	$11.0^{+7.1}_{-4.5}$	$0.19^{+0.05}_{-0.04}$	…	$0.10^{+0.01}_{-0.00}$	$0.29^{+0.02}_{-0.02}$	0.35	$0.06^{+0.01}_{-0.00}$	0.03	$0.05^{+0.00}_{-0.01}$	…	…
WR133	WN2–5w + O	II91	$1.8^{+0.0}_{-0.1}$	1.2 ± 0.1	…	2	$-9.66^{+0.08}_{-0.09}$	1700	$3.0^{+0.8}_{-0.7}$	…	…	…	…	0.14	$0.10^{+0.01}_{-0.00}$	0.12	0.00	$0.20^{+0.01}_{-0.01}$	$0.24^{+0.01}_{-0.02}$
WR134	WN3–7s	II91	$1.9^{+0.0}_{-0.1}$	1.9 ± 0.2	$5.67^{+0.09}_{-0.08}$	1	$-9.14^{+0.08}_{-0.09}$	2600	$25.9^{+8.1}_{-7.2}$	$1.43^{+0.14}_{-0.12}$	$0.55^{+0.03}_{-0.03}$	—	$0.43^{+0.02}_{-0.01}$	—	0.16	$0.13^{+0.01}_{-0.00}$	$0.06^{+0.00}_{-0.01}$	0.04	$0.16^{+0.01}_{-0.02}$	$0.20^{+0.02}_{-0.01}$
WR136	WN3–7s	II91	$1.7^{+0.0}_{-0.1}$	1.7 ± 0.2	$5.68^{+0.07}_{-0.08}$	1	$-8.92^{+0.07}_{-0.10}$	1900	$27.2^{+7.9}_{-7.2}$	$1.49^{+0.12}_{-0.11}$	$0.33^{+0.02}_{-0.02}$	—	$0.56^{+0.02}_{-0.01}$	—	0.34	$0.15^{+0.01}_{-0.01}$	$0.05^{+0.00}_{-0.01}$	0.06	$0.24^{+0.01}_{-0.02}$	$0.18^{+0.01}_{-0.02}$
WR138	WN2–5w + O	II91	2.2 ± 0.1	1.9 ± 0.2	…	2	$-9.84^{+0.08}_{-0.09}$	1400	$7.2^{+2.3}_{-2.0}$	…	…	$0.19^{+0.01}_{-0.00}$	$0.21^{+0.01}_{-0.00}$	$0.28^{+0.01}_{-0.00}$	$0.15^{+0.01}_{-0.00}$	$0.07^{+0.01}_{-0.00}$	0.05	$0.29^{+0.02}_{-0.02}$	$0.28^{+0.02}_{-0.03}$
WR138-1	WN9–11	II13	$7.0^{+0.8}_{-0.6}$	$7.0^{+0.7}_{-0.7}$	…	2	$-13.68^{+0.08}_{-0.10}$	500	$3.3^{+4.0}_{-1.9}$	…	…	0.00	$1.25^{+0.14}_{-0.12}$	$1.17^{+0.02}_{-0.01}$	$0.07^{+0.01}_{-0.01}$	0.00	$1.04^{+0.22}_{-0.19}$	$1.59^{+0.40}_{-0.28}$	$0.01^{+0.01}_{-0.00}$
WR139	WN2–5w + O	II91	$1.4^{+0.0}_{-0.1}$	$2.5^{+0.3}_{-0.2}$	…	2	$-9.93^{+0.08}_{-0.10}$	1600	$4.5^{+1.8}_{-1.4}$	…	…	…	…	0.25	$0.14^{+0.01}_{-0.01}$	$0.14^{+0.01}_{-0.01}$	0.05	$0.21^{+0.02}_{-0.02}$	$0.28^{+0.04}_{-0.03}$
WR141	WN2–5w + O	II91	$1.9^{+0.0}_{-0.1}$	$3.7^{+0.3}_{-0.4}$	…	2	$-10.27^{+0.08}_{-0.09}$	1700	$14.0^{+7.6}_{-5.5}$	…	…	…	…	0.25	$0.12^{+0.01}_{-0.00}$	$0.08^{+0.00}_{-0.01}$	$0.04^{+0.01}_{-0.00}$	$0.13^{+0.01}_{-0.02}$	$0.13^{+0.03}_{-0.02}$
WR147	WN6–8 + B	II96	$1.7^{+0.1}_{-0.1}$	10.7 ± 1.1	$6.58^{+0.43}_{-0.44}$	1	$-13.43^{+0.04}_{-0.05}$	700	$20.1^{+47.0}_{-14.4}$	$0.14^{+0.07}_{-0.05}$	…	$0.06^{+0.01}_{-0.01}$	$0.54^{+0.09}_{-0.08}$	$0.86^{+0.02}_{-0.02}$	$0.11^{+0.03}_{-0.02}$	$0.02^{+0.00}_{-0.01}$	$0.81^{+0.27}_{-0.21}$	$0.60^{+0.32}_{-0.20}$	…
WR148	WN6–8	II91	8.1 ± 0.7	3.0 ± 0.3	$6.25^{+0.15}_{-0.14}$	1	$-11.27^{+0.08}_{-0.10}$	600	$12.6^{+5.8}_{-4.5}$	$0.18^{+0.04}_{-0.03}$	…	$0.09^{+0.00}_{-0.01}$	$0.38^{+0.01}_{-0.02}$	0.51	$0.07^{+0.01}_{-0.00}$	0.03	$0.16^{+0.01}_{-0.01}$	$0.38^{+0.07}_{-0.04}$	…
WR149	WN2–5w	II13	$5.3^{+0.4}_{-0.3}$	$5.3^{+0.6}_{-0.5}$	$5.48^{+0.22}_{-0.22}$	1	$-12.20^{+0.08}_{-0.09}$	1300	$8.5^{+7.2}_{-4.2}$	$0.73^{+0.18}_{-0.15}$	…	$0.20^{+0.01}_{-0.02}$	$0.23^{+0.02}_{-0.02}$	$0.21^{+0.00}_{-0.00}$	$0.13^{+0.01}_{-0.02}$	$0.09^{+0.01}_{-0.01}$	$0.04^{+0.01}_{-0.00}$	$0.13^{+0.02}_{-0.03}$	$0.16^{+0.04}_{-0.04}$
WR152	WN2–5w	II91	$3.5^{+0.3}_{-0.2}$	1.9 ± 0.2	$5.46^{+0.09}_{-0.09}$	1	$-10.96^{+0.08}_{-0.10}$	2000	$1.4^{+0.5}_{-0.4}$	$0.13^{+0.02}_{-0.01}$	…	0.00	0.04	0.34	0.09	0.01	0.00	$0.18^{+0.01}_{-0.01}$	$0.04^{+0.00}_{-0.01}$
WR155	WN6–8 + O	II91	2.7 ± 0.1	2.2 ± 0.2	…	2	$-10.42^{+0.08}_{-0.10}$	1200	$4.1^{+1.4}_{-1.2}$	…	…	…	…	$0.44^{+0.00}_{-0.01}$	$0.09^{+0.00}_{-0.01}$	0.05	$0.06^{+0.01}_{-0.00}$	$0.30^{+0.03}_{-0.02}$	$0.13^{+0.01}_{-0.01}$

Table A1 – *continued*

Star	Category	Data ID	d kpc	A_V mag	log $L_{Bol}/L_\odot$	Ref	log $F_{HeII\ 4686}$ erg s^{-1} cm^{-2}	HeII 4686 FWHM	$L_{HeII\ 4686}$ 10^{35} erg s^{-1}	$L_{HeII\ 4686}$ 10^{-3} L_{Bol}	$\frac{L_{NIV\ 3478,85}}{L_{HeII\ 4686}}$	$\frac{L_{NIV\ 4058}}{L_{HeII\ 4686}}$	$\frac{L_{4100}}{L_{HeII\ 4686}}$	$\frac{L_{4630}}{L_{HeII\ 4686}}$	$\frac{L_{HeII\ 5412}}{L_{HeII\ 4686}}$	$\frac{L_{CIV\ 5801,12}}{L_{HeII\ 4686}}$	$\frac{L_{HeI\ 5876}}{L_{HeII\ 4686}}$	$\frac{L_{H\alpha}}{L_{HeII\ 4686}}$	$\frac{L_{NIV\ 7103,29}}{L_{HeII\ 4686}}$
WR156	WN6–8	II91	$3.3^{+0.2}_{-0.1}$	$4.6^{+0.4}_{-0.5}$	$5.81^{+0.19}_{-0.18}$	1	$-11.61^{+0.07}_{-0.10}$	500	$5.5^{+3.9}_{-2.5}$	$0.22^{+0.04}_{-0.03}$	...	...	...	$2.02^{+0.02}_{-0.02}$	$0.05^{+0.01}_{-0.00}$	$0.03^{+0.01}_{-0.00}$	$0.45^{+0.06}_{-0.05}$	$1.27^{+0.25}_{-0.21}$	...
WR157	WN2–5w	II91	$2.8^{+0.2}_{-0.1}$	2.8 ± 0.3	...	2	$-10.53^{+0.08}_{-0.10}$	1300	$6.6^{+2.8}_{-2.3}$	...	...	...	...	0.22	$0.16^{+0.00}_{-0.01}$	...	...	...	...
BAT99-1	WN3–7s	NE	49.6 ± 1.0	$0.5^{+0.1}_{-0.0}$	$5.29^{+0.03}_{-0.02}$	7	$-12.19^{+0.04}_{-0.04}$	2000	$3.4^{+0.4}_{-0.4}$	$0.45^{+0.02}_{-0.01}$	[b]0.13	0.00	0.05	0.18	0.14	0.01	0.00	0.19	0.00
BAT99-3	WN3–7s	NE	49.6 ± 1.0	$0.5^{+0.0}_{-0.1}$	$5.50^{+0.03}_{-0.02}$	7	$-11.77^{+0.04}_{-0.05}$	2000	$8.2^{+0.9}_{-0.9}$	$0.67^{+0.02}_{-0.02}$	[b]$0.66^{+0.01}_{-0.02}$	0.03	0.08	0.17	0.14	0.05	0.02	$0.16^{+0.00}_{-0.01}$	$0.08^{+0.00}_{-0.01}$
BAT99-5	WN2–5w	NE	49.6 ± 1.0	1.0 ± 0.1	$5.44^{+0.05}_{-0.04}$	7	$-12.72^{+0.04}_{-0.05}$	2400	$1.7^{+0.3}_{-0.2}$	$0.16^{+0.01}_{-0.01}$	...	0.00	$0.04^{+0.01}_{-0.00}$	0.04	$0.15^{+0.00}_{-0.01}$	0.00	0.00	$0.17^{+0.01}_{-0.00}$	0.00
BAT99-7	WN3–7s	NE	49.6 ± 1.0	0.3 ± 0.0	$5.83^{+0.02}_{-0.02}$	7	$-11.11^{+0.04}_{-0.05}$	3800	$31.7^{+3.4}_{-3.4}$	$1.21^{+0.03}_{-0.03}$	[b]$0.30^{+0.00}_{-0.01}$	0.00	$0.05^{+0.00}_{-0.01}$	0.09	0.11	0.03	0.00	$0.15^{+0.00}_{-0.01}$	0.02
BAT99-13	WN9–11	AR + SC	49.6 ± 1.0	$0.8^{+0.0}_{-0.1}$	$5.55^{+0.04}_{-0.03}$	7	$-12.98^{+0.04}_{-0.05}$	200	$0.7^{+0.1}_{-0.1}$	$0.05^{+0.00}_{-0.00}$	...	0.00	$3.7^{+0.0}_{-0.1}$	2.4	0.01	0.00	$3.3^{+0.0}_{-0.0}$	$11.1^{+0.3}_{-0.3}$	...
BAT99-15	WN3–7s	NE	49.6 ± 1.0	0.3 ± 0.0	$5.56^{+0.02}_{-0.02}$	7	$-11.53^{+0.04}_{-0.04}$	2200	$12.2^{+1.3}_{-1.3}$	$0.87^{+0.02}_{-0.02}$	[b]$0.55^{+0.01}_{-0.01}$	0.04	0.12	0.16	0.13	0.07	0.03	$0.16^{+0.00}_{-0.01}$	0.07
BAT99-16	WN6–8	AR + SC	49.6 ± 1.0	$0.3^{+0.1}_{-0.0}$	$5.79^{+0.02}_{-0.02}$	7	$-11.61^{+0.05}_{-0.04}$	700	$10.6^{+1.2}_{-1.1}$	$0.44^{+0.02}_{-0.01}$	[b]$0.16^{+0.01}_{-0.00}$	0.23	$0.50^{+0.01}_{-0.00}$	0.54	0.10	0.04	$0.19^{+0.00}_{-0.01}$	$0.51^{+0.01}_{-0.00}$	...
BAT99-17	WN2–5w + B	NE	49.6 ± 1.0	$0.4^{+0.0}_{-0.1}$	$5.63^{+0.03}_{-0.02}$	8	$-11.78^{+0.04}_{-0.04}$	1800	$7.4^{+0.8}_{-0.8}$	$0.45^{+0.01}_{-0.01}$	[b]$0.75^{+0.02}_{-0.01}$	0.08	0.10	0.18	0.13	0.07	0.01	$0.15^{+0.01}_{-0.00}$	0.10
BAT99-18	WN2–5w	NE	49.6 ± 1.0	$0.4^{+0.0}_{-0.1}$	$5.62^{+0.03}_{-0.02}$	7	$-12.00^{+0.04}_{-0.05}$	1800	$4.5^{+0.5}_{-0.5}$	$0.28^{+0.00}_{-0.01}$	[b]$0.80^{+0.01}_{-0.02}$	0.09	0.11	0.18	$0.10^{+0.01}_{-0.00}$	0.03	0.00	0.20	0.07
BAT99-22	WN9–11	AR + SC	49.6 ± 1.0	$0.5^{+0.0}_{-0.1}$	$5.74^{+0.03}_{-0.02}$	7	$-12.17^{+0.04}_{-0.05}$	300	$3.4^{+0.4}_{-0.4}$	$0.16^{+0.01}_{-0.01}$	[b]0.00	0.00	$1.18^{+0.01}_{-0.01}$	1.52	0.00	0.03	$0.77^{+0.01}_{-0.01}$	$3.27^{+0.06}_{-0.06}$	...
BAT99-23	WN2–5w	NE	49.6 ± 1.0	$2.3^{+0.2}_{-0.3}$	$5.54^{+0.09}_{-0.09}$	7	$-13.20^{+0.04}_{-0.05}$	1800	$2.2^{+0.7}_{-0.5}$	$0.17^{+0.01}_{-0.02}$	...	$0.08^{+0.00}_{-0.01}$	$0.19^{+0.01}_{-0.01}$	0.25	0.10	0.00	0.00	$0.26^{+0.02}_{-0.02}$	$0.04^{+0.00}_{-0.01}$
BAT99-24	WN3–7s	NE	49.6 ± 1.0	$0.4^{+0.0}_{-0.1}$	$5.53^{+0.03}_{-0.02}$	7	$-11.51^{+0.04}_{-0.05}$	2600	$13.7^{+1.5}_{-1.5}$	$1.04^{+0.03}_{-0.03}$	[b]$0.54^{+0.01}_{-0.01}$	0.04	0.11	0.14	0.13	0.04	0.02	$0.15^{+0.01}_{-0.00}$	0.09
BAT99-25	WN2–5w	NE	49.6 ± 1.0	$0.6^{+0.0}_{-0.1}$	$5.54^{+0.03}_{-0.03}$	7	$-12.71^{+0.05}_{-0.04}$	1700	$1.1^{+0.1}_{-0.1}$	$0.08^{+0.00}_{-0.00}$	...	0.07	0.00	0.11	0.08	0.01	0.00	$0.30^{+0.00}_{-0.01}$	0.06
BAT99-26	WN3–7s	NE	49.6 ± 1.0	$0.5^{+0.1}_{-0.0}$	$5.61^{+0.03}_{-0.02}$	7	$-11.78^{+0.04}_{-0.05}$	1800	$8.7^{+1.0}_{-1.0}$	$0.55^{+0.02}_{-0.02}$	[b]$0.83^{+0.02}_{-0.02}$	0.07	0.11	0.18	0.13	$0.09^{+0.00}_{-0.01}$	0.01	0.13	$0.10^{+0.01}_{-0.00}$
BAT99-30	WN6–8	AR	49.6 ± 1.0	$0.3^{+0.0}_{-0.1}$	$5.64^{+0.02}_{-0.02}$	7	$-11.76^{+0.04}_{-0.05}$	1000	$6.8^{+0.7}_{-0.7}$	$0.40^{+0.01}_{-0.01}$	[b]$0.29^{+0.00}_{-0.01}$	0.20	0.39	0.28	0.10	0.05	0.05	[b]$0.50^{+0.01}_{-0.00}$	...
BAT99-31	WN3–7s	NE	49.6 ± 1.0	$0.6^{+0.1}_{-0.0}$	$5.32^{+0.03}_{-0.03}$	7	$-12.08^{+0.04}_{-0.05}$	2000	$4.9^{+0.6}_{-0.6}$	$0.61^{+0.02}_{-0.02}$	[b]$0.57^{+0.02}_{-0.01}$	0.05	0.10	0.19	$0.13^{+0.00}_{-0.01}$	$0.07^{+0.00}_{-0.01}$	0.01	$0.27^{+0.00}_{-0.01}$	0.08
BAT99-32	WN6–8 + O	AR + SC	49.6 ± 1.0	0.3 ± 0.0	$5.93^{+0.02}_{-0.02}$	7	$-11.36^{+0.04}_{-0.05}$	1400	$17.9^{+1.9}_{-1.9}$	$0.54^{+0.01}_{-0.01}$	[b]0.36	0.19	0.26	0.14	0.12	0.03	0.04	$0.24^{+0.01}_{-0.00}$	...
BAT99-35	WN2–5w	NE	49.6 ± 1.0	$0.4^{+0.1}_{-0.0}$	$5.59^{+0.03}_{-0.02}$	7	$-11.97^{+0.04}_{-0.05}$	1800	$4.9^{+0.6}_{-0.5}$	$0.33^{+0.01}_{-0.01}$	[b]$0.80^{+0.02}_{-0.01}$	0.03	0.07	0.23	0.13	0.01	0.00	0.19	0.06
BAT99-37	WN2–5w	NE	49.6 ± 1.0	1.9 ± 0.2	$5.64^{+0.08}_{-0.07}$	7	$-12.62^{+0.04}_{-0.05}$	2000	$5.6^{+1.4}_{-1.2}$	$0.33^{+0.03}_{-0.02}$	...	$0.04^{+0.00}_{-0.01}$	$0.09^{+0.01}_{-0.00}$	0.25	$0.12^{+0.00}_{-0.01}$	0.02	0.00	$0.14^{+0.02}_{-0.00}$	0.03
BAT99-40	WN2–5w + O	NE	49.6 ± 1.0	$0.6^{+0.0}_{-0.1}$	$5.61^{+0.03}_{-0.03}$	7	$-12.34^{+0.04}_{-0.05}$	1600	$2.5^{+0.3}_{-0.3}$	$0.16^{+0.01}_{-0.01}$	[b]$0.63^{+0.02}_{-0.02}$	0.06	0.12	$0.08^{+0.01}_{-0.00}$	0.08	$0.08^{+0.01}_{-0.00}$	0.00	$0.23^{+0.00}_{-0.01}$	0.07
BAT99-41	WN3–7s	NE	49.6 ± 1.0	$0.5^{+0.0}_{-0.1}$	$5.59^{+0.03}_{-0.02}$	7	$-11.82^{+0.04}_{-0.05}$	1600	$7.3^{+0.8}_{-0.8}$	$0.48^{+0.02}_{-0.01}$	[b]0.07	0.04	$0.10^{+0.01}_{-0.00}$	0.18	$0.13^{+0.01}_{-0.00}$	0.08	0.01	0.14	0.10
BAT99-44	WN6–8	AR	49.6 ± 1.0	$0.5^{+0.0}_{-0.1}$	$5.65^{+0.03}_{-0.02}$	7	$-12.13^{+0.04}_{-0.05}$	900	$3.6^{+0.4}_{-0.4}$	$0.21^{+0.00}_{-0.01}$	[b]$0.15^{+0.01}_{-0.00}$	0.18	$0.63^{+0.01}_{-0.01}$	0.74	0.08	0.04	0.19	[b]$1.01^{+0.02}_{-0.02}$	...
BAT99-45	WN9–11	AR + SC	49.6 ± 1.0	$0.3^{+0.0}_{-0.0}$	$5.75^{+0.02}_{-0.02}$	9	$-12.40^{+0.05}_{-0.05}$	200	$1.6^{+0.2}_{-0.2}$	$0.07^{+0.01}_{-0.00}$	...	0.03	$2.2^{+0.0}_{-0.0}$	2.3	0.05	0.00	2.8	$6.8^{+0.0}_{-0.1}$	...
BAT99-46	WN2–5w	NE	49.6 ± 1.0	0.8 ± 0.1	$5.43^{+0.04}_{-0.03}$	7	$-12.27^{+0.04}_{-0.04}$	1700	$3.8^{+0.5}_{-0.5}$	$0.36^{+0.02}_{-0.01}$	[b]$0.78^{+0.03}_{-0.03}$	0.05	$0.11^{+0.00}_{-0.01}$	0.16	$0.12^{+0.01}_{-0.00}$	0.03	0.01	$0.17^{+0.00}_{-0.01}$	0.10
BAT99-47	WN3–7s	NE	49.6 ± 1.0	$0.8^{+0.0}_{-0.1}$	$5.58^{+0.04}_{-0.03}$	7	$-12.00^{+0.04}_{-0.05}$	1600	$6.8^{+0.9}_{-0.9}$	$0.46^{+0.02}_{-0.02}$	...	0.01	0.07	$0.19^{+0.01}_{-0.00}$	0.13	0.02	0.00	$0.13^{+0.01}_{-0.00}$	0.02
BAT99-48	WN3–7s	NE	49.6 ± 1.0	$0.4^{+0.0}_{-0.1}$	$5.39^{+0.03}_{-0.02}$	7	$-11.74^{+0.05}_{-0.05}$	2000	$8.0^{+0.9}_{-0.9}$	$0.84^{+0.03}_{-0.02}$	[b]$0.70^{+0.01}_{-0.01}$	0.03	0.09	0.19	0.13	$0.08^{+0.00}_{-0.01}$	0.02	$0.14^{+0.00}_{-0.01}$	0.08
BAT99-50	WN2–5w	NE	49.6 ± 1.0	$0.7^{+0.0}_{-0.1}$	$5.64^{+0.03}_{-0.03}$	7	$-12.54^{+0.04}_{-0.04}$	1200	$1.8^{+0.2}_{-0.2}$	$0.11^{+0.00}_{-0.01}$	...	0.27	0.20	0.05	0.07	0.03	0.00	$0.27^{+0.01}_{-0.01}$	$0.15^{+0.00}_{-0.01}$
BAT99-51	WN3–7s	NE	49.6 ± 1.0	$0.1^{+0.0}_{-0.0}$	$5.29^{+0.02}_{-0.01}$	7	$-11.91^{+0.04}_{-0.05}$	2900	$3.9^{+0.4}_{-0.4}$	$0.52^{+0.01}_{-0.00}$	[b]$0.48^{+0.01}_{-0.00}$	0.03	0.06	0.11	0.15	0.01	0.00	0.19	0.05
BAT99-54	WN9–11	AR	49.6 ± 1.0	1.9 ± 0.2	$5.74^{+0.08}_{-0.07}$	7	$-13.15^{+0.04}_{-0.05}$	300	$1.7^{+0.4}_{-0.4}$	$0.08^{+0.00}_{-0.01}$	...	0.03	$0.17^{+0.00}_{-0.01}$	0.74	0.04	0.01	$0.17^{+0.00}_{-0.01}$	...	...
BAT99-56	WN3–7s	NE	49.6 ± 1.0	$0.5^{+0.0}_{-0.1}$	$5.55^{+0.03}_{-0.02}$	7	$-11.80^{+0.05}_{-0.04}$	1800	$7.8^{+0.9}_{-0.9}$	$0.56^{+0.02}_{-0.01}$	[b]$0.85^{+0.01}_{-0.02}$	0.04	0.10	0.21	0.13	0.07	0.02	0.14	0.08
BAT99-57	WN3–7s	NE	49.6 ± 1.0	$0.4^{+0.0}_{-0.1}$	$5.39^{+0.03}_{-0.02}$	7	$-11.80^{+0.04}_{-0.04}$	1800	$7.1^{+0.8}_{-0.8}$	$0.75^{+0.02}_{-0.02}$	[b]$0.66^{+0.01}_{-0.02}$	0.02	$0.10^{+0.00}_{-0.01}$	0.20	0.13	0.07	0.01	0.15	$0.07^{+0.00}_{-0.01}$
BAT99-58	WN6–8	AR	49.6 ± 1.0	1.9 ± 0.2	$5.63^{+0.08}_{-0.07}$	7	$-12.71^{+0.04}_{-0.04}$	1000	$4.6^{+1.2}_{-1.0}$	$0.28^{+0.02}_{-0.02}$	[b]$0.21^{+0.01}_{-0.02}$	$0.19^{+0.01}_{-0.01}$	$0.41^{+0.01}_{-0.02}$	0.36	0.10	0.06	$0.06^{+0.00}_{-0.01}$	[b]$0.40^{+0.03}_{-0.02}$	...
BAT99-60	WN2–5w + O	NE	49.6 ± 1.0	$0.4^{+0.0}_{-0.1}$	$5.46^{+0.03}_{-0.02}$	8	$-12.37^{+0.04}_{-0.05}$	1800	$1.9^{+0.2}_{-0.2}$	$0.17^{+0.00}_{-0.01}$	[b]$0.75^{+0.02}_{-0.01}$	$0.15^{+0.00}_{-0.01}$	0.00	0.19	0.10	0.02	0.00	$0.22^{+0.01}_{-0.00}$	0.03

Table A1 – *continued*

Star	Category	Data	d	A_V	log	Ref	log $F_{\rm HeII\ 4686}$	HeII 4686	$L_{\rm HeII\ 4686}$		$\frac{L_{\rm NIV\ 3478,85}}{L_{\rm HeII\ 4686}}$	$\frac{L_{\rm NIV\ 4058}}{L_{\rm HeII\ 4686}}$	$\frac{L_{4100}}{L_{\rm HeII\ 4686}}$	$\frac{L_{4630}}{L_{\rm HeII\ 4686}}$	$\frac{L_{\rm HeII\ 5412}}{L_{\rm HeII\ 4686}}$	$\frac{L_{\rm CIV\ 5801,12}}{L_{\rm HeII\ 4686}}$	$\frac{L_{\rm HeI\ 5876}}{L_{\rm HeII\ 4686}}$	$\frac{L_{\rm H\alpha}}{L_{\rm HeII\ 4686}}$	$\frac{L_{\rm NIV\ 7103.29}}{L_{\rm HeII\ 4686}}$
		ID	kpc	mag	$L_{\rm Bol}/L_\odot$		erg s^{-1} cm^{-2}	FWHM	10^{35} erg s^{-1}	10^{-3} $L_{\rm Bol}$									
BAT99-62	WN2–5w	NE	49.6 ± 1.0	$0.5^{+0.0}_{-0.1}$	$5.40^{+0.03}_{-0.02}$	7	$-12.23^{+0.04}_{-0.05}$	1800	$2.8^{+0.4}_{-0.3}$	$0.29^{+0.01}_{-0.01}$	[b]$1.02^{+0.02}_{-0.02}$	0.01	$0.09^{+0.00}_{-0.01}$	0.29	0.13	0.01	0.00	0.20	0.05
BAT99-63	WN2–5w	NE	49.6 ± 1.0	$0.4^{+0.0}_{-0.1}$	$5.57^{+0.03}_{-0.02}$	7	$-12.26^{+0.04}_{-0.04}$	1800	$2.5^{+0.3}_{-0.3}$	$0.17^{+0.01}_{-0.00}$	[b]$0.70^{+0.02}_{-0.01}$	$0.13^{+0.01}_{-0.00}$	$0.15^{+0.00}_{-0.01}$	0.12	$0.09^{+0.00}_{-0.01}$	0.05	0.00	$0.25^{+0.01}_{-0.00}$	$0.08^{+0.00}_{-0.01}$
BAT99-65	WN2–5w	NE	49.6 ± 1.0	1.74 ± 0.2	$5.74^{+0.07}_{-0.07}$	7	$-12.32^{+0.04}_{-0.04}$	1800	$9.2^{+2.1}_{-1.8}$	$0.43^{+0.03}_{-0.03}$	···	0.05	$0.10^{+0.01}_{-0.00}$	0.20	0.12	0.07	0.01	$0.12^{+0.01}_{-0.00}$	$0.08^{+0.00}_{-0.01}$
BAT99-66	WN2–5w	NE	49.6 ± 1.0	$0.5^{+0.0}_{-0.1}$	$5.77^{+0.03}_{-0.02}$	7	$-12.48^{+0.04}_{-0.05}$	2000	$1.7^{+0.2}_{-0.2}$	$0.07^{+0.01}_{-0.00}$	···	0.00	0.08	0.35	0.12	0.01	0.00	$0.24^{+0.00}_{-0.01}$	0.02
BAT99-67	WN2–5w	NE	49.6 ± 1.0	$1.2^{+0.2}_{-0.1}$	$5.95^{+0.06}_{-0.05}$	7	$-12.18^{+0.04}_{-0.05}$	1600	$7.7^{+1.3}_{-1.3}$	$0.22^{+0.01}_{-0.01}$	[b]$0.55^{+0.03}_{-0.03}$	$0.27^{+0.01}_{-0.01}$	$0.52^{+0.01}_{-0.01}$	0.00	$0.13^{+0.01}_{-0.00}$	0.03	0.00	$0.30^{+0.01}_{-0.02}$	$0.15^{+0.01}_{-0.00}$
BAT99-73	WN2–5w	NE	49.6 ± 1.0	$0.8^{+0.0}_{-0.1}$	$5.71^{+0.04}_{-0.03}$	7	$-12.68^{+0.04}_{-0.05}$	1300	$1.4^{+0.2}_{-0.2}$	$0.07^{+0.00}_{-0.00}$	···	0.22	0.13	0.00	0.08	0.03	0.00	$0.32^{+0.01}_{-0.01}$	$0.15^{+0.00}_{-0.01}$
BAT99-74	WN2–5w	NE	49.6 ± 1.0	$0.8^{+0.0}_{-0.1}$	$5.68^{+0.04}_{-0.03}$	7	$-12.82^{+0.05}_{-0.04}$	2200	$1.0^{+0.1}_{-0.1}$	$0.06^{+0.00}_{-0.01}$	···	0.00	0.00	0.50	0.09	0.01	0.00	$0.21^{+0.01}_{-0.00}$	0.00
BAT99-75	WN2–5w	NE	49.6 ± 1.0	$0.3^{+0.0}_{-0.1}$	$5.55^{+0.02}_{-0.02}$	7	$-11.95^{+0.04}_{-0.04}$	1700	$4.4^{+0.5}_{-0.4}$	$0.32^{+0.01}_{-0.00}$	···	0.11	0.17	0.18	$0.14^{+0.00}_{-0.01}$	0.09	0.02	0.17	$0.11^{+0.01}_{-0.00}$
BAT99-76	WN9–11	AR + SC	49.6 ± 1.0	1.0 ± 0.1	$5.65^{+0.05}_{-0.04}$	7	$-12.55^{+0.04}_{-0.05}$	200	$2.4^{+0.4}_{-0.3}$	$0.14^{+0.01}_{-0.01}$	[b]0.00	0.00	$0.88^{+0.01}_{-0.02}$	1.07	0.01	0.01	$0.57^{+0.01}_{-0.02}$	$1.66^{+0.06}_{-0.06}$	···
BAT99-78	WN2–5w	HF	49.6 ± 1.0	$0.8^{+0.0}_{-0.1}$	$5.69^{+0.04}_{-0.03}$	7	$-13.08^{+0.04}_{-0.05}$	1500	$0.6^{+0.0}_{-0.1}$	$0.03^{+0.00}_{-0.00}$	$0.56^{+0.02}_{-0.01}$	0.11	$0.15^{+0.00}_{-0.01}$	0.11	···	···	···	···	···
BAT99-81	WN2–5w	NE	49.6 ± 1.0	$1.2^{+0.2}_{-0.1}$	$5.47^{+0.06}_{-0.05}$	7	$-12.87^{+0.04}_{-0.04}$	1100	$1.6^{+0.3}_{-0.3}$	$0.14^{+0.01}_{-0.01}$	···	$0.43^{+0.01}_{-0.01}$	$0.42^{+0.01}_{-0.01}$	0.12	0.08	$0.12^{+0.01}_{-0.00}$	0.00	$0.35^{+0.02}_{-0.01}$	$0.11^{+0.00}_{-0.01}$
BAT99-82	WN3–7s	NE	49.6 ± 1.0	1.0 ± 0.1	$5.52^{+0.05}_{-0.04}$	7	$-12.30^{+0.04}_{-0.04}$	2000	$4.6^{+0.7}_{-0.7}$	$0.36^{+0.01}_{-0.02}$	[b]$0.13^{+0.01}_{-0.00}$	0.00	0.06	0.17	0.13	0.00	0.00	$0.15^{+0.01}_{-0.01}$	···
BAT99-86	WN2–5w	NE	49.6 ± 1.0	$1.4^{+0.1}_{-0.2}$	$5.32^{+0.06}_{-0.05}$	7	$-12.98^{+0.04}_{-0.04}$	1900	$1.4^{+0.2}_{-0.3}$	$0.17^{+0.01}_{-0.01}$	[b]$1.25^{+0.08}_{-0.07}$	0.02	0.10	0.23	$0.12^{+0.01}_{-0.00}$	0.02	0.01	$0.28^{+0.01}_{-0.02}$	0.02
BAT99-89	WN6–8	AR	49.6 ± 1.0	$1.1^{+0.1}_{-0.2}$	$5.77^{+0.05}_{-0.04}$	7	$-11.97^{+0.04}_{-0.05}$	1100	$10.0^{+1.6}_{-1.5}$	$0.44^{+0.02}_{-0.02}$	···	$0.17^{+0.00}_{-0.01}$	$0.32^{+0.01}_{-0.00}$	0.30	0.12	$0.04^{+0.00}_{-0.01}$	$0.10^{+0.01}_{-0.00}$	···	···
BAT99-91	WN6–8	HF	49.6 ± 1.0	$1.2^{+0.1}_{-0.2}$	$5.41^{+0.06}_{-0.05}$	7	$-12.43^{+0.04}_{-0.05}$	900	$4.3^{+0.7}_{-0.7}$	$0.43^{+0.02}_{-0.02}$	$0.17^{+0.01}_{-0.01}$	$0.16^{+0.00}_{-0.01}$	$0.28^{+0.00}_{-0.01}$	$0.24^{+0.00}_{-0.01}$	···	···	···	···	···
BAT99-94	WN3–7s	NE	49.6 ± 1.0	1.1 ± 0.1	$5.79^{+0.05}_{-0.04}$	7	$-11.69^{+0.04}_{-0.05}$	3300	$20.0^{+3.3}_{-3.0}$	$0.83^{+0.05}_{-0.04}$	[b]$0.65^{+0.03}_{-0.03}$	0.00	0.10	0.10	0.13	0.06	0.00	$0.15^{+0.01}_{-0.00}$	$0.09^{+0.01}_{-0.00}$
BAT99-95	WN6–8	AR + SC	49.6 ± 1.0	0.9 ± 0.1	$5.99^{+0.04}_{-0.04}$	7	$-11.48^{+0.05}_{-0.04}$	1600	$27.8^{+4.2}_{-3.9}$	$0.73^{+0.04}_{-0.03}$	···	0.14	$0.32^{+0.01}_{-0.00}$	0.27	$0.11^{+0.00}_{-0.01}$	0.02	$0.13^{+0.00}_{-0.01}$	$0.28^{+0.01}_{-0.01}$	···
BAT99-96	WN6–8	VM	49.6 ± 1.0	$2.6^{+0.3}_{-0.2}$	$6.34^{+0.11}_{-0.10}$	7	$-12.24^{+0.08}_{-0.09}$	900	$31.3^{+12.3}_{-10.1}$	$0.37^{+0.03}_{-0.03}$	···	···	···	$0.51^{+0.01}_{-0.00}$	$0.10^{+0.00}_{-0.01}$	0.01	$0.15^{+0.01}_{-0.01}$	$0.21^{+0.02}_{-0.02}$	$0.05^{+0.01}_{-0.00}$
BAT99-97	Of/WN	VM	49.6 ± 1.0	$2.3^{+0.2}_{-0.3}$	$6.29^{+0.09}_{-0.09}$	7	$-12.83^{+0.08}_{-0.10}$	800	$5.3^{+1.8}_{-1.6}$	$0.07^{+0.01}_{-0.01}$	···	···	···	$0.41^{+0.01}_{-0.00}$	0.01	0.02	0.00	$0.58^{+0.05}_{-0.4}$	···
BAT99-98	WN6–8	VM	49.6 ± 1.0	$1.5^{+0.1}_{-0.2}$	···	2	$-11.93^{+0.08}_{-0.10}$	1260	$17.6^{+4.7}_{-4.4}$	···	···	···	···	0.21	0.08	0.02	0.02	$0.35^{+0.02}_{-0.02}$	$0.07^{+0.00}_{-0.01}$
BAT99-99	Of/WN + O	VM	49.6 ± 1.0	$1.1^{+0.1}_{-0.1}$	$5.89^{+0.05}_{-0.05}$	7	$-12.65^{+0.08}_{-0.09}$	1100	$2.3^{+0.6}_{-0.5}$	$0.08^{+0.00}_{-0.01}$	···	···	···	0.19	0.01	0.08	0.00	$0.82^{+0.03}_{-0.04}$	$0.15^{+0.01}_{-0.01}$
BAT99-100	WN6–8	HF + VM	49.6 ± 1.0	$1.1^{+0.1}_{-0.2}$	$6.14^{+0.05}_{-0.04}$	7	$-11.52^{+0.04}_{-0.05}$	1000	$28.2^{+4.5}_{-4.2}$	$0.53^{+0.02}_{-0.03}$	$0.10^{+0.01}_{-0.00}$	0.12	$0.25^{+0.01}_{-0.00}$	0.25	$0.10^{+0.00}_{-0.01}$	0.02	$0.12^{+0.00}_{-0.01}$	$0.24^{+0.01}_{-0.01}$	0.04
BAT99-103	WN6–8 + O	VM	49.6 ± 1.0	0.9 ± 0.1	$6.08^{+0.03}_{-0.04}$	8	$-11.67^{+0.08}_{-0.09}$	1300	$17.8^{+4.1}_{-4.0}$	$0.38^{+0.03}_{-0.02}$	···	···	···	0.25	$0.10^{+0.01}_{-0.00}$	0.01	0.05	$0.21^{+0.01}_{-0.01}$	$0.07^{+0.01}_{-0.00}$
BAT99-104	Of/WN	VM	49.6 ± 1.0	$1.4^{+0.2}_{-0.1}$	$6.05^{+0.06}_{-0.06}$	7	$-12.74^{+0.08}_{-0.09}$	1100	$2.6^{+0.7}_{-0.6}$	$0.06^{+0.00}_{-0.00}$	···	···	···	0.10	0.04	0.01	0.00	$0.46^{+0.02}_{-0.02}$	$0.06^{+0.00}_{-0.01}$
BAT99-106	WN5–7h	HF	49.6 ± 1.0	1.7 ± 0.2	$6.52^{+0.07}_{-0.07}$	5	$-11.74^{+0.04}_{-0.05}$	2000	$32.4^{+7.2}_{-6.3}$	$0.25^{+0.02}_{-0.01}$	$0.43^{+0.03}_{-0.02}$	$0.22^{+0.01}_{-0.00}$	$0.21^{+0.00}_{-0.01}$	0.07	$0.10^{+0.00}_{-0.01}$	0.04	0.00	$0.40^{+0.02}_{-0.02}$	···
BAT99-108	WN5–7h	HF	49.6 ± 1.0	1.8 ± 0.2	$6.88^{+0.07}_{-0.07}$	5	$-11.61^{+0.04}_{-0.05}$	2000	$49.1^{+11.5}_{-9.9}$	$0.17^{+0.01}_{-0.01}$	$0.48^{+0.03}_{-0.03}$	$0.19^{+0.00}_{-0.01}$	$0.18^{+0.00}_{-0.01}$	0.10	$0.12^{+0.00}_{-0.01}$	0.05	0.0	$0.36^{+0.02}_{-0.02}$	···
BAT99-109	WN5–7h	HF	49.6 ± 1.0	1.9 ± 0.2	$6.70^{+0.08}_{-0.08}$	5	$-11.79^{+0.05}_{-0.04}$	2000	$36.5^{+8.9}_{-7.7}$	$0.19^{+0.01}_{-0.01}$	$0.45^{+0.03}_{-0.03}$	$0.19^{+0.00}_{-0.01}$	$0.17^{+0.00}_{-0.01}$	0.08	0.11	0.04	0.00	$0.33^{+0.02}_{-0.01}$	···
BAT99-110	Of/WN	HF	49.6 ± 1.0	$1.7^{+0.2}_{-0.1}$	$6.32^{+0.07}_{-0.07}$	5,10	$-12.83^{+0.04}_{-0.04}$	1700	$2.8^{+0.6}_{-0.6}$	$0.03^{+0.01}_{-0.00}$	$0.30^{+0.02}_{-0.01}$	$0.22^{+0.01}_{-0.01}$	0.00	0.19	0.00	0.00	0.00	$0.55^{+0.03}_{-0.03}$	···
BAT99-111	WN6–8[c]	HF	49.6 ± 1.0	$1.6^{+0.2}_{-0.1}$	$6.24^{+0.07}_{-0.06}$	7	$-12.75^{+0.04}_{-0.05}$	600	$3.1^{+0.7}_{-0.6}$	$0.05^{+0.00}_{-0.01}$	0.00	$0.13^{+0.00}_{-0.01}$	0.11	0.63	0.00	0.00	0.04	$0.69^{+0.05}_{-0.04}$	···
BAT99-112	WN5–7h	HF + VM	49.6 ± 1.0	$2.5^{+0.3}_{-0.2}$	$6.49^{+0.10}_{-0.10}$	5	$-11.97^{+0.04}_{-0.05}$	1600	$45.2^{+14.6}_{-11.5}$	$0.38^{+0.03}_{-0.03}$	$0.33^{+0.03}_{-0.03}$	$0.15^{+0.01}_{-0.00}$	$0.16^{+0.01}_{-0.00}$	0.06	$0.06^{+0.01}_{-0.00}$	0.01	0.00	$0.24^{+0.02}_{-0.02}$	$0.06^{+0.01}_{-0.00}$
BAT99-113	Of/WN + O	VM	49.6 ± 1.0	$1.2^{+0.2}_{-0.1}$	$6.13^{+0.06}_{-0.05}$	8	$-12.54^{+0.07}_{-0.10}$	1100	$2.9^{+0.7}_{-0.7}$	$0.06^{+0.00}_{-0.01}$	···	···	···	0.09	0.03	0.04	0.00	$0.50^{+0.02}_{-0.02}$	···
BAT99-114	Of/WN	VM	49.6 ± 1.0	$1.2^{+0.2}_{-0.1}$	$6.43^{+0.05}_{-0.05}$	7	$-12.74^{+0.08}_{-0.09}$	1000	$2.0^{+0.4}_{-0.5}$	$0.02^{+0.00}_{-0.00}$	···	···	···	0.12	0.03	0.07	0.00	$0.64^{+0.03}_{-0.03}$	$0.13^{+0.01}_{-0.00}$
BAT99-116	2×WN5–7h	VM	49.6 ± 1.0	2.0 ± 0.2	$6.70^{+0.08}_{-0.09}$	11	$-11.87^{+0.08}_{-0.10}$	1800	$33.3^{+10.4}_{-9.3}$	$0.17^{+0.01}_{-0.01}$	···	···	···	0.05	0.07	$0.04^{+0.00}_{-0.01}$	$0.03^{+0.01}_{-0.00}$	$0.39^{+0.03}_{-0.02}$	$0.11^{+0.01}_{-0.01}$
BAT99-117	WN5–7h	NE	49.6 ± 1.0	0.7 ± 0.1	$6.39^{+0.04}_{-0.03}$	7	$-11.82^{+0.05}_{-0.04}$	2000	$9.9^{+1.3}_{-1.12}$	$0.10^{+0.01}_{-0.00}$	[b]$0.68^{+0.02}_{-0.02}$	$0.09^{+0.01}_{-0.00}$	0.03	0.00	$0.07^{+0.01}_{-0.00}$	0.01	0.00	$0.24^{+0.01}_{-0.01}$	0.11
BAT99-118	2×WN6–8	AR + SC	49.6 ± 1.0	$0.6^{+0.1}_{-0.0}$	$6.71^{+0.03}_{-0.03}$	12	$-10.86^{+0.04}_{-0.05}$	1400	$80.1^{+10.0}_{-9.7}$	$0.41^{+0.01}_{-0.02}$	···	0.15	$0.26^{+0.00}_{-0.01}$	0.15	0.09	0.04	0.04	$0.41^{+0.00}_{-0.01}$	···

Table A1 – *continued*

Star	Category	Data ID	d kpc	A_V mag	log $L_{Bol}/L_\odot$	Ref	log $F_{HeII\ 4686}$ erg s^{-1} cm^{-2}	HeII 4686 FWHM	$L_{HeII\ 4686}$ 10^{35} erg s^{-1}	$L_{HeII\ 4686}$ 10^{-3} L_{Bol}	$L_{NIV\ 3478,85}$ / $L_{HeII\ 4686}$	$L_{NIV\ 4058}$ / $L_{HeII\ 4686}$	L_{4100} / $L_{HeII\ 4686}$	L_{4630} / $L_{HeII\ 4686}$	$L_{HeII\ 5412}$ / $L_{HeII\ 4686}$	$L_{CIV\ 5801,12}$ / $L_{HeII\ 4686}$	$L_{HeI\ 5876}$ / $L_{HeII\ 4686}$	$L_{H\alpha}$ / $L_{HeII\ 4686}$	$L_{NIV\ 7103,29}$ / $L_{HeII\ 4686}$
BAT99-119	WN6–8 + O	AR + SC	49.6 ± 1.0	$1.1^{+0.1}_{-0.2}$	$6.63^{+0.05}_{-0.04}$	8	$-11.34^{+0.04}_{-0.04}$	1100	$43.3^{+7.0}_{-6.5}$	$0.26^{+0.01}_{-0.01}$	$0.17^{+0.01}_{-0.01}$	0.17	$0.23^{+0.01}_{-0.00}$	0.17	$0.10^{+0.01}_{-0.00}$	0.05	0.03	$0.32^{+0.02}_{-0.01}$	···
BAT99-120	WN9–11	AR + SC	49.6 ± 1.0	$0.6^{+0.0}_{-0.1}$	$5.57^{+0.03}_{-0.03}$	7	$-12.30^{+0.04}_{-0.05}$	300	$2.7^{+0.4}_{-0.3}$	$0.19^{+0.01}_{-0.01}$	···	0.03	$0.86^{+0.01}_{-0.01}$	$1.34^{+0.01}_{-0.00}$	0.02	0.01	$0.45^{+0.00}_{-0.01}$	$1.54^{+0.03}_{-0.03}$	···
BAT99-122	WN5–7h	NE	49.6 ± 1.0	$1.1^{+0.1}_{-0.2}$	$6.22^{+0.05}_{-0.04}$	7	$-11.50^{+0.04}_{-0.05}$	1300	$29.5^{+4.7}_{-4.4}$	$0.46^{+0.02}_{-0.02}$	[b]$0.23^{+0.01}_{-0.01}$	$0.25^{+0.00}_{-0.01}$	$0.35^{+0.01}_{-0.01}$	$0.10^{+0.00}_{-0.01}$	0.11	0.04	0.02	$0.31^{+0.01}_{-0.02}$	$0.11^{+0.01}_{-0.00}$
BAT99-128	WN3–7s	NE	49.6 ± 1.0	$0.6^{+0.1}_{-0.0}$	$5.43^{+0.03}_{-0.03}$	7	$-12.00^{+0.05}_{-0.04}$	1800	$6.0^{+0.8}_{-0.7}$	$0.58^{+0.02}_{-0.02}$	···	0.01	0.06	0.18	$0.15^{+0.00}_{-0.01}$	0.01	0.08	$0.17^{+0.01}_{-0.00}$	0.01
BAT99-130	WN9–11	AR + SC	49.6 ± 1.0	$0.9^{+0.1}_{-0.1}$	$5.67^{+0.04}_{-0.04}$	7	$-13.42^{+0.04}_{-0.05}$	200	$0.3^{+0.1}_{-0.0}$	$0.02^{+0.00}_{-0.00}$	···	0.00	$2.2^{+0.1}_{-0.0}$	$4.2^{+0.0}_{-0.0}$	0.00	0.00	$3.3^{+0.1}_{-0.1}$	12^{+0}_{-0}	···
BAT99-131	WN3–7s	NE	49.6 ± 1.0	$0.5^{+0.0}_{-0.1}$	$5.66^{+0.03}_{-0.02}$	7	$-11.65^{+0.04}_{-0.04}$	1600	$11.4^{+1.3}_{-1.3}$	$0.64^{+0.02}_{-0.02}$	···	0.06	$0.10^{+0.00}_{-0.01}$	0.19	0.14	0.04	0.01	$0.14^{+0.01}_{-0.00}$	$0.09^{+0.01}_{-0.00}$
BAT99-132	WN3–7s	NE	49.6 ± 1.0	$0.9^{+0.0}_{-0.1}$	$5.57^{+0.04}_{-0.04}$	7	$-11.69^{+0.05}_{-0.04}$	1900	$15.8^{+2.2}_{-2.2}$	$1.10^{+0.05}_{-0.06}$	[b]$0.64^{+0.03}_{-0.02}$	0.06	$0.11^{+0.01}_{-0.00}$	0.16	0.14	0.04	0.01	$0.18^{+0.01}_{-0.01}$	$0.11^{+0.01}_{-0.00}$
BAT99-133	WN9–11	AR + SC	49.6 ± 1.0	$0.4^{+0.1}_{-0.0}$	$5.68^{+0.02}_{-0.02}$	7	$-12.98^{+0.04}_{-0.05}$	200	$0.5^{+0.0}_{-0.1}$	$0.03^{+0.00}_{-0.01}$	···	0.00	$1.5^{+0.0}_{-0.1}$	$1.7^{+0.0}_{-0.0}$	0.00	0.00	$2.2^{+0.0}_{-0.1}$	$5.4^{+0.1}_{-0.1}$	···
BAT99-134	WN3–7s	NE	49.6 ± 1.0	0.2 ± 0.0	$5.50^{+0.02}_{-0.02}$	7	$-11.62^{+0.04}_{-0.05}$	2100	$9.0^{+0.9}_{-0.9}$	$0.73^{+0.02}_{-0.01}$	[b]$0.57^{+0.01}_{-0.01}$	0.04	0.08	0.17	$0.12^{+0.01}_{-0.00}$	0.06	0.02	$0.15^{+0.01}_{-0.00}$	$0.05^{+0.01}_{-0.00}$
LMC 170–2	WN2–5w	MM	49.6 ± 1.0	0.4 ± 0.0	$5.68^{+0.03}_{-0.02}$	14	$-13.45^{+0.04}_{-0.05}$	1900	$0.16^{+0.02}_{-0.02}$	$0.01^{+0.00}_{-0.00}$	0.00	0.01	0.00	0.38	0.04	0.01	0.00	0.19	0.00
VFTS 682	WN5–7h	VX	49.6 ± 1.0	4.6 ± 0.5	$6.46^{+0.19}_{-0.18}$	13	$-13.21^{+0.04}_{-0.05}$	1800	$22.2^{+14.0}_{-8.8}$	$0.20^{+0.02}_{-0.02}$	$0.50^{+0.07}_{-0.06}$	$0.18^{+0.01}_{-0.02}$	$0.17^{+0.01}_{-0.01}$	0.10	0.08	0.04	0.00	$0.46^{+0.06}_{-0.05}$	$0.17^{+0.02}_{-0.02}$
AB1	WN2–5w	NE	61.2 ± 1.2	0.8 ± 0.1	$6.08^{+0.04}_{-0.03}$	15	$-12.92^{+0.04}_{-0.04}$	1500	$1.4^{+0.2}_{-0.2}$	$0.03^{+0.00}_{-0.00}$	···	0.06	0.00	0.26	0.10	0.00	0.00	$0.38^{+0.01}_{-0.01}$	0.00
AB2	WN2–5w	NE	61.2 ± 1.2	$0.4^{+0.0}_{-0.1}$	$5.58^{+0.03}_{-0.02}$	15	$-12.76^{+0.04}_{-0.05}$	1000	$1.2^{+0.1}_{-0.2}$	$0.08^{+0.00}_{-0.00}$	···	0.25	0.00	0.00	0.05	0.05	0.00	$0.46^{+0.01}_{-0.00}$	0.22
AB3	WN2–5w + O	CS	61.2 ± 1.2	$0.6^{+0.0}_{-0.1}$	$5.94^{+0.03}_{-0.02}$	16	$-12.36^{+0.04}_{-0.04}$	1600	$3.6^{+0.5}_{-0.4}$	$0.11^{+0.00}_{-0.01}$	$0.58^{+0.02}_{-0.01}$	0.05	0.03	0.23	···	···	···	···	···
AB4	WN6–8	AR	61.2 ± 1.2	$0.3^{+0.1}_{-0.0}$	$5.79^{+0.03}_{-0.02}$	15	$-11.94^{+0.04}_{-0.05}$	900	$7.4^{+0.8}_{-0.8}$	$0.31^{+0.01}_{-0.01}$	[b]$0.28^{+0.00}_{-0.01}$	0.13	0.12	0.06	0.10	0.02	0.00	0.24	0.07
AB5	2×WN6–8	HS	61.2 ± 1.2	$0.2^{+0.1}_{-0.0}$	$6.49^{+0.02}_{-0.02}$	17,18	$-11.09^{+0.04}_{-0.05}$	1300	$47.0^{+5.0}_{-4.9}$	$0.39^{+0.01}_{-0.01}$	$0.18^{+0.01}_{-0.00}$	0.04	0.08	0.01	0.10	0.04	0.04	$0.22^{+0.00}_{-0.01}$	0.06
AB6	WN2–5w + O	AR + CS	61.2 ± 1.2	0.2 ± 0.0	$6.29^{+0.02}_{-0.02}$	16	$-12.35^{+0.04}_{-0.05}$	1900	$2.5^{+0.3}_{-0.3}$	$0.03^{+0.00}_{-0.00}$	···	0.00	0.00	0.21	···	···	···	···	···
AB7	WN2–5w + O	AR	61.2 ± 1.2	$0.2^{+0.1}_{-0.0}$	$6.11^{+0.02}_{-0.02}$	16	$-12.20^{+0.04}_{-0.05}$	1700	$3.7^{+0.4}_{-0.4}$	$0.07^{+0.01}_{-0.00}$	···	0.00	0.00	0.00	0.05	0.00	0.00	$0.13^{+0.01}_{-0.00}$	0.00
AB9	WN2–5w	NE	61.2 ± 1.2	$0.3^{+0.1}_{-0.0}$	$6.06^{+0.03}_{-0.02}$	15	$-12.96^{+0.04}_{-0.05}$	1700	$0.7^{+0.1}_{-0.1}$	$0.02^{+0.00}_{-0.00}$	···	0.00	0.00	0.19	0.07	0.00	0.00	0.18	0.00
AB10	WN2–5w	NE	61.2 ± 1.2	$0.5^{+0.0}_{-0.1}$	$5.66^{+0.03}_{-0.02}$	15	$-13.02^{+0.04}_{-0.04}$	1900	$0.7^{+0.1}_{-0.1}$	$0.04^{+0.00}_{-0.00}$	···	0.02	0.00	0.35	0.06	0.00	0.00	[d]0.33	0.00
AB11	WN2–5w	NE	61.2 ± 1.2	$0.4^{+0.1}_{-0.0}$	$5.86^{+0.03}_{-0.02}$	15	$-13.15^{+0.04}_{-0.04}$	1700	$0.5^{+0.1}_{-0.1}$	$0.02^{+0.00}_{-0.00}$	···	0.00	0.00	0.36	0.02	0.03	0.00	$0.20^{+0.01}_{-0.00}$	0.00
AB12	WN2–5w	NE	61.2 ± 1.2	$0.5^{+0.1}_{-0.0}$	$5.91^{+0.03}_{-0.02}$	15	$-13.06^{+0.04}_{-0.05}$	1700	$0.7^{+0.1}_{-0.1}$	$0.02^{+0.00}_{-0.00}$	···	0.00	0.00	0.13	0.05	0.00	0.00	$0.14^{+0.00}_{-0.01}$	0.00

Notes. 1: Hamann et al. (2006); 2: Crowther & Hadfield (2006); 3: Crowther et al. (1995a); 4: Smith, Crowther & Prinja (1994); 5: Crowther et al. (2010); 6: Bohannan & Crowther (1999); 7: Hainich et al. (2014); 8: Shenar et al. (2019); 9: Crowther & Smith (1997); 10: Brands et al. (2022); 11: Tehrani et al. (2019); 12: Shenar et al. (2021); 13: M. Rubio-Diez et al. (in preparation); 14: Neugent et al. (2017); 15: Hainich et al. (2015); 16: Shenar et al. (2016); 17: Koenigsberger et al. (2014); 18: Hillier et al. (2019).
[a] CASPEC observations (Schmutz 1997). [b] SIT observations (Torres-Dodgen & Massey 1988). [c] MUSE/NFM observations (Castro et al. 2021). [d] *CTIO*/R-C spectrograph observations (Foellmi, Moffat & Guerrero 2003).

Table A2. Luminosities of prominent optical emission lines of Galactic (WR) and LMC (BAT99) WN/C, categorized as either strong-lined (WN3–7s/C) or early/late weak-lined (WN2–5w/C or WN6–8/C) for consistency with WN stars. He II λ4686 FWHM are also provided in km s^{-1} (±100 km s^{-1}). The feature at λ4100 involves N III λλ4097,4103, Si IV λλ4088,4116, and He II λ4100 + H δ, while the feature at λλ4630 involves N V λλ4603,20, N III λλ4634,41, and C III λλ4647,51. Stars included in spectral templates are indicated in bold.

Star	Category	Data ID	d kpc	A_V mag	log $L_{Bol}/L_\odot$	Ref	log $F_{HeII\ 4686}$ erg s^{-1} cm^{-2}	HeII 4686 FWHM	$L_{HeII\ 4686}$ 10^{35} erg s^{-1}	$L_{HeII\ 4686}$ 10^{-3} L_{Bol}	$L_{NIV\ 3478.85}/L_{HeII\ 4686}$	$L_{NIV\ 4058}/L_{HeII\ 4686}$	$L_{4100}/L_{HeII\ 4686}$	$L_{4630}/L_{HeII\ 4686}$	$L_{HeII\ 5412}/L_{HeII\ 4686}$	$L_{CIII\ 5696}/L_{HeII\ 4686}$	$L_{CIV\ 5801.12}/L_{HeII\ 4686}$	$L_{HeII\ 6560}/L_{HeII\ 4686}$	$L_{NIV\ 7103.29}/L_{HeII\ 4686}$
WR8	WN6–8/C	CS	3.5 ± 0.2	2.7 ± 0.3	$5.61^{+0.11}_{-0.12}$	1	$-10.64^{+0.04}_{-0.05}$	1300	$6.9^{+2.6}_{-2.0}$	$0.45^{+0.06}_{-0.06}$	$0.82^{+0.07}_{-0.06}$	$0.91^{+0.04}_{-0.04}$	$0.87^{+0.04}_{-0.03}$	$3.36^{+0.01}_{-0.01}$	$0.13^{+0.01}_{-0.00}$	$0.03^{+0.01}_{-0.00}$	$0.67^{+0.06}_{-0.04}$	$0.15^{+0.02}_{-0.01}$	...
WR26	WN3–7s/C	CS	$6.6^{+0.8}_{-0.6}$	4.7 ± 0.5	$5.72^{+0.21}_{-0.21}$	1	$-12.07^{+0.04}_{-0.04}$	2400	$8.8^{+6.3}_{-3.8}$	$0.44^{+0.13}_{-0.10}$	$0.64^{+0.09}_{-0.08}$	—	$0.68^{+0.04}_{-0.05}$	—	$3.09^{+0.01}_{-0.01}$	$0.21^{+0.02}_{-0.02}$	0.00	$2.28^{+0.32}_{-0.27}$	$0.17^{+0.04}_{-0.03}$	...
WR58	WN3–7s/C	CS	$6.7^{+0.5}_{-0.4}$	1.9 ± 0.2	$5.01^{+0.10}_{-0.11}$	1	$-11.13^{+0.04}_{-0.04}$	2200	$3.6^{+1.0}_{--0.8}$	$0.93^{+0.14}_{-0.12}$	$0.67^{+0.04}_{-0.04}$	$0.17^{+0.01}_{-0.00}$	$0.21^{+0.01}_{-0.01}$	0.28	$0.15^{+0.01}_{-0.00}$	0.00	$0.26^{+0.02}_{-0.01}$	$0.21^{+0.02}_{-0.02}$	...
WR98	WN6–8/C	CS	2.2 ± 0.1	5.0 ± 0.5	$5.69^{+0.20}_{-0.21}$	1	$-11.80^{+0.04}_{-0.04}$	1100	$3.1^{+2.5}_{-1.4}$	$0.17^{+0.04}_{-0.03}$	...	...	...	$2.29^{+0.01}_{-0.01}$	$0.12^{+0.01}_{-0.01}$	$0.18^{+0.03}_{-0.03}$	$0.30^{+0.06}_{-0.04}$	$0.11^{+0.04}_{-0.02}$	...
WR126	WN2–5w/C	KI	$11.3^{+1.1}_{-1.0}$	$3.6^{+0.3}_{-0.4}$	$6.25^{+0.16}_{-0.17}$	1	$-12.20^{+0.04}_{-0.05}$	1700	$5.2^{+2.7}_{-1.9}$	$0.08^{+0.02}_{-0.02}$	...	—	$0.73^{+0.04}_{-0.04}$	—	$3.93^{+-0.01}_{-0.02}$	$0.30^{+0.02}_{-0.02}$	0.00	$3.97^{+0.41}_{-0.38}$	$0.33^{+0.05}_{-0.05}$	$0.34^{+0.06}_{-0.06}$
WR145	WN6–8/C + O	WI94	1.6 ± 0.0	7.0 ± 0.7	$5.71^{+0.28}_{-0.28}$	1	$-11.94^{+0.04}_{-0.05}$	1300	$9.5^{+11.4}_{-5.3}$	$0.48^{+0.10}_{-0.09}$	...	...	...	$0.82^{+0.01}_{-0.00}$	$0.13^{+0.02}_{-0.02}$	0.01	$0.63^{+0.14}_{-0.11}$	...	...
WR153	WN6–8/C + O	II91	4.5 ± 0.3	$2.1^{+0.3}_{-0.2}$	...	2	$-10.45^{+0.08}_{-0.09}$	1400	$9.7^{+3.4}_{-2.9}$	...	...	...	...	0.52	$0.22^{+0.01}_{-0.01}$	0.00	$0.53^{+0.03}_{-0.03}$	$0.28^{+0.02}_{-0.02}$	$0.20^{+0.02}_{-0.02}$
BAT99-36	WN3–7s/C	AR	49.6 ± 1.0	$0.5^{+0.0}_{-0.1}$	$5.70^{+0.03}_{-0.02}$	3	$-11.73^{+0.05}_{-0.04}$	2100	$9.5^{+1.1}_{-1.1}$	$0.49^{+0.02}_{-0.02}$	[a]$0.60^{+0.01}_{-0.01}$	0.03	0.08	0.24	0.12	0.00	$1.17^{+0.02}_{-0.01}$	...	...
BAT99-88	WN3–7s/C	NE	49.6 ± 1.0	$3.2^{+0.3}_{-0.4}$	$5.79^{+0.13}_{-0.12}$	3	$-12.97^{+0.04}_{-0.05}$	2900	$10.3^{+4.5}_{-3.2}$	$0.43^{+0.05}_{-0.04}$	...	0.00	$0.09^{+0.00}_{-0.01}$	0.17	$0.11^{+0.01}_{-0.01}$	0.00	$1.52^{+0.12}_{-0.12}$	$0.15^{+0.02}_{-0.02}$	$0.05^{+0.01}_{-0.01}$

Notes. 1: Sander et al. (2012); 2: Crowther & Hadfield (2006); 3: Hainich et al. (2014).
[a]SIT observations (Torres-Dodgen & Massey 1988).

Table A3. Luminosities of prominent optical emission lines of Galactic (WR) and LMC (BAT99) WC stars, categorised as early-type (WC4–5), mid-type (WC6–7) or late-type (WC8–9) stars. C IV λλ5801,12 FWHM are also provided in km s^{-1} (±100 km s^{-1}). The feature at 6559–81 involves He II 6560 and C II λλ6559,81. Stars included in spectral templates are indicated in bold (the remainder are excluded owing to limited spectral coverage).

WR	Category	Data ID	d kpc	A_V mag	log $L_{Bol}/L_\odot$	Ref	log $F_{CIV\ 5801,\ 12}$ erg s^{-1} cm^{-2}	CIV 5801,12 FWHM	$L_{CIV\ 5801,\ 12}$ 10^{35} erg s^{-1}	$L_{CIV\ 5801,\ 12}$ 10^{-3} L_{Bol}	$L_{OIV\ 3403,13}/L_{5801,\ 12}$	$L_{CIII\ 4647,51}/L_{5801,\ 12}$	$L_{HeII\ 4686}/L_{5801,\ 12}$	$L_{CIII\ 5696}/L_{5801,\ 12}$	$L_{HeI\ 5876}/L_{5801-12}$	$L_{6559-81}/L_{5801,\ 12}$	$L_{CIII\ 6727,73}/L_{5801,\ 12}$	$L_{CIV\ 7725}/L_{5801,\ 12}$	$L_{CIII\ 9701,19}/L_{5801,\ 12}$
WR4	WC4–5	WI02	$2.6^{+0.2}_{-0.1}$	$2.3^{+0.2}_{-0.3}$	$5.41^{+0.10}_{-0.10}$	1	$-9.72^{+0.04}_{-0.05}$	2200	$10.9^{+2.6}_{-2.3}$	$1.10^{+0.08}_{-0.08}$	$1.01^{+0.14}_{-0.13}$	—	$2.60^{+0.16}_{-0.16}$	—	0.07	0.06	0.06	$0.11^{+0.01}_{-0.00}$	$0.10^{+0.00}_{-0.01}$	···
WR5	WC6–7	WI02	$2.8^{+0.2}_{-0.1}$	3.2 ± 0.3	$5.49^{+0.14}_{-0.13}$	1	$-9.95^{+0.04}_{-0.04}$	1900	$16.9^{+5.7}_{-4.5}$	$1.41^{+0.11}_{-0.09}$	$0.87^{+0.18}_{-0.15}$	$2.58^{+0.23}_{-0.22}$	$0.38^{+0.04}_{-0.03}$	$0.09^{+0.01}_{-0.00}$	0.08	0.08	$0.13^{+0.01}_{-0.01}$	$0.08^{+0.01}_{-0.00}$	[a]$0.17^{+0.03}_{-0.02}$
WR9	WC4–5 + O	CS	3.5 ± 0.2	$3.9^{+0.4}_{-0.4}$	···	2	$-10.19^{+0.04}_{-0.05}$	3200	$27.0^{+11.2}_{-8.2}$	···	···	—	$2.70^{+0.31}_{-0.27}$	—	0.00	0.00	$0.10^{+0.01}_{-0.00}$	$0.15^{+0.00}_{-0.01}$	···	···
WR13	WC6–7	CS	$4.3^{+0.3}_{-0.2}$	$4.5^{+0.5}_{-0.4}$	$5.45^{+0.19}_{-0.18}$	1	$-10.92^{+0.04}_{-0.05}$	2000	$13.1^{+6.4}_{-4.5}$	$1.20^{+0.09}_{-0.07}$	···	—	$2.49^{+0.34}_{-0.29}$	—	0.08	0.08	$0.10^{+0.00}_{-0.01}$	$0.15^{+0.01}_{-0.01}$	···	···
WR14	WC6–7	AD	$1.7^{+0.1}_{-0.0}$	$2.4^{+0.3}_{-0.2}$	$5.56^{+0.10}_{-0.10}$	1	$-9.46^{+0.05}_{-0.04}$	1900	$10.3^{+2.6}_{-2.2}$	$0.73^{+0.03}_{-0.03}$	$0.75^{+0.12}_{-0.10}$	$2.73^{+0.19}_{-0.18}$	$0.66^{+0.04}_{-0.05}$		0.32	0.12	$0.16^{+0.00}_{-0.01}$	$0.19^{+0.00}_{-0.01}$	$0.12^{+0.00}_{-0.01}$	$0.33^{+0.04}_{-0.03}$
WR15	WC6–7	CS	2.5 ± 0.1	$4.6^{+0.5}_{-0.4}$	$5.83^{+0.19}_{-0.18}$	1	$-10.07^{+0.04}_{-0.04}$	2900	$33.4^{+16.6}_{-11.5}$	$1.27^{+0.05}_{-0.05}$	···	—	$2.37^{+0.33}_{-0.27}$	—	0.17	0.18	$0.10^{+0.01}_{-0.00}$	$0.12^{+0.01}_{-0.01}$	···	···
WR17	WC4–5	AD	$5.0^{+0.5}_{-0.4}$	$1.2^{+0.1}_{-0.2}$	$5.30^{+0.09}_{-0.09}$	1	$-9.97^{+0.04}_{-0.05}$	1900	$8.6^{+1.5}_{-1.4}$	$1.12^{+0.08}_{-0.08}$	$0.36^{+0.03}_{-0.02}$	$2.03^{+0.06}_{-0.07}$	$0.51^{+0.02}_{-0.01}$		0.03	0.07	$0.08^{+0.00}_{-0.01}$	0.11	0.08	$0.13^{+0.00}_{-0.01}$
WR19	WC4–5 + O	AD	4.7 ± 0.3	$5.1^{+0.5}_{-0.5}$	···	2	$-11.11^{+0.04}_{-0.04}$	4000	$16.3^{+9.2}_{-6.1}$	···	$0.74^{+0.26}_{-0.19}$	—	$1.98^{+0.30}_{-0.26}$	—	0.00	0.00	0.03	$0.08^{+0.01}_{-0.01}$	$0.08^{+0.01}_{-0.01}$	$0.18^{+0.05}_{-0.04}$
WR23	WC6–7	AD	2.3 ± 0.1	$2.3^{+0.3}_{-0.2}$	$5.51^{+0.09}_{-0.10}$	1	$-9.49^{+0.04}_{-0.05}$	2100	$15.4^{+3.8}_{-3.2}$	$1.24^{+0.06}_{-0.05}$	$0.79^{+0.11}_{-0.09}$	$2.50^{+0.15}_{-0.14}$	$0.65^{+0.04}_{-0.03}$		0.23	0.13	$0.13^{+0.00}_{-0.01}$	$0.17^{+0.01}_{-0.00}$	$0.12^{+0.01}_{-0.01}$	$0.29^{+0.03}_{-0.03}$
WR27	WC6–7	CS	$2.3^{+0.1}_{-0.0}$	$6.3^{+0.6}_{-0.7}$	$5.17^{+0.25}_{-0.26}$	1	$-11.29^{+0.04}_{-0.04}$	2200	$7.8^{+5.8}_{-3.4}$	$1.39^{+0.05}_{-0.05}$	$0.71^{+0.26}_{-0.11}$	$2.63^{+0.40}_{-0.36}$	$0.45^{+0.06}_{-0.06}$	$0.14^{+0.00}_{-0.01}$	0.07	$0.11^{+0.01}_{-0.00}$	$0.19^{+0.02}_{-0.01}$	···	···	
WR30	WC6–7 + O	CS	5.9 ± 0.5	$2.1^{+0.3}_{-0.2}$	···	2	$-10.48^{+0.04}_{-0.04}$	2100	$8.8^{+2.1}_{-1.9}$	···	$0.28^{+0.04}_{-0.03}$	$1.84^{+0.12}_{-0.10}$	$0.78^{+0.04}_{-0.04}$		0.07	0.08	$0.13^{+0.00}_{-0.01}$	$0.13^{+0.00}_{-0.01}$	···	···
WR33	WC4–5	CS	$6.6^{+0.9}_{-0.7}$	$2.3^{+0.2}_{-0.3}$	$5.31^{+0.14}_{-0.13}$	1	$-10.34^{+0.04}_{-0.05}$	3400	$16.4^{+4.4}_{-3.7}$	$2.08^{+0.25}_{-0.22}$	···	—	$2.50^{+0.16}_{-0.15}$	—	0.00	0.00	0.10	0.13	···	···
WR38	WC4–5	AD	$6.3^{+0.9}_{-0.7}$	$4.2^{+0.4}_{-0.5}$	$5.14^{+0.20}_{-0.20}$	1	$-11.32^{+0.05}_{-0.04}$	3300	$8.6^{+4.0}_{-2.9}$	$1.62^{+0.27}_{-0.22}$	$0.38^{+0.11}_{-0.08}$	—	$1.70^{+0.20}_{-0.19}$	—	0.00	0.00	0.02	0.05	$0.06^{+0.01}_{-0.01}$	$0.04^{+0.01}_{-0.00}$
WR39	WC6–7 + O	CS	$4.4^{+1.4}_{-1.0}$	$6.4^{+0.6}_{-0.7}$	$6.12^{+0.35}_{-0.33}$	1	$-12.05^{+0.04}_{-0.05}$	2900	$5.1^{+4.1}_{-2.5}$	$0.10^{+0.04}_{-0.02}$	···	—	$3.61^{+0.69}_{-0.58}$	—	$0.42^{+0.00}_{-0.01}$	0.25	$0.32^{+0.02}_{-0.03}$	$0.21^{+0.02}_{-0.02}$	···	···
WR50	WC6–7 + O	CS	3.4 ± 0.2	$3.9^{+0.4}_{-0.4}$	$5.39^{+0.16}_{-0.16}$	1	$-10.82^{+0.04}_{-0.04}$	2400	$6.1^{+2.6}_{-1.9}$	$0.65^{+0.05}_{-0.05}$	$0.91^{+0.21}_{-0.18}$	—	$2.98^{+0.32}_{-0.28}$	—	0.43	0.09	$0.19^{+0.01}_{-0.00}$	$0.16^{+0.01}_{-0.00}$	···	···
WR53	WC8–9	AD	2.9 ± 0.1	$2.8^{+0.3}_{-0.3}$	$5.14^{+0.12}_{-0.12}$	1	$-10.64^{+0.04}_{-0.05}$	1500	$2.5^{+0.7}_{-0.6}$	$0.47^{+0.03}_{-0.03}$	$0.84^{+0.15}_{-0.12}$	$3.43^{+0.27}_{-0.26}$	$1.10^{+0.09}_{-0.08}$	$2.60^{+0.01}_{-0.02}$	0.29	$0.62^{+0.02}_{-0.02}$	$0.44^{+0.02}_{-0.02}$	$0.14^{+0.02}_{-0.01}$	$0.88^{+0.12}_{-0.11}$	
WR56	WC6–7	CS	7.5 ± 0.7	$2.6^{+0.3}_{-0.2}$	$5.00^{+0.13}_{-0.14}$	1	$-11.42^{+0.04}_{-0.05}$	1700	$2.4^{+1.0}_{-0.8}$	$0.63^{+0.07}_{-0.07}$	$1.08^{+0.18}_{-0.16}$	$2.95^{+0.22}_{-0.21}$	$0.81^{+0.06}_{-0.06}$	0.56	0.15	$0.20^{+0.00}_{-0.01}$	$0.18^{+0.01}_{-0.01}$	···	···	
WR57	WC8–9	CS	$3.0^{+0.2}_{-0.1}$	$1.7^{+0.1}_{-0.2}$	$5.16^{+0.08}_{-0.07}$	1	$-10.06^{+0.04}_{-0.05}$	1700	$3.9^{+0.7}_{-0.7}$	$0.69^{+0.05}_{-0.04}$	$3.21^{+0.28}_{-0.26}$	$3.37^{+0.13}_{-0.13}$	$0.93^{+0.04}_{-0.03}$	$1.14^{+0.00}_{-0.01}$	0.18	$0.32^{+0.01}_{-0.00}$	$0.25^{+0.00}_{-0.01}$	···	···	
WR59	WC8–9	CS	3.4 ± 0.2	$7.6^{+0.8}_{-0.7}$	$5.67^{+0.31}_{-0.30}$	1	$-12.28^{+0.04}_{-0.04}$	1400	$5.1^{+4.9}_{-2.5}$	$0.28^{+0.02}_{-0.01}$	···	$5.55^{+1.27}_{1.04}$	$1.54^{+0.34}_{-0.28}$	$3.68^{+0.05}_{-0.06}$	$0.57^{+0.01}_{-0.00}$	$1.21^{+0.12}_{-0.11}$	$1.01^{+0.12}_{-0.11}$	···	···	
WR60	WC8–9	CS	3.4 ± 0.3	$5.4^{+0.6}_{-0.5}$	$5.73^{+0.23}_{-0.22}$	1	$-11.03^{+0.04}_{-0.05}$	1800	$13.4^{+8.2}_{-5.3}$	$0.64^{+0.08}_{-0.06}$	$1.57^{+0.59}_{-0.43}$	$2.40^{+0.38}_{-0.34}$	$1.26^{+0.20}_{-0.17}$	$1.87^{+0.02}_{-0.02}$	0.39	$0.42^{+0.02}_{-0.03}$	$0.28^{+0.02}_{-0.02}$	···	···	
WR65	WC8–9 + B	CS	2.8 ± 0.2	$7.5^{+0.8}_{-0.7}$	$5.71^{+0.34}_{-0.33}$	1	$-12.46^{+0.04}_{-0.04}$	1400	$2.0^{+1.8}_{-1.0}$	$0.10^{+0.01}_{-0.00}$	···	$5.56^{+1.28}_{-1.04}$	$1.32^{+0.29}_{-0.24}$	$4.14^{+0.06}_{-0.07}$	$0.86^{+0.01}_{-0.01}$	$1.51^{+0.15}_{-0.14}$	$0.86^{+0.11}_{-0.09}$	···	···	
WR68	WC6–7	CS	$5.9^{+0.6}_{-0.5}$	$5.3^{+0.5}_{-0.6}$	$5.87^{+0.22}_{-0.22}$	1	$-11.31^{+0.05}_{-0.04}$	1900	$19.0^{+11.1}_{-7.3}$	$0.67^{+0.08}_{-0.07}$	···	$2.55^{+0.39}_{-0.35}$	$0.81^{+0.12}_{-0.11}$	$0.51^{+0.01}_{-0.00}$	0.26	$0.20^{+0.01}_{-0.01}$	$0.17^{+0.02}_{-0.01}$	···	···	
WR69	WC8–9	CS	2.6 ± 0.1	2.0 ± 0.2	$5.06^{+0.10}_{-0.09}$	1	$-10.63^{+0.04}_{-0.05}$	1500	$1.1^{+0.2}_{-0.2}$	$0.24^{+0.02}_{-0.02}$	···	$4.33^{+0.26}_{-0.24}$	$1.18^{+0.07}_{-0.06}$	$4.48^{+0.01}_{-0.02}$	0.70	$1.70^{+0.04}_{-0.05}$	···	···	···	
WR70	WC8–9 + B	CS	$3.1^{+0.1}_{-0.2}$	$4.7^{+0.5}_{-0.4}$	···	2	$-11.41^{+0.04}_{-0.04}$	1200	$2.6^{+1.3}_{-0.9}$	···	···	$3.44^{+0.48}_{-0.42}$	$1.19^{+0.16}_{-0.14}$	$3.52^{+0.03}_{-0.04}$	$0.35^{+0.00}_{-0.01}$	$1.65^{+0.10}_{-0.09}$	···	···	···	
WR73	WC8–9	CS	$6.9^{+1.0}_{-0.8}$	$5.7^{+0.6}_{-0.5}$	···	2	$-12.20^{+0.04}_{-0.05}$	1600	$4.9^{+3.3}_{-2.0}$	···	···	$3.36^{+0.57}_{-0.49}$	$0.99^{+0.16}_{-0.14}$	$3.20^{+0.04}_{-0.03}$	$0.36^{+0.00}_{-0.01}$	$1.10^{+0.09}_{-0.07}$	$0.49^{+0.04}_{-0.04}$	···	···	
WR77	WC8–9 + O	CS	3.1 ± 0.2	$3.4^{+0.4}_{-0.3}$	···	2	$-11.49^{+0.04}_{-0.05}$	1600	$0.7^{+0.3}_{-0.2}$	···	···	$1.81^{+0.17}_{-0.17}$	$0.87^{+0.09}_{-0.07}$	$2.15^{+0.01}_{-0.01}$	0.25	$0.60^{+0.03}_{-0.02}$	$0.47^{+0.02}_{-0.02}$	···	···	
WR80	WC8–9 + O	CS	3.8 ± 0.3	$7.0^{+0.7}_{-0.7}$	$5.23^{+0.29}_{-0.29}$	1	$-12.19^{+0.04}_{-0.05}$	1500	$4.4^{+3.7}_{-2.1}$	$0.68^{+0.07}_{-0.06}$	···	$3.58^{+0.73}_{-0.61}$	$1.06^{+0.20}_{-0.18}$	$3.77^{+0.06}_{-0.05}$	$0.49^{+0.00}_{-0.01}$	$1.31^{+0.12}_{-0.11}$	$1.00^{+0.11}_{-0.09}$	···	···	
WR81	WC8–9	CS	2.5 ± 0.1	$6.0^{+0.6}_{-0.6}$	$5.38^{+0.24}_{-0.24}$	1	$-11.56^{+0.04}_{-0.05}$	1500	$3.5^{+2.4}_{-1.5}$	$0.38^{+0.02}_{-0.02}$	···	$3.48^{+0.59}_{-0.50}$	$1.30^{+0.21}_{-0.18}$	$3.90^{+0.05}_{-0.04}$	$0.91^{+0.01}_{-0.00}$	$1.37^{+0.10}_{-0.10}$	$0.51^{+0.05}_{-0.04}$	···	···	
WR88	WC8–9	CS	$2.7^{+0.2}_{-0.1}$	$5.9^{+0.6}_{-0.6}$	$5.27^{+0.24}_{-0.24}$	1	$-11.86^{+0.04}_{-0.04}$	1400	$2.1^{+1.5}_{-0.9}$	$0.30^{+0.02}_{-0.02}$	···	$5.32^{+0.72}_{-0.72}$	$1.54^{+0.23}_{-0.20}$	$3.23^{+0.04}_{-0.03}$	$0.86^{+0.01}_{-0.00}$	$0.85^{+0.06}_{-0.06}$	$0.35^{+0.03}_{-0.03}$	···	···	
WR90	WC6–7	VU	1.3 ± 0.0	$1.5^{+0.2}_{-0.1}$	$5.67^{+0.06}_{-0.07}$	1	$-8.74^{+0.04}_{-0.04}$	1900	$13.8^{+2.4}_{-2.2}$	$0.77^{+0.04}_{-0.03}$	$0.95^{+0.08}_{-0.08}$	$2.73^{+0.11}_{-0.11}$	$0.94^{+0.03}_{-0.04}$	0.40	0.14	$0.17^{+0.00}_{-0.01}$	$0.16^{+0.01}_{-0.00}$	$0.11^{+0.00}_{-0.01}$	$0.25^{+0.02}_{-0.01}$	
WR92	WC8–9	CS	$4.5^{+0.4}_{-0.3}$	$1.8^{+0.2}_{-0.2}$	$5.09^{+0.10}_{-0.10}$	1	$-11.03^{+0.04}_{-0.05}$	1400	$1.1^{+0.2}_{-0.2}$	$0.23^{+0.02}_{-0.02}$	···	$5.17^{+0.28}_{-0.27}$	$1.62^{+0.09}_{-0.08}$	$4.36^{+0.01}_{-0.02}$	$0.81^{+0.01}_{-0.00}$	$1.86^{+0.04}_{-0.05}$	$0.50^{+0.01}_{-0.02}$	···	···	
WR93	WC6–7 + O	CS	1.9 ± 0.1	$5.3^{+0.6}_{-0.5}$	···	2	$-10.43^{+0.04}_{-0.05}$	2000	$8.4^{+4.9}_{-3.2}$	···	···	$2.06^{+0.32}_{-0.28}$	$0.99^{+0.16}_{-0.13}$	$0.56^{+0.00}_{-0.01}$	$0.52^{+0.00}_{-0.01}$	$0.20^{+0.02}_{-0.01}$	$0.15^{+0.01}_{-0.01}$	···	···	
WR95	WC8–9	CS	$2.2^{+0.1}_{-0.2}$	$6.9^{+0.7}_{-0.6}$	$5.22^{+0.28}_{-0.28}$	1	$-11.92^{+0.04}_{-0.05}$	1400	$2.7^{+2.2}_{-1.3}$	$0.41^{+0.03}_{-0.02}$	···	$3.98^{+0.79}_{-0.65}$	$1.11^{+0.20}_{-0.18}$	$3.92^{+0.06}_{-0.05}$	$0.54^{+0.00}_{-0.01}$	$1.19^{+0.10}_{-0.09}$	$1.15^{+0.12}_{-0.11}$	···	···	
WR103	WC8–9	II91	$2.5^{+0.2}_{-0.1}$	$2.0^{+0.1}_{-0.2}$	$5.19^{+0.09}_{-0.10}$	1	$-10.25^{+0.08}_{-0.10}$	1400	$2.3^{+0.6}_{-0.6}$	$0.38^{+0.03}_{-0.02}$	···	$3.43^{+0.19}_{-0.18}$	$1.00^{+0.06}_{-0.05}$	$3.78^{+0.02}_{-0.01}$	$0.83^{+0.01}_{-0.00}$	$1.16^{+0.03}_{-0.03}$	$0.54^{+0.01}_{-0.02}$	···	···	
WR106	WC8–9	WI02	2.9 ± 0.2	$4.6^{+0.5}_{-0.4}$	$5.10^{+0.20}_{-0.19}$	1	$-11.59^{+0.05}_{-0.04}$	1400	$1.4^{+0.6}_{-0.4}$	$0.29^{+0.02}_{-0.02}$	$0.43^{+0.13}_{-0.10}$	$2.79^{+0.39}_{-0.33}$	$0.78^{+0.10}_{-0.09}$	$3.66^{+0.03}_{-0.04}$	$0.84^{+0.01}_{-0.00}$	$1.77^{+0.10}_{-0.10}$	$0.95^{+0.07}_{-0.06}$	$0.09^{+0.01}_{-0.01}$	[a]$1.25^{+0.29}_{-0.23}$	

Table A3 – *continued*

WR	Category	Data	d	A_V	log	Ref	log $F_{\rm CIV\ 5801,12}$	CIV 5801,12	$L_{\rm CIV\ 5801,12}$		$\frac{L_{\rm OIV\ 3403,13}}{L_{5801,12}}$	$\frac{L_{\rm CIII\ 4647,51}}{L_{5801,12}}$	$\frac{L_{\rm HeII\ 4686}}{L_{5801,12}}$	$\frac{L_{\rm CIII\ 5696}}{L_{5801,12}}$	$\frac{L_{\rm HeI\ 5876}}{L_{5801-12}}$	$\frac{L_{6559-81}}{L_{5801,12}}$	$\frac{L_{\rm CIII\ 6727,73}}{L_{5801,12}}$	$\frac{L_{\rm CIV\ 7725}}{L_{5801,12}}$	$\frac{L_{\rm CIII\ 9701,19}}{L_{5801,12}}$
		ID	kpc	mag	$L_{\rm Bol}/L_\odot$		erg s^{-1} cm^{-2}	FWHM	10^{35} erg s^{-1}	10^{-3} $L_{\rm Bol}$									
WR111	WC4–5	WI02	$1.3^{+0.1}_{-0.0}$	$1.3^{+0.1}_{-0.2}$	$5.20^{+0.07}_{-0.07}$	1	$-8.86^{+0.04}_{-0.05}$	2200	$8.7^{+1.4}_{-1.3}$	$1.44^{+0.09}_{-0.08}$	$0.69^{+0.05}_{-0.05}$	—	$2.64^{+0.10}_{-0.08}$	—	0.06	0.08	0.08	$0.14^{+0.00}_{-0.01}$	$0.10^{+0.00}_{-0.01}$	[a]$0.18^{+0.01}_{-0.01}$
WR113	WC8–9 + O	KI	$1.9^{+0.1}_{-0.0}$	$4.1^{+0.5}_{-0.4}$	$6.01^{+0.16}_{-0.17}$	1	$-10.47^{+0.04}_{-0.04}$	1500	$5.5^{+2.5}_{-1.8}$	$0.14^{+0.01}_{-0.00}$	$1.11^{+0.24}_{-0.20}$	$4.05^{+0.39}_{-0.36}$	$0.87^{+0.08}_{-0.07}$	$2.20^{+0.02}_{-0.01}$	0.29	$0.75^{+0.04}_{-0.03}$	$0.60^{+0.03}_{-0.03}$	···	···
WR114	WC4–5	KI	1.9 ± 0.1	$5.1^{+0.5}_{-0.5}$	$5.29^{+0.21}_{-0.20}$	1	$-10.54^{+0.04}_{-0.05}$	2100	$9.4^{+5.2}_{-3.5}$	$1.25^{+0.07}_{-0.07}$	$0.59^{+0.20}_{-0.15}$	$2.41^{+0.36}_{-0.32}$	$0.49^{+0.07}_{-0.06}$	0.07	0.09	$0.08^{+0.00}_{-0.01}$	$0.14^{+0.01}_{-0.01}$	···	···
WR117	WC8–9	WI02	$5.0^{+0.6}_{-0.5}$	$5.9^{+0.5}_{-0.6}$	$5.57^{+0.25}_{-0.25}$	1	$-11.57^{+0.04}_{-0.05}$	1700	$12.2^{+8.2}_{-5.1}$	$0.85^{+0.14}_{-0.10}$	$0.72^{+0.29}_{-0.21}$	$2.95^{+0.51}_{-0.44}$	$0.87^{+0.14}_{-0.13}$	$2.90^{+0.03}_{-0.04}$	$0.38^{+0.00}_{-0.01}$	$0.99^{+0.07}_{-0.07}$	$0.48^{+0.05}_{-0.04}$	$0.14^{+0.03}_{-0.02}$	···
WR119	WC8–9	KI	$4.1^{+0.3}_{-0.2}$	$3.4^{+0.3}_{-0.4}$	$4.85^{+0.14}_{-0.15}$	1	$-11.65^{+0.04}_{-0.05}$	1300	$0.8^{+0.3}_{-0.2}$	$0.31^{+0.02}_{-0.03}$	···	$3.31^{+0.32}_{-0.30}$	$1.03^{+0.09}_{-0.09}$	$4.14^{+0.03}_{-0.02}$	$0.73^{+0.00}_{-0.01}$	$1.56^{+0.07}_{-0.07}$	$0.64^{+0.04}_{-0.03}$	···	[a]$1.26^{+0.21}_{-0.19}$
WR121	WC8–9	WI02	3.4 ± 0.2	$5.3^{+0.5}_{-0.6}$	$5.51^{+0.22}_{-0.21}$	1	$-11.55^{+0.04}_{-0.05}$	1400	$3.4^{+2.0}_{-1.1}$	$0.27^{+0.02}_{-0.01}$	···	$3.29^{+0.51}_{-0.45}$	$0.99^{+0.15}_{-0.13}$	$3.64^{+0.03}_{-0.04}$	$0.91^{+0.01}_{-0.00}$	$1.24^{+0.09}_{-0.07}$	$0.65^{+0.06}_{-0.05}$	$0.06^{+0.01}_{-0.01}$	[a]$0.96^{+0.26}_{-0.21}$
WR125	WC6–7 + O	KI	$5.9^{+0.7}_{-0.6}$	$6.0^{+0.6}_{-0.6}$	$6.28^{+0.26}_{-0.25}$	1	$-11.38^{+0.04}_{-0.05}$	2800	$29.7^{+20.5}_{-12.7}$	$0.40^{+0.07}_{-0.05}$	···	—	$2.98^{+0.52}_{-0.46}$	—	$1.03^{+0.01}_{-0.01}$	0.29	$0.21^{+0.02}_{-0.01}$	$0.23^{+0.02}_{-0.02}$	···	···
WR132	WC6–7	KI	$4.2^{+0.3}_{-0.2}$	$4.3^{+0.4}_{-0.4}$	$5.34^{+0.18}_{-0.18}$	1	$-10.87^{+0.04}_{-0.04}$	2000	$11.8^{+5.5}_{-3.9}$	$1.41^{+0.10}_{-0.09}$	$0.80^{+0.23}_{-0.18}$	$2.56^{+0.22}_{-0.29}$	$0.64^{+0.08}_{-0.07}$	0.19	0.10	$0.11^{+0.00}_{-0.01}$	$0.16^{+0.01}_{-0.01}$	···	···
WR135	WC8–9	WI02	$2.4^{+0.1}_{-0.2}$	$1.5^{+0.2}_{-0.1}$	$5.54^{+0.08}_{-0.07}$	1	$-9.45^{+0.04}_{-0.04}$	1400	$8.6^{+1.5}_{-1.4}$	$0.64^{+0.04}_{-0.04}$	$1.35^{+0.13}_{-0.09}$	$3.34^{+0.14}_{-0.14}$	$0.85^{+0.03}_{-0.03}$	1.06	0.23	$0.31^{+0.00}_{-0.01}$	$0.28^{+0.00}_{-0.01}$	$0.13^{+0.00}_{-0.01}$	[a]$0.59^{+0.04}_{-0.04}$
WR137	WC6–7 + O	KI	2.0 ± 0.1	$2.4^{+0.3}_{-0.2}$	$5.89^{+0.10}_{-0.10}$	1	$-9.54^{+0.04}_{-0.05}$	1700	$11.1^{+2.9}_{-2.4}$	$0.37^{+0.02}_{-0.01}$	$0.98^{+0.15}_{-0.13}$	$3.38^{+0.24}_{-0.22}$	$0.75^{+0.05}_{-0.04}$	0.59	0.13	$0.26^{+0.01}_{-0.01}$	$0.22^{+0.01}_{-0.00}$	···	[a]$0.36^{+0.05}_{-0.03}$
WR140	WC6–7 + O	II13	$1.8^{+0.0}_{-0.1}$	$2.1^{+0.3}_{-0.2}$	···	2	$-8.90^{+0.08}_{-0.09}$	2900	$29.3^{+8.4}_{-7.7}$	···	$0.36^{+0.05}_{-0.04}$	—	$2.24^{+0.13}_{-0.12}$	—	0.34	0.08	$0.11^{+0.01}_{-0.00}$	$0.12^{+0.00}_{-0.01}$	$0.10^{+0.01}_{-0.01}$	[a]$0.30^{+0.04}_{-0.02}$
WR143	WC4–5 + O	KI	1.8 ± 0.1	$4.4^{+0.4}_{-0.5}$	$5.45^{+0.18}_{-0.18}$	1	$-10.31^{+0.04}_{-0.04}$	2900	$7.3^{+3.3}_{-2.4}$	$0.66^{+0.04}_{-0.03}$	$0.37^{+0.16}_{-0.09}$	—	$2.36^{+0.41}_{-0.35}$	—	0.00	0.00	0.04	$0.08^{+0.01}_{-0.01}$	···	···
WR144	WC4–5	WI02	$1.7^{+0.0}_{-0.1}$	$7.0^{+0.7}_{-0.7}$	$5.15^{+0.28}_{-0.28}$	1	$-11.14^{+0.04}_{-0.04}$	2800	$10.3^{+8.6}_{-4.8}$	$1.89^{+0.06}_{-0.05}$	···	—	$1.13^{+0.21}_{-0.17}$	—	0.00	0.00	$0.05^{+0.00}_{-0.01}$	$0.12^{+0.01}_{-0.01}$	$0.12^{+0.03}_{-0.01}$	···
WR150	WC4–5	KI	$6.8^{+0.8}_{-0.6}$	$3.5^{+0.3}_{-0.4}$	$5.54^{+0.17}_{-0.16}$	1	$-10.70^{+0.04}_{-0.04}$	2900	$23.1^{+8.9}_{-6.9}$	$1.73^{+0.24}_{-0.20}$	$0.28^{+0.05}_{-0.04}$	—	$2.29^{+0.20}_{-0.19}$	—	0.00	0.09	$0.11^{+0.00}_{-0.01}$	$0.14^{+0.01}_{-0.01}$	···	···
WR154	WC6–7	WI02	4.7 ± 0.3	$2.9^{+0.3}_{-0.3}$	$5.76^{+0.13}_{-0.14}$	1	$-10.18^{+0.05}_{-0.04}$	2100	$25.9^{+8.6}_{-6.8}$	$1.17^{+0.10}_{-0.08}$	$0.70^{+0.13}_{-0.11}$	$2.37^{+0.20}_{-0.18}$	$0.64^{+0.05}_{-0.05}$	0.18	0.12	$0.10^{+0.01}_{-0.00}$	$0.16^{+0.01}_{-0.00}$	$0.11^{+0.01}_{-0.01}$	[a]$0.22^{+0.04}_{-0.02}$
BAT99-8	WC4–5	MM	49.6 ± 1.0	$0.4^{+0.0}_{-0.0}$	$5.47^{+0.03}_{-0.02}$	3	$-11.31^{+0.04}_{-0.05}$	2600	$20.2^{+2.2}_{-2.2}$	$1.76^{+0.04}_{-0.03}$	$0.52^{+0.02}_{-0.01}$	—	$1.71^{+0.02}_{-0.01}$	—	0.03	0.08	0.04	0.07	0.08	0.07
BAT99-9	WC4–5	MM	49.6 ± 1.0	$0.5^{+0.0}_{-0.1}$	$5.47^{+0.03}_{-0.02}$	3	$-11.20^{+0.05}_{-0.04}$	2600	$28.7^{+3.2}_{-3.2}$	$2.51^{+0.06}_{-0.05}$	$0.25^{+0.01}_{-0.00}$	—	$1.05^{+0.01}_{-0.02}$	—	0.01	0.06	0.04	0.03	0.05	0.02
BAT99-10	WC4–5 + O	AD	49.6 ± 1.0	$0.1^{+0.0}_{-0.0}$	···	2	$-11.09^{+0.04}_{-0.05}$	3200	$25.4^{+2.6}_{-2.6}$	···	···	—	1.26	—	0.00	0.00	···	0.09	0.06	···
BAT99-11	WC4–5	MM	49.6 ± 1.0	$0.4^{+0.1}_{-0.0}$	$5.85^{+0.03}_{-0.02}$	3	$-10.81^{+0.04}_{-0.04}$	3500	$66.7^{+7.2}_{-7.2}$	$2.43^{+0.05}_{-0.05}$	$0.40^{+0.01}_{-0.02}$	—	$1.73^{+0.02}_{-0.02}$	—	0.01	0.10	0.05	0.08	0.06	0.06
BAT99-20	WC4–5 + O	AD	49.6 ± 1.0	$1.2^{+0.1}_{-0.2}$	···	2	$-11.72^{+0.04}_{-0.05}$	3900	$15.2^{+2.2}_{-2.1}$	···	···	—	$1.81^{+0.05}_{-0.06}$	—	0.00	0.00	···	0.05	0.05	···
BAT99-28	WC4–5 + O	AD	49.6 ± 1.0	$0.2^{+0.0}_{-0.1}$	···	2	$-11.10^{+0.04}_{-0.04}$	3400	$26.8^{+2.7}_{-2.8}$	···	···	—	$2.20^{+0.00}_{-0.01}$	—	0.13	0.00	0.09	0.09	0.07	···
BAT99-34	WC4–5 + O	AD	49.6 ± 1.0	$0.1^{+0.0}_{-0.0}$	···	2	$-11.19^{+0.04}_{-0.04}$	2700	$20.4^{+2.1}_{-2.1}$	···	···	—	$1.41^{+0.01}_{-0.00}$	—	0.01	0.00	0.05	0.05	0.05	···
BAT99-38	WC4–5 + O	AD	49.6 ± 1.0	$0.2^{+0.0}_{-0.1}$	···	2	$-11.14^{+0.04}_{-0.04}$	3600	$24.4^{+2.6}_{-2.5}$	···	···	—	$1.26^{+0.00}_{-0.01}$	—	0.01	0.00	···	0.03	0.06	···
BAT99-39	WC4–5 + O	AD	49.6 ± 1.0	$0.1^{+0.0}_{-0.0}$	···	2	$-11.18^{+0.04}_{-0.05}$	3900	$21.4^{+2.2}_{-2.2}$	···	···	—	$1.45^{+0.00}_{-0.01}$	—	0.02	0.00	···	0.04	0.05	···
BAT99-52	WC4–5	MM	49.6 ± 1.0	$0.3^{+0.1}_{-0.0}$	$5.64^{+0.02}_{-0.02}$	3	$-11.06^{+0.04}_{-0.05}$	3000	$34.3^{+3.7}_{-3.6}$	$2.03^{+0.04}_{-0.04}$	$0.68^{+0.02}_{-0.02}$	—	$2.05^{+0.01}_{-0.02}$	—	0.03	0.09	0.04	0.08	0.07	0.07
BAT99-53	WC4–5 + O	AD	49.6 ± 1.0	$0.4^{+0.1}_{-0.0}$	···	2	$-11.07^{+0.04}_{-0.05}$	3700	$35.7^{+3.8}_{-3.9}$	···	···	—	$1.60^{+0.01}_{-0.02}$	—	0.00	0.00	···	0.05	0.06	···
BAT99-61	WC4–5	MM	49.6 ± 1.0	$0.5^{+0.0}_{-0.1}$	$5.87^{+0.03}_{-0.02}$	4	$-10.85^{+0.04}_{-0.05}$	3400	$63.5^{+7.1}_{-7.0}$	$2.21^{+0.05}_{-0.05}$	$0.31^{+0.01}_{-0.01}$	—	$1.68^{+0.02}_{-0.02}$	—	0.01	0.14	0.06	0.07	0.05	0.06
BAT99-70	WC4–5 + O	AD	49.6 ± 1.0	$1.5^{+0.2}_{-0.1}$	···	2	$-11.09^{+0.04}_{-0.05}$	4300	$89.4^{+15.6}_{-14.3}$	···	···	—	$1.03^{+0.04}_{-0.04}$	—	0.00	0.00	0.05	0.03	0.04	···
BAT99-84	WC4–5 + O	AD	49.6 ± 1.0	$0.5^{+0.0}_{-0.1}$	···	2	$-11.09^{+0.05}_{-0.04}$	3200	$36.7^{+4.0}_{-4.0}$	···	···	—	$1.96^{+0.03}_{-0.02}$	—	0.01	0.00	0.05	0.09	0.07	···
BAT99-85	WC4–5 + O	AD	49.6 ± 1.0	$1.1^{+0.1}_{-0.1}$	···	2	$-11.34^{+0.04}_{-0.04}$	3700	$35.6^{+5.1}_{-4.9}$	···	···	—	$1.25^{+0.04}_{-0.04}$	—	0.00	0.00	···	0.10	0.06	···
BAT99-90	WC4–5	MM	49.6 ± 1.0	$1.1^{+0.1}_{-0.1}$	$5.48^{+0.05}_{-0.04}$	4	$-11.46^{+0.04}_{-0.05}$	2800	$25.9^{+3.7}_{-3.5}$	$2.22^{+0.05}_{-0.06}$	$0.50^{+0.05}_{-0.03}$	—	$1.60^{+0.04}_{-0.05}$	—	0.02	0.08	0.04	0.06	0.06	0.06
BAT99-115	WC4–5	MM	49.6 ± 1.0	$1.6^{+0.1}_{-0.2}$	···	4	$-11.56^{+0.08}_{-0.10}$	4000	$30.7^{+7.5}_{-7.3}$	···	[b]$1.07^{+0.13}_{-0.11}$	—	$2.49^{+0.10}_{-0.10}$	—	0.03	0.02	$0.04^{+0.01}_{-0.00}$	$0.07^{+0.01}_{-0.00}$	$0.08^{+0.01}_{-0.00}$	···
BAT99-121	WC4–5	MM	49.6 ± 1.0	$2.2^{+0.2}_{-0.2}$	···	2	$-12.16^{+0.04}_{-0.05}$	3000	$13.6^{+3.1}_{-2.8}$	···	$0.70^{+0.12}_{-0.10}$	—	$1.85^{+0.11}_{-0.10}$	—	0.02	0.10	0.05	0.06	$0.07^{+0.01}_{-0.00}$	$0.12^{+0.01}_{-0.01}$

Notes. $E_{\rm B-V} = 1.21\ E_{b-v}$ and $(b-v)_0 = -0.30$ mag adopted. 1: Sander et al. (2012); 2: Aadland et al. (2022a); 3: Aadland et al. (2022b); 4: Bartzakos, Moffat & Niemela (2001).
[a] *IRTF*/SpeX observations (Crowther et al. 2006a). [b] FOS observations (Massey & Hunter 1998).

Table A4. Luminosities of prominent optical emission lines of Galactic (WR), LMC (BAT99, LMC, and LH), and SMC (AB) WO stars. C IV λλ5801,12 FWHM are also provided in km s^{-1} (±200 km s^{-1}). Stars included in spectral templates are indicated in bold (the remainder are excluded owing to limited spectral coverage).

Star	Category	Data ID	d kpc	A_V mag	log $L_{Bol}/L_\odot$	Ref	log $F_{CIV\ 5801,\ 12}$ erg s^{-1} cm^{-2}	CIV 5801,12 FWHM	$L_{CIV\ 5801,\ 12}$ 10^{35} erg s^{-1}	$L_{CIV\ 5801,\ 12}$ 10^{-3} L_{Bol}	$\frac{L_{OIV\ 3403,13}}{L_{CIV\ 5801,\ 12}}$	$\frac{L_{OVI\ 3811,34}}{L_{CIV\ 5801,\ 12}}$	$\frac{L_{CIV\ 4658+HeII\ 4686}}{L_{CIV\ 5801,\ 12}}$	$\frac{L_{OV\ 5572,5607}}{L_{CIV\ 5801,\ 12}}$	$\frac{L_{HeII\ 6560}}{L_{CIV\ 5801,\ 12}}$	$\frac{L_{CIV\ 7725}}{L_{CIV\ 5801,\ 12}}$
WR30a	WO + O	AD	$8.0^{+0.7}_{-0.5}$	4.1 ± 0.4	···	1	$-11.47^{+0.04}_{-0.05}$	5200	$8.7^{+3.8}_{-2.8}$	···	$0.66^{+0.18}_{-0.14}$	$0.35^{+0.08}_{-0.06}$	$0.81^{+0.09}_{-0.09}$	0.14	···	$0.05^{+0.00}_{-0.01}$
WR93b	WO	VX	$2.1^{+0.1}_{-0.1}$	6.3 ± 0.6	$4.88^{+0.26}_{-0.26}$	2	$-11.90^{+0.05}_{-0.04}$	8400	$1.5^{+1.1}_{-0.6}$	$0.52^{+0.04}_{-0.03}$	$1.6^{+0.6}_{-0.5}$	$1.7^{+0.5}_{-0.4}$	$0.71^{+0.13}_{-0.10}$	$0.12^{+0.01}_{-0.00}$	0.06	$0.14^{+0.02}_{-0.02}$
WR102	WO	WI02	$2.6^{+0.1}_{-0.1}$	3.9 ± 0.4	$4.95^{+0.17}_{-0.16}$	2	$-12.10^{+0.04}_{-0.04}$	6600	$0.2^{+0.1}_{-0.1}$	$0.05^{+0.01}_{-0.00}$	$3.1^{+0.8}_{-0.6}$	25^{+5}_{-4}	$3.2^{+0.3}_{-0.3}$	$1.31^{+0.02}_{-0.02}$	$0.38^{+0.02}_{-0.02}$	$1.10^{+0.13}_{-0.09}$
WR142	WO	WI02	$1.6^{+0.1}_{-0.0}$	4.9 ± 0.5	$5.33^{+0.20}_{-0.20}$	2	$-11.16^{+0.04}_{-0.04}$	7000	$1.5^{+0.7}_{-0.6}$	$0.18^{+0.00}_{-0.00}$	$2.0^{+0.7}_{-0.5}$	$7.1^{+2.1}_{-1.6}$	$2.2^{+0.3}_{-0.3}$	$0.43^{+0.01}_{-0.01}$	$0.22^{+0.01}_{-0.02}$	$0.53^{+0.09}_{-0.07}$
LH41-1042	WO	VX	49.6 ± 1.0	0.4 ± 0.0	$5.25^{+0.02}_{-0.02}$	2	$-11.52^{+0.04}_{-0.04}$	5600	$12.7^{+1.3}_{-1.4}$	$1.85^{+0.03}_{-0.04}$	$0.78^{+0.02}_{-0.02}$	$0.33^{+0.00}_{-0.01}$	$0.78^{+0.01}_{-0.01}$	0.10	0.03	0.06
LMC195–1	WO	MM	49.6 ± 1.0	0.4 ± 0.0	$5.40^{+0.03}_{-0.02}$	3	$-12.26^{+0.04}_{-0.04}$	4900	$2.3^{+0.2}_{-0.2}$	$0.24^{+0.0}_{-0.1}$	$4.3^{+0.1}_{-0.2}$	$5.8^{+0.1}_{-0.1}$	$1.5^{+0.1}_{-0.0}$	0.32	0.17	0.29
BAT99-123	WO	MM	49.6 ± 1.0	$0.5^{+0.0}_{-0.1}$	$5.40^{+0.03}_{-0.02}$	3	$-11.50^{+0.04}_{-0.05}$	5400	$14.2^{+1.6}_{-1.5}$	$1.46^{+0.04}_{-0.03}$	$0.64^{+0.03}_{-0.02}$	$0.40^{+0.02}_{-0.01}$	$0.45^{+0.00}_{-0.01}$	0.05	$0.02^{+0.01}_{-0.00}$	0.06
AB 8	WO + O	AD	61.2 ± 1.2	0.2 ± 0.0	$6.16^{+0.02}_{-0.02}$	4	$-11.22^{+0.05}_{-0.04}$	5300	$32.9^{+3.4}_{-3.4}$	$0.59^{+0.01}_{-0.01}$	$0.96^{+0.01}_{-0.02}$	$0.70^{+0.01}_{-0.01}$	$0.65^{+0.01}_{-0.00}$	0.16	0.04	0.19

Note. 1: Rate & Crowther (2020); 2: Tramper et al. (2015); 3: Aadland et al. (2022b); 4: Shenar et al. (2016).

APPENDIX B: TEMPLATES

Continuum-subtracted WR emission line templates are provided for the Milky Way, LMC, and SMC in Figs B1–B6. Templates are degraded to a uniform spectra resolution of 10 Å, and are provided from single and single + binary WR stars, since the latter are often contaminated by (Balmer) absorption lines from companion OB stars. Average velocity corrections of 284 and 162 km s^{-1} have been applied for the LMC and SMC, respectively (Tully et al. 2016).

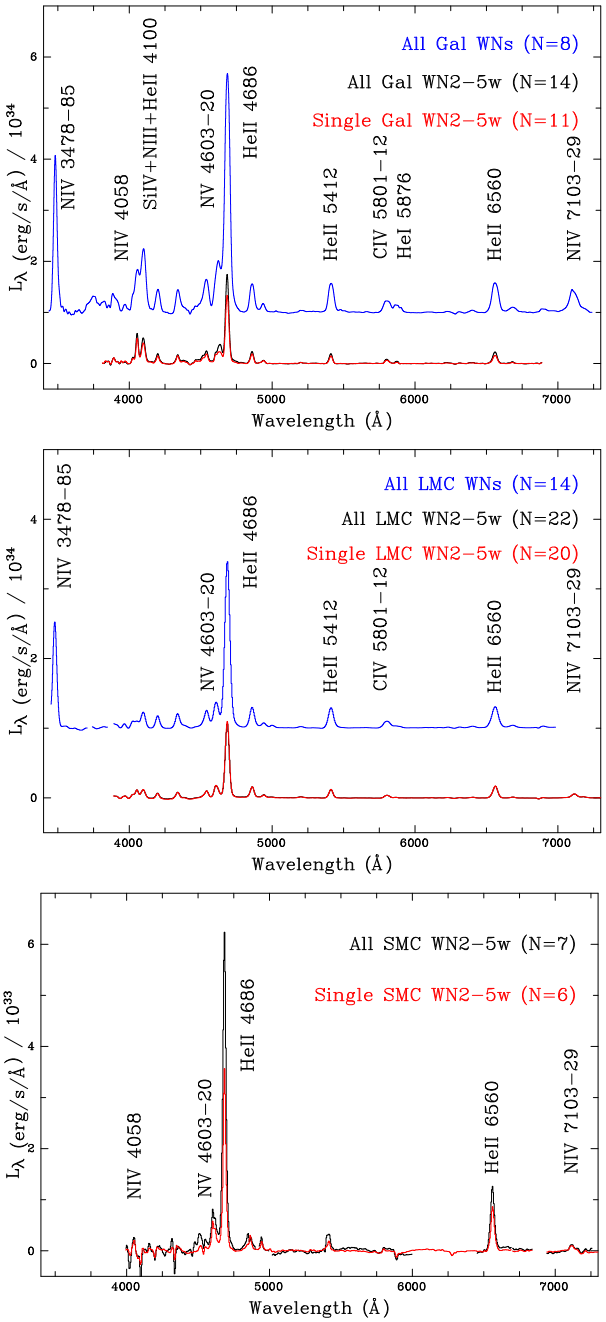

Figure B1. Upper panel: Galactic WN2–5w emission line templates based on single (red) and all (black) stars, and WN3–7s templates (blue, offset by 10^{34} erg s^{-1} Å^{-1}). Middle panel: LMC emission line templates. Lower panel: SMC emission line templates (no strong-lined WN stars are known).

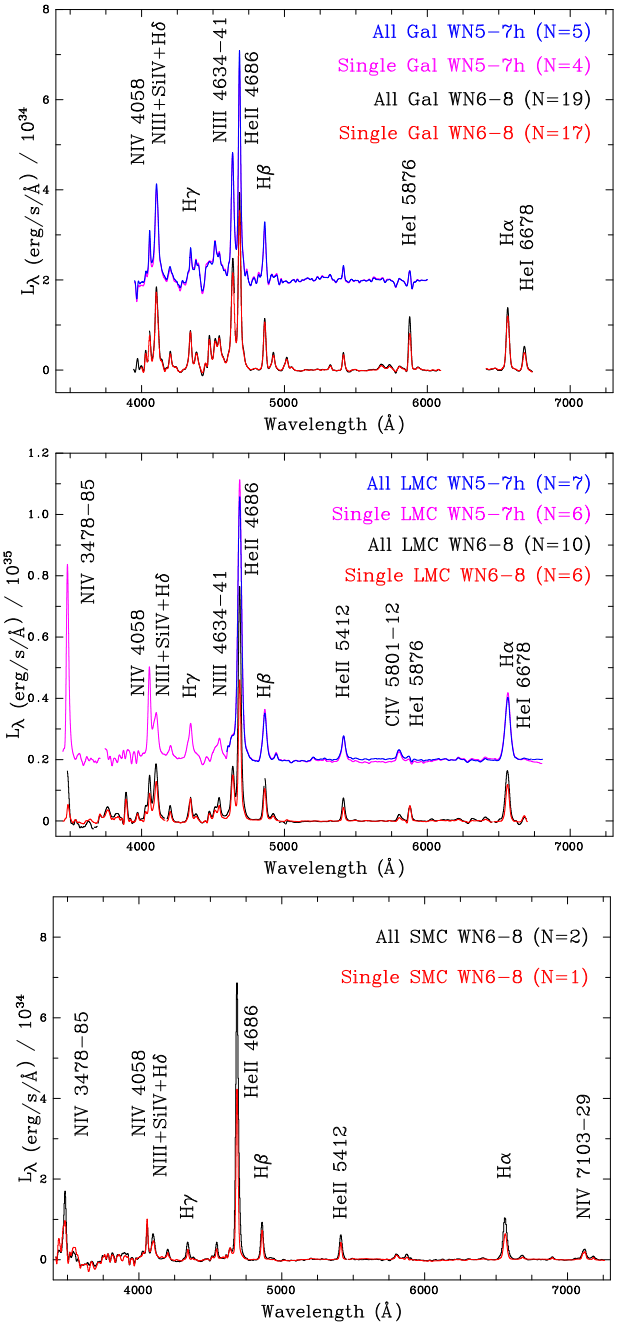

Figure B2. Upper panel: Galactic WN6–8 emission line templates based on single (red) and all (black) stars, and WN5–7h templates (pink and blue, offset by 2 × 10^{34} erg s^{-1} Å^{-1}). Middle panel: LMC WN6–8 and WN5–7h emission line templates. Lower panel: SMC WN6–8 emission line templates. LMC WN5–7h templates exclude the region shortward of λ4600 owing to the use of VLT/MUSE data sets (Castro et al. 2018).

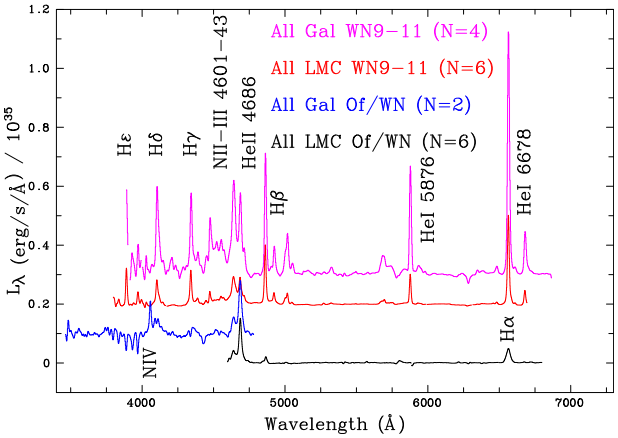

Figure B3. Emission line templates for LMC (black) and Milky Way (blue, offset by 10^{34} erg s^{-1} Å^{-1}) Of/WN stars, and LMC (red, offset by 2×10^{34} erg s^{-1} Å^{-1}) and Milky Way (pink, offset by 3×10^{34} erg s^{-1} Å^{-1}) WN9–11 stars. LMC Of/WN templates exclude the region shortward of λ4600 owing to the use of VLT/MUSE data sets (Castro et al. 2018).

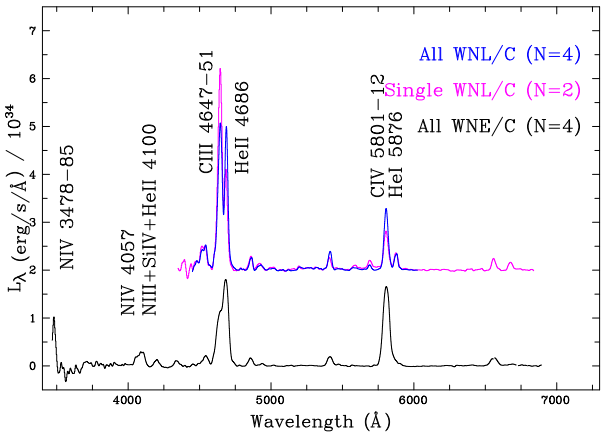

Figure B4. WN/C emission line templates for single WNE/C (black, three Milky Way and two LMC), single WNL/C (two Milky Way, pink), and all WNL/C (four Milky Way, blue) the latter group offset by 2×10^{34} erg s^{-1} Å^{-1}.

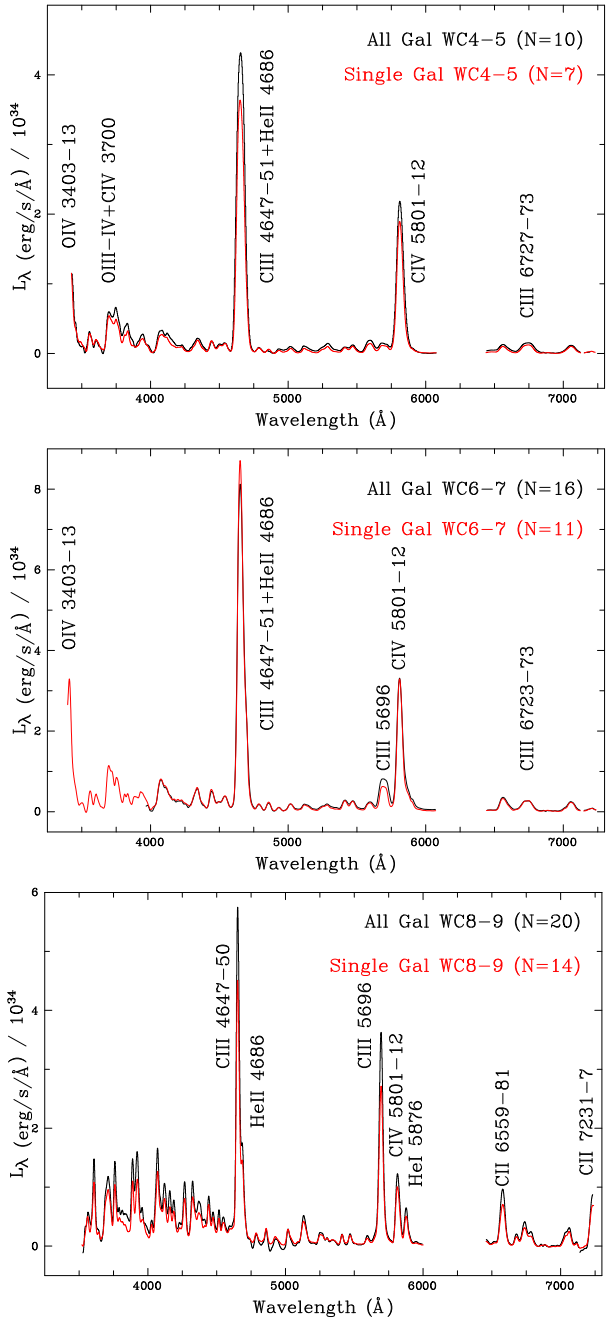

Figure B5. Upper panel: Galactic WC4–5 emission line templates based on single (red) and all (black) stars. Middle panel: Galactic WC6–7 emission line templates. Lower panel: Galactic WC8–9 emission line templates. The forest of blue features in WC8–9 stars primarily involves C II–III (Crowther et al. 2006b).

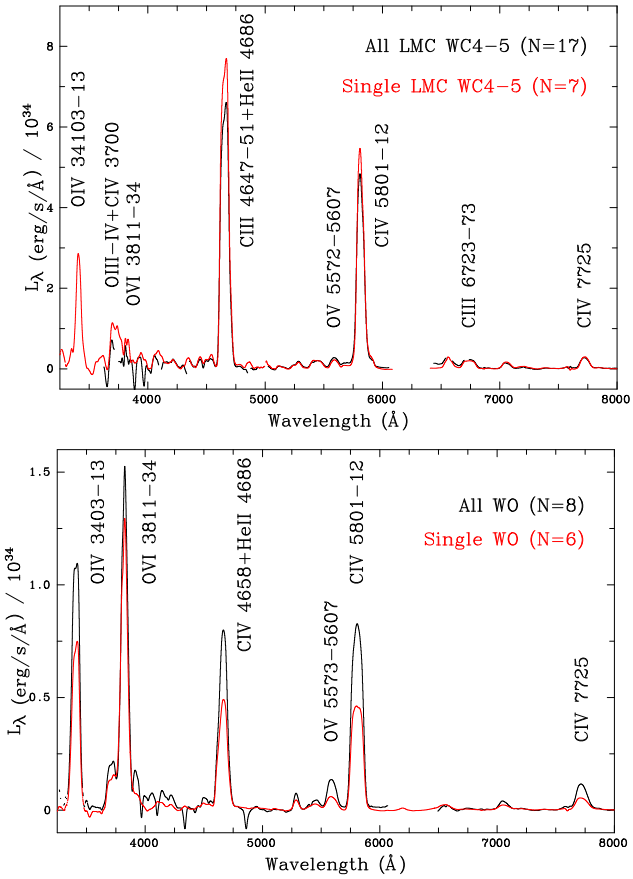

Figure B6. Upper panel: LMC WC4–5 emission line templates based on single (red) and all (black) stars. Lower panel: WO emission line templates based on single (red) and all (black) stars, incorporating all Milky Way (four), LMC (three), and SMC (one) stars.

This paper has been typeset from a TEX/LATEX file prepared by the author.